Title

Rational Chemical Design of Molecular Glue Degraders

Author

Toriki, Ethan Shigeru

Publication Date

2024

Rational Chemical Design of Molecular Glue Degraders

By

Ethan Shigeru Toriki

A dissertation submitted in partial satisfaction of the

requirements for the degree of

Doctor of Philosophy

in

Chemistry

in the

Graduate Division

of the

University of California, Berkeley

Committee in charge:

Professor Daniel K. Nomura, Chair
Professor Evan W. Miller
Professor James A. Olzmann

Spring 2024

Abstract

Rational Chemical Design of Molecular Glue Degraders

by

Ethan Shigeru Toriki

Doctor of Philosophy in Chemistry

University of California, Berkeley

Professor Daniel K. Nomura, Chair

One of the largest obstacles in modern drug discovery is that a significant portion (>90%) of the proteome is considered “undruggable”, in that these proteins lack a characterized, functional binding pocket or “ligandable hotspot” which small molecules can bind to and modulate the protein’s function for therapeutic benefit. To overcome such disease-causing proteins, targeted protein degradation (TPD) strategies have arisen, where the cell’s endogenous degradation machinery is hijacked to ubiquitinate and degrade the classically undruggable protein. Molecular glue degraders serve as a promising modality to achieve TPD. These are monovalent compounds that induce the proximity of a target protein with a component of the ubiquitin proteasome system to degrade the protein of interest. The systematic and modular synthesis of such small molecules, however, has not been possible due to a lack of known rational chemical design principles for converting protein-targeting ligands into molecular glue degraders.

This dissertation discusses the elucidation of novel design principles for the synthesis of covalent molecular glue degraders through the discovery of a transplantable chemical moiety that converts protein-targeting ligands into monovalent degraders of their corresponding targets. We first discovered a covalent handle which, when appended to the CDK4/6 inhibitor ribociclib, resulted in the degradation of CDK4 in a proteasome-dependent manner. Structural optimization of the initial covalent handle led to the synthesis of a but-2-ene-1,4-dione (fumarate) moiety that induced a more potent dose-responsive degradation of CDK4. Utilizing quantitative chemoproteomic platforms to profile global cysteine reactivity throughout the proteome, we identified that the RING-family E3 ligase RNF126 was binding covalently to the monovalent CDK4 degraders. Transplanting this covalent fumarate handle onto various inhibitors and protein-targeting ligands allowed for the degradation of protein targets BCR-ABL and c-ABL, PDE5, SMARCA2/4, LRRK2, BRD4, BTK, HDAC1/3, and AR and AR-V7. We have identified a first-in-class minimal covalent chemical handle that can convert protein targeting ligands into molecular glue degraders of their corresponding targets across diverse chemical and protein classes.

Table of Contents

List of Figures

Abbreviations

ABPP	Activity-based protein profiling
ANOVA	Analysis of variance
AR	Androgen receptor
AR-V7	Androgen receptor splice variant 7
ATCC	American Type Culture Collection
ATP	Adenosine triphosphate
BAF	BRG1- or BRM-associated factors
BAG6	BAG cochaperone 6
BCA	Bicinchoninic acid
BCL6	B cell lymphoma 6 protein
BCR-ABL	Breakpoint cluster region-Abelson tyrosine protein kinase 1
BET	Bromodomain and extra-terminal domain
BRD2	Bromodomain-containing protein 2
BRD3	Bromodomain-containing protein 3
BRD4	Bromodomain-containing protein 4
BRG1	SMARCA4
BRM	SMARCA2
BRSM	Based on recovered starting material
BSA	Bovine serum albumin
BTB	Broad-complex, Tramtrack and Bric-a-brac domain
BTK	Bruton tyrosine kinase
BTZ	Bortezomib
c-ABL	Abelson tyrosine protein kinase 1
CDK4	Cyclin-dependent kinase 4
CDK6	Cyclin-dependent kinase 6
CDK12	Cyclin-dependent kinase 12
CRISPR	Clustered regularly interspaced short palindromic repeats
CRL4B	Cullin-RING ubiquitin ligase 4B
CRPC	Castration-resistant prostate cancer
CSP	Chemical shift perturbation
CuAAC	Copper-catalyzed azide-alkyne cycloaddition
CUL4	Cullin-4
CV	Compensation voltages
CV	Column volume
C13	Cysteine at position 13
C16	Cysteine at position 16
C29	Cysteine at position 29
C32	Cysteine at position 32

C481	Cysteine at position 481
DCAF16	DDB1 and CUL4 Associated Factor 16
DCC	N,N′-Dicyclohexylcarbodiimide
DCM	Dichloromethane
DDB1	DNA damage-binding protein 1
DIPEA	N,N-diisopropylethylamine
DMAP	4-Dimethylaminopyridine
DMEM	Dulbecco's Modified Eagle Medium
DMF	N,N-dimethylformamide
DMP	Dess–Martin periodinane
DMSO	Dimethyl sulfoxide
DNA	Deoxyribonucleic acid
DSS	Sodium trimethylsilylpropanesulfonate
DTT	Dithiothreitol
ESI	Electrospray ionization
ESI-LC/MS	Liquid chromatography-electrospray ionization-mass spectrometry
EtOAc	Ethyl acetate
FA	Formic acid
FAIMS	High-field asymmetric waveform ion mobility spectroscopy
FBS	Fetal bovine serum
FDA	Food and Drug Administration
FDR	False discovery rate
FEM1B	Fem-1 homolog B
FLAG Tag	DYKDDDDK polypeptide protein tag
FPLC	Fast protein liquid chromatography
F12-K	Kaighn's Modification of Ham's F-12 Medium
GAPDH	Glyceraldehyde 3-phosphate dehydrogenase
GSPT1	G1 To S Phase Transition 1
GSPT2	G1 To S Phase Transition 2
HATU	Hexafluorophosphate azabenzotriazole tetramethyl uronium
HCD	Higher-energy collision dissociation
HDAC1	Histone deacetylase 1
HDAC2	Histone deacetylase 2
HDAC3	Histone deacetylase 3
HDAC6	Histone deacetylase 6
HEK	Human embryonic kidney
HEPES	4-(2-hydroxyethyl)-1-piperazineethanesulfonic acid
HMQC	Heteronuclear multiple quantum coherence
HPLC	High-performance liquid chromatography
HRMS	High-resolution mass spectrometry

IA	Iodoacetamide
IMAC	Immobilized metal affinity chromatography
IMDM	Iscove's Modified Dulbecco's Medium
IMiD	Immunomodulatory drug
IPTMs	Induced proximity-based therapeutic modalities
IPTG	Isopropyl β-D-1-thiogalactopyranoside
IR	Infrared
isoDTB-ABPP	Isotopically labeled desthiobiotin azide-tag-based activity-based protein profiling
LB	Lysogeny broth
LC	Liquid chromatography
LCMS	Liquid chromatography-mass spectrometry
LC-MS/MS	Liquid chromatography-tandem mass spectrometry
LNCaP	Lymph node carcinoma of the prostate
LRMS	Low-resolution mass spectrometry
LRRK2	Leucine-rich repeat kinase 2
LRSAM1	Leucine rich repeat and sterile alpha motif containing 1
MDA-MB-231	MD Anderson-metastatic breast-231
MeCN	Acetonitrile
MEM	Minimal Essential Medium
MeOH	Methanol
MID2	Midline 2
MS	Mass spectrometry
MS1	First MS for detection of initial ionization in MS/MS
MS2	Second MS for detection of fragment ionization in MS/MS
MWCO	Molecular weight cut-off
n-BuLi	n-Butyllithium
NEB	New England Biolabs
NFκB	Nuclear factor kappa-light-chain-enhancer of activated B cells
NMR	Nuclear magnetic resonance
NP-40	Nonyl phenoxypolyethoxylethanol
NTA	Nitrilotriacetic acid
OD	Optical density
PBS	Phosphate-buffered saline
PDE5	Phosphodiesterase 5
POI	Protein of interest
PROTAC	Proteolysis-targeting chimera
p97	Valosin-containing protein
RING	Really interesting new gene
RIPA	Radio-immunoprecipitation assay
RNA	Ribonucleic acid

RNF126	Ring finger protein 126
RNF14	Ring finger protein 14
RNF219	Ring finger protein 219
RNF4	Ring finger protein 4
RNF40	Ring finger protein 40
RPMI	Roswell Park Memorial Institute Medium
RT	Room temperature
SAR	Structure-activity relationship
SALL4	Spalt-like transcription factor 4
SDS	Sodium dodecyl sulfate
SDS/PAGE	Sodium dodecyl sulfate-polyacrylamide gel electrophoresis
SEC	Size exclusion chromatography
SFC	Supercritical fluid chromatography
shRNA	Short hairpin RNA
SIAH1	Seven in absentia homolog 1
SMARCA2	SWI/SNF related, matrix associated, actin dependent regulator of chromatin, subfamily A, member 2
SMARCA4	SWI/SNF related, matrix associated, actin dependent regulator of chromatin, subfamily A, member 4
SOFAST	Band-selective optimized flip angle short transient
SQD	Single quadrupole detector
TBS-T	Tris-buffered saline containing Tween 20
TBTA	Tris(benzyltriazolylmethyl)amine
TCEP	Tris(2-carboxyethyl)phosphine
TEAB	Triethylammonium bicarbonate
TEV	Tobacco etch virus protease
TFA	Trifluoroacetic acid
TGX	Tris-Glycine eXtended
THF	Tetrahydrofuran
TLC	Thin layer chromatography
TMT	Tandem mass tag
TMSCl	Trimethylsilyl chloride
TPD	Targeted protein degradation
tBuOH	tert-Butyl alcohol
T3P	Propylphosphonic anhydride
UBE2D	Ubiquitin-conjugating enzyme E2 D
UPLC-MS	Ultra-performance liquid chromatography-mass spectrometry
UV	Ultraviolet
VHL	Von Hippel-Lindau tumor suppressor

Dedication

It would be incredibly arrogant of myself to claim that my accomplishments as a graduate student (and throughout life) are mine alone. The significance of my family, friends, and mentors throughout my journey as a growing scientist and person cannot be overstated.

To Mom and Dad, thank you for being the most loving and supportive parents a child could ask for. From as early as I can remember, you strove for me to become the best version of myself in everything I pursued, whether that was in school, baseball, or beyond. And no matter how many times I struggled or failed, your belief that I could achieve things far beyond my imagination never wavered. I will forever be grateful for your continuous support and belief in me, even as I was over an ocean away from home. I strive every day to better myself as a scientist and person, so I can be a son you are proud of. This doctorate is as much yours as it is mine. Thank you for everything you've given and taught me. To Gram, Gramps, Grandma Toriki, Aunty Ri, and Uncle Pat, I always love coming home from the mainland to see you. Thank you for always supporting me in every endeavor I pursue and being the best family ever.

Throughout my life, I have been incredibly blessed to meet and befriend so many of the most wonderful individuals on the face of this planet, many of whom I have met in Berkeley. To my brother James, words cannot express how grateful I am to have met you. We made quite the spectacular team here in the Nomura Research Group. You were the most brilliant and dedicated co-author I could have ever teamed up with, and I learned so much from you about what it means to be a good scientist and a good person. To Kaila and Claire, it was an absolute pleasure to mentor and work alongside each of you, and I cannot wait to see the incredible accomplishments you make in the future. To Daniela, it was wonderful to talk science and sports with you every day, thank you for being the best conference buddy I could ask for. Throughout my time in graduate school, I was able to work those long hours and on weekends because of all my lab mates in the Nomura Research Group, who made coming into lab every day so enjoyable. To all my wonderful friends I have met while at UC Berkeley, thank you for letting me be a part of your life. I will treasure all the memories I made here.

All my accomplishments at Berkeley, of course, would not have been possible without one man who took a chance on a prospective graduate student coming all the way from Rochester. To my mentor and advisor, Dan Nomura, thank you so much for allowing me to join your lab those four years ago. You always supported me through my development as a scientist, challenged me to become the best version of myself I could be, and never lost belief in me even when my experiments were not working well. I will forever be grateful for your mentorship.

Acknowledgments

Thank you to the members of the Nomura Research Group, Novartis Institutes for BioMedical Research, and Novartis-Berkeley Translational Chemical Biology Institute (NB-TCBI).

For chapter 2, this work was supported by Novartis Institutes for BioMedical Research and the Novartis-Berkeley Translational Chemical Biology Institute (NB-TCBI) for all listed authors. This work was also supported by the Nomura Research Group and the Mark Foundation for Cancer Research ASPIRE Award for DKN, EST, JP, and KN. JP was also supported by the Mark Foundation for Cancer Research Momentum Postdoctoral Award and the Canadian NSERC CRSNG Postdoctoral Fellowship. This work was also supported by grants from the National Institutes of Health (R01CA240981 and R35CA263814 for DKN) and the National Science Foundation Molecular Foundations for Biotechnology Award (2127788). We also thank Drs. Hasan Celik, Alicia Lund, and UC Berkeley's NMR facility in the College of Chemistry (CoC-NMR) for spectroscopic assistance. Instruments in the College of Chemistry NMR facility are supported in part by NIH S10OD024998.

Adapted with permission from co-authors, Ethan S. Toriki, James W. Papatzimas, Kaila Nishikawa, Dustin Dovala, Andreas O. Frank, Matthew J. Hesse, Daniela Dankova, Jae-Geun Song, Megan Bruce-Smythe, Heidi Struble, Francisco J. Garcia, Scott M. Brittain, Andrew C. Kile, Lynn M. McGregor, Jeffrey M. McKenna, John A. Tallarico, Markus Schirle, Daniel K. Nomura, "Rational Chemical Design of Molecular Glue Degraders." Copyright © 2023 ACS Central Science.

CHAPTER 1

Background on Targeted Protein Degradation and Molecular Glue Degraders

1.1 Modalities of Targeted Protein Degradation

Advances in drug discovery over the last several decades have been mainly achieved through occupancy-driven pharmacology. In this model, organic small molecular bind to the active site of a protein of interest, modulating the protein's function for therapeutic benefit. However, one of the biggest challenges in developing new therapies for diseases like cancer is that most (>90%) of the proteome is deemed "undruggable" in that these proteins are devoid of characterized, functional binding pockets or "ligandable hotspots" that can be targeted by small molecules to achieve protein function modulation.[1] To successfully target undruggable proteins involved in disease, induced proximity-based therapeutic modalities (IPTMs) have been developed that exploit small molecules to induce the proximity of proteins that usually do not interact to alter the protein target's stability, function, or interactome for therapeutic benefit.[1-4] One such IPTM is centered around targeted protein degradation (TPD), where proximity is induced between a target protein and a component of the cellular degradation machinery, resulting in the degradation of the protein target. Traditional strategies in TPD involve heterobifunctional degraders, or proteolysis-targeting chimeras (PROTACs), that consist of a ligand targeting the protein of interest (POI) and a ligand targeting a E3 ubiquitin ligase, connected by a chemical linker. The nature of this type of small molecule allows for a ternary complex to form between the POI and E3 ligase, causing ubiquitination and degradation of the protein target (Figure 1.1a).[1-4] While PROTACs have shown great therapeutic promise, concerns persist regarding their non-drug-like physiochemical properties due to their high molecular weights and the lack of known ligandable E3 ligases that can be utilized by PROTACs. To overcome these challenges, molecular glue degraders serve as a second powerful strategy in TPD that combine the low-molecular weight properties seen in traditional inhibitors with the benefits of event-driven pharmacology. These are monovalent small molecules that promote degradation of substrate proteins through inducing protein-protein interactions between a target of interest and a component of the ubiquitin proteosome system (Figure 1.1b).[1-4] While PROTACs primarily rely on protein-targeting ligands capable of recruiting either the POI or E3 ligase through direct engagement of a distinct binding pocket, molecular glue degraders access shallower protein interfaces to trigger ternary complex formation and degradation of the protein target. Thalidomide is one example of a molecular glue degrader, as it triggers protein-protein interactions between cereblon, an E3 ubiquitin ligase substrate receptor, and multiple neo-substrate proteins like Ikaros and SALL4, leading to the ubiquitination and degradation of these targets.[7,12-14] Various immunomodulatory drug (IMiD) analogs of thalidomide have since been synthesized, such as lenalidomide and pomalidomide, and serve as anticancer treatments.

While molecular glue degraders could serve as a powerful therapeutic modality in tackling the undruggable proteome, one glaring issue remains that has hindered the transition of these types of compounds into the clinic. The design of PROTACs is quite modular, where E3 ligase recruiters can be connected to protein-targeting ligands via a linker in a very systematic approach. This is not possible for monovalent compounds like molecular glue degraders, as discovery of these compounds has mainly been achieved fortuitously or through the repurposing of already well-characterized E3 ligase recruiters.[5-11] For molecular glue degraders to be a viable and powerful therapeutic strategy in

degrading high value, intractable protein targets, advancements in the rational discovery and design of such compounds must be achieved. Here, I will discuss recent advances in the rational discovery of molecular glue degraders through cell-based phenotypic screening. I will also review several independent examples regarding specific small molecules and protein targets that suggest molecular glue degraders could be synthesized through small chemical structural changes to protein-targeting ligands.

1.2 Rational Discovery of Molecular Glue Degraders

Chemical screening for anticancer small molecules has arisen as a novel strategy to facilitate the rational discovery of molecular glue degraders. Mayor-Ruiz et al. demonstrated the utility of this technique, where a screen for compounds with anticancer phenotypes was paired with a counter-screen for an attenuated anticancer phenotype in hyponeddylation cell lines.[15] This allowed for the identification of compounds that rely on a Cullin E3 ligase-dependent mechanism of action to induce cancer cell toxicity. This strategy, coupled with whole genome-wide CRISPR screens, facilitated the discovery of molecular glue degraders that target cyclin K through ternary complex formation between CDK12-cyclin K and the CRL4B complex.[15] King et al. also utilized this counter-screening approach in hyponeddylation cell lines and coupled it with covalent chemoproteomic platforms for rapid mechanistic elucidation.[16] Screening a library of covalent ligands for anticancer phenotypes, followed by subsequent use of quantitative proteomic approaches yielded a monovalent degrader that utilizes the E2 ubiquitin-conjugating enzyme UBE2D to degrade NFκB.[16]

1.3 Converting Protein-Targeting Ligands into Molecular Glue Degraders

Recent evidence has emerged that suggest small structural alterations to protein-targeting ligands can convert such small molecules into molecular glue degraders of their corresponding targets. In a study from Slabicki et al., a genome-wide CRISPR screen of E3 ligase components was utilized to elucidate correlations between drugs showing anticancer effects and ligase expression.[17] The CDK inhibitor CR8 was shown to induce cytotoxic effects through the expression of DBB1, a CUL4 adaptor protein. Subsequent quantitative mass spectrometry experiments revealed selective degradation of cyclin K mediated by CR8 through the formation of a ternary complex between CDK12-cyclin K and DDB1.[17] CR8 is a structural analog of the CDK12 inhibitor roscovitine, differing only through the presence of a phenyl-pyridine moiety (Figure 1.2a). These results suggest that molecular glue degraders could be synthesized from protein-targeting ligands through subtle chemical changes to those ligands' structure. Roscovitine is converted to CR8 through the addition of a pyridine group at its solvent exposed exit vector, resulting in CR8 being able to induce an interaction between two protein complexes that, under normal physiological conditions, do not associate.

Single point mutations on proteins, such as the glutamate to valine mutation on hemoglobin, completely alters the interactome of that protein. In the case of hemoglobin, the mutation of glutamate to valine increases the protein's affinity for itself, polymerizing

hemoglobin to trigger sickle cell anemia. In a similar type of mechanism, it is likely that small molecules can serve to modify the surface of the proteins they bind to and have a significant impact on that protein's interactome. One further example of the potential for small molecules to alter protein interaction landscape is illustrated in another study from Slabicki et al. BI-3802, an analog of the oncogenic transcription factor B cell lymphoma 6 (BCL6) inhibitor BI-3812, was shown to trigger the proteasome-mediated degradation of BCL6.[18] BI-3802 binds to the Broad-complex, Tramtrack and Bric-a-brac (BTB) domain of BCL6 and induces interactions between BCL6 homodimers to form supramolecular filaments of the protein that are degraded by the E3 ligase SIAH1.[18] The key difference between BI-3812 and BI-3802 is in their piperidine group at their exit vectors, again illustrating that small structural changes to inhibitors or protein-binding ligands can drastically alter their mechanism of action and the interactome of the protein it binds to (Figure 1.2b).

The bromodomain-containing protein 4 (BRD4) inhibitor JQ1 has also been derivatized into a degrader of its respective protein target. A proporgyl amine moiety conjugated onto JQ1 resulted in the compound GNE-0011, which repurposes the CUL4 ligase substrate receptor DCAF16 to ubiquitinate and degrade BRD4 (Figure 1.2c).[19-22] GNE-0011 is another case of a protein inhibitor that is converted into a monovalent degrader through a small modification to its structure. These examples suggest that rational chemical design principles to aid in the synthesis of molecular glue degraders can be developed that would allow for the systematic and modular development of these compounds. A rational design strategy to streamline the synthesis of monovalent degraders would be a marked improvement from our current endeavors in using phenotypic screens of thousands of compounds to discover such degraders. The following work described in this dissertation covers the discovery of a minimal covalent handle that when appended onto various protein targeting ligands, converts these ligands into molecular glue degraders of their respective protein targets.

1.4 Figures

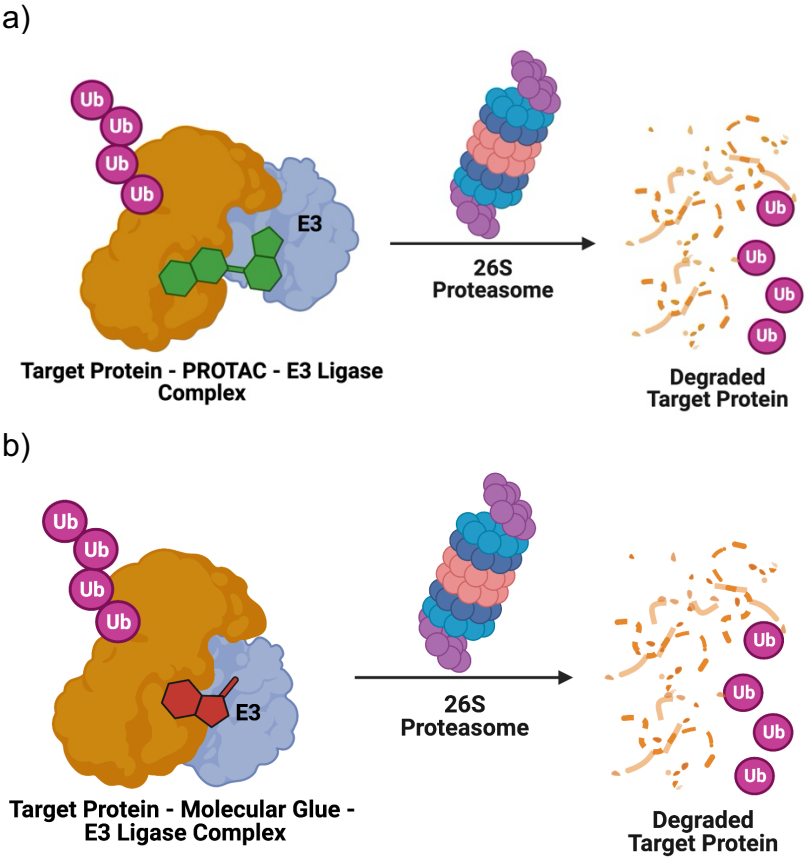

Figure 1.1 Targeted protein degradation utilizing PROTACs and molecular glue degraders. (a) Heterobifunctional PROTAC molecule induces ternary complex formation with target protein and E3 ligase complex. Subsequent ubiquitination of the target protein leads to degradation of the target via the 26S proteasome. (b) Monovalent molecular glue degrader induces ternary complex formation with target protein and E3 ligase complex. Subsequent ubiquitination of the target protein leads to degradation of the target via the 26S proteasome.

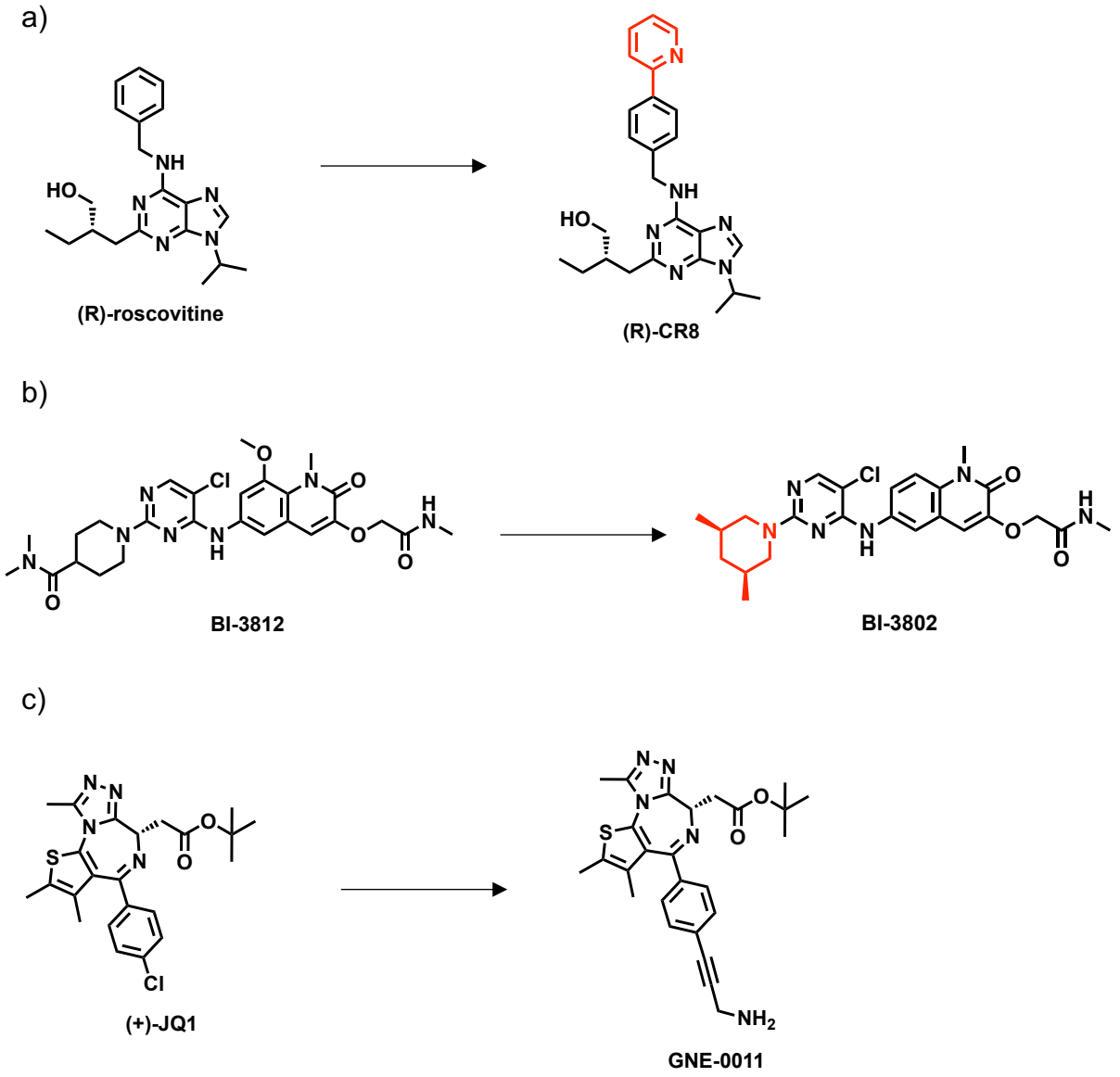

Figure 1.2 Examples of protein-targeting ligands being converted into molecular glue degraders through subtle chemical changes. (a) Roscovitine (CDK12 inhibitor) is converted to CR8 (cyclin K degrader) through addition of a pyridine group. (b) BI-3812 (BCL6 inhibitor) is converted to BI-3802 (BCL6 degrader) through conversion to a dimethyl-piperidine group. (c) JQ1 (BRD4 inhibitor) is converted to GNE-0011 (BRD4 degrader) through addition of a propargyl amine group.

CHAPTER 2

Discovery of a Transplantable Covalent Chemical Handle for Rational Molecular Glue Degrader Design

This chapter is based on the *ACS Central Science* publication “Rational Chemical Design of Molecular Glue Degraders”[41] and has been adapted with permission from all co-authors

2.1 Summary

Targeted protein degradation with molecular glue degraders has arisen as a powerful therapeutic modality for eliminating classically undruggable disease-causing proteins through proteasome-mediated degradation. However, we currently lack rational chemical design principles for converting protein-targeting ligands into molecular glue degraders. To overcome this challenge, we sought to identify a transposable chemical handle that would convert protein-targeting ligands into molecular degraders of their corresponding targets. Using the CDK4/6 inhibitor ribociclib as a prototype, we identified a covalent handle that, when appended to the exit vector of ribociclib, induced the proteasome-mediated degradation of CDK4 in cancer cells. Further modification of our initial covalent scaffold led to an improved CDK4 degrader with the development of a but-2-ene-1,4-dione ("fumarate") handle that showed improved interactions with RNF126. Subsequent chemoproteomic profiling revealed interactions of the CDK4 degrader and the optimized fumarate handle with RNF126 as well as additional RING-family E3 ligases. We then transplanted this covalent handle onto a diverse set of protein-targeting ligands to induce the degradation of BRD4, BCR-ABL and c-ABL, PDE5, AR and AR-V7, BTK, LRRK2, HDAC1/3, and SMARCA2/4. Our study undercovers a design strategy for converting protein-targeting ligands into covalent molecular glue degraders.

2.2 Introduction

Targeted protein degradation (TPD) has arisen as a powerful approach for destroying classically undruggable disease-causing proteins through ubiquitination and proteasome-mediated degradation. Two major strategic medicinal chemistry approaches exist for TPD: heterobifunctional proteolysis targeting chimeras (PROTACs) and monovalent molecular glue degraders. Both induce the proximity of an E3 ubiquitin ligase with a target protein leading to the ubiquitination and degradation of the protein in a proteasome-dependent manner.[1−4] While PROTAC design is more modular wherein protein-targeting ligands can be connected via a linker to an E3 ligase recruiter, the discovery of novel molecular glue degraders has mostly been either fortuitous from phenotypic screens or via specific well-characterized E3 ligase-targeting recruiters (e.g., for cereblon).[5−11] Given this landscape, a rational chemical design principle for converting protein-targeting ligands into molecular glue degraders is highly desired and would thereby facilitate a modular target-based design strategy of molecular glue degraders, which is currently lacking.

There are several emerging innovative strategies for discovering novel molecular glue degraders, as discussed in the previous chapter, but these discoveries have only been made through cell-based phenotypic screens of large compound libraries. There does exist, though, several independent one-off examples of minor structural modifications to nondegradative inhibitors that have converted these compounds into degraders of their targets or associated protein complexes. This indicates that rational chemical design principles may exist to convert nondegradative protein-targeting ligands more systematically and modularly into molecular glue degraders of those targets, but such design principles are still poorly understood. Here, we have discovered a minimal

covalent chemical moiety that can be appended onto various protein-targeting ligands to induce the degradation of their target proteins.

2.3 Results

2.3.1 Synthesis and Testing of Analogs with Chemical Handles Appended to the Exit Vector of the CDK4/6 Inhibitor Ribociclib

To identify potential chemical handles that could convert protein-targeting ligands into molecular glue degraders of their targets, we appended various moieties onto the solvent-exposed piperazine of the CDK4/6 inhibitor ribociclib (Figure 2.1a).[23] Among the nine initial ribociclib analogs tested, we found one compound, EST1027, a trifluoromethylphenyl cinnamamide, that led to >50% reduction in CDK4, but not CDK6, levels in C33A cervical cancer cells treated for 24 h at 3 μM (Figures 2.1b−d and S1a). This EST1027-mediated reduction in CDK4 occurred via proteasome-mediated degradation, since pretreatment of C33A cells with the proteasome inhibitor bortezomib attenuated EST1027-mediated CDK4 degradation (Figure 2.1e,f). Tandem mass tagging (TMT)-based quantitative proteomic analysis revealed a significant reduction in CDK4 levels in C33A cells after treatment with EST1027, alongside 100 other proteins that were significantly reduced out of >5000 total proteins quantified (Figure S1b and Table S1). The moderate selectivity observed may be due to downstream protein level changes resulting from CDK4 degradation or potential off-target effects of the cinnamamide handle. The cinnamamide motif is a possible covalent substrate that can undergo 1,4-addition with a cysteine thiolate anion. Confirming the necessity of this covalent functionality for the degradation of CDK4, a nonreactive trifluoromethylphenyl propionamide analog, EST1036, did not induce the degradation of CDK4 in C33A cells (Figure 2.1g−i).

2.3.2 Structure-Activity Relationship of CDK4 Degrader

Encouraged by these data, we postulated that this trifluoromethylphenyl cinnamamide moiety could be appended onto other protein-targeting ligands to induce their degradation. Thus, we next appended this motif onto another structurally similar CDK4/6 inhibitor, palbociclib, to generate EST1090 (Figure S1c). Disappointingly, EST1090 did not degrade CDK4 in C33A cells (Figure S1d), indicating that this chemical motif was not generalizable and could not be transplanted onto other even very similar protein-targeting ligands to induce targeted degradation.

We therefore sought to explore structure−activity relationships of the cinnamamide motif for CDK4 degradation. Still using ribociclib as our testbed, we generated seven additional analogs to identify a better covalent chemical module (Figure 2.2a). Interestingly, moving the trifluoromethyl moiety from the para- to ortho- or meta- positions with EST1051, EST1054, and KN1002 abrogated CDK4 degradation in C33A cells, giving further support to specific interactions of these degrader compounds with an E3 ligase rather than nonspecific mechanisms (Figure 2.2a,b). We note that EST1027 caused a modest degree of C33A cytotoxicity that was also observed with close structural analogs EST1051 and EST1054, which did not degrade CDK4, indicating that general cytotoxicity was likely not mediating CDK4 loss (Figure S1e). Merely appending an acrylamide handle

with EST1057 also did not cause CDK4 degradation (Figure 2.2a,b). Among additional derivatives tested, we observed improved dose-responsive CDK4 degradation with EST1060, containing a methoxyphenyl but-2-ene-1,4-dione ("fumarate derivative"), in C33A cells (Figure 2.2a−d). A nonreactive derivative of EST1060, JP-2-230, did not degrade CDK4 in C33A cells (Figure S2a,b). EST1060 also did not degrade CDK6 (Figure S2c). We next appended this fumarate module onto palbociclib to generate EST1089 (Figure S2d). EST1089 was now capable of degrading CDK4 (Figure S2e), suggesting that this moiety may be a more versatile chemical handle when compared to our original cinnamamide handle.

2.3.3 Mapping the Proteome-Wide Targets of the Covalent Handle

Based on our data indicating that the covalent functionality on EST1027 and EST1060 was necessary to induce the degradation of CDK4 (Figures 2.1g−i and S2b), we postulated that this motif was leading to the covalent recognition of E3 ubiquitin ligases, leading to molecular glue interactions between E3 ligases and CDK4 and subsequent ubiquitination and proteasome-mediated degradation of CDK4. To identify E3 ligases covalently targeted by our original EST1027 CDK4 degrader, we performed isotopically labeled desthiobiotin azide-tag-based activity-based protein profiling (isoDTB-ABPP)[24] in which we treated C33A cells in situ with vehicle or EST1027 and subsequently labeled resulting cell lysates with an alkyne-functionalized iodoacetamide probe to identify cysteines that were highly engaged by EST1027 across the proteome.[25−28] Out of 3772 quantified probe-modified cysteines, we identified 49 targets that showed control/EST1027 ratios of >2 with a p-value of $p < 0.05$. Among these 49 targets, we identified a zinc-coordinating cysteine 32 (C32) on the RING-family E3 ubiquitin ligase RNF126 as a putative target of EST1027 that showed a control/EST1027 ratio of 2.0 (Figure 2.3a and Table S2).[29] We posited that labeling by EST1027 of only one of the zinc-coordinating cysteines still allows functional zinc coordination with the other cysteines (C13, C16, and C29), maintaining RNF126 function. RNF126 was the only protein involved in the ubiquitin proteasome system among these targets, and as such, the other targets were not pursued for further characterization. RNF126 is an important E3 ligase involved in cellular protein quality control and is necessary to ubiquitinate and degrade mislocalized proteins in the cytosol or membrane proteins from the endoplasmic reticulum through its association with BAG6 and ubiquitination of BAG6-associated client proteins.[30,31]

We next confirmed the interaction of EST1027 with RNF126 by gel-based ABPP, showing dose-responsive competition of EST1027 against rhodamine-functionalized iodoacetamide cysteine labeling of recombinant RNF126 (Figure 2.3b). RNF126 knockdown completely attenuated EST1027-mediated CDK4 degradation in C33A cells, demonstrating that RNF126 was at least partially involved in the degradation of CDK4 with EST1027 (Figures 2.3c and S3a). Interestingly, we also observed significant reduction in RNF126 levels with EST1027 treatment, which was potentially achieved through the proteasomal degradation of the CDK4-EST027-RNF126 ternary complex (Figures 2.3c and S3b). EST1090, the palbociclib derivative with the cinnamamide handle which did not degrade CDK4, did not bind to RNF126 (Figure S3c).

Interestingly, we found that EST1060, with the fumarate handle, displaced cysteine-reactive probe labeling of pure RNF126 much more potently compared to

EST1027 (Figure 2.3d). The nonreactive derivative of EST1060, JP-2-230, interestingly still showed binding to RNF126, albeit weaker than EST1060, indicating the fumarate motif may possess reversible binding affinity to RNF126 beyond its inherent reactivity (Figure S3d). We observed similar potent interactions with the palbociclib-based, fumarate CDK4 degrader EST1089 as EST1060 (Figure S3e). Mass spectrometry analysis of tryptic digests from RNF126 incubated with EST1027 or EST1060 further confirmed C32 as the site of modification (Figure S4a−d).

2.3.4 Identifying the Minimal Covalent Chemical Handle Required for RNF126 Interactions

We next sought to understand the minimal chemical functionality and pharmacophore necessary to covalently interact with RNF126. To achieve this, we reverse engineered the EST1027 and EST1060 structures by taking their respective covalent handles and iteratively appending increasing portions of the ribociclib scaffold to assess their labeling of RNF126 by gel-based ABPP (Figure 2.3e). With trifluoromethylphenyl cinnamic acid appended to the minimal diethylamine moiety, KN1026, no RNF126 labeling was observed. In contrast, the methoxyphenyl fumarate handle linked to the diethylamine moiety, KN1025, showed labeling of RNF126, albeit weaker than EST1060 (Figure 2.3e). While appending a piperazine moiety onto trifluoromethylphenyl cinnamic acid to form EST1102 still did not confer labeling of RNF126, appending this substituent to the methoxyphenyl fumarate handle yielded JP-2-196, which showed significant potency comparable to that of EST1060 (Figure 2.3e). With the trifluoromethylphenyl cinnamamide handle, installing phenylpiperazine or pyridinyl-piperazine substituents, KN1023 or KN1017, respectively, began to show binding to RNF126 with comparable potency to that observed with EST1027 (Figure 2.3e). However, this required linking a substantial portion of the ribociclib structure as exemplified by JP-2-200 (Figure 2.3e). In contrast, growing substituents on the methoxyphenyl fumarate handle with equivalent moieties, KN1021, KN1018, and JP-2-199, did not substantially improve potency against RNF126 beyond that observed with the piperazine substituent alone of JP-2-196 (Figure 2.3e). These data collectively showed that the covalent fumarate-derived motif is a better ligand for RNF126 and the p-methoxyphenylpiperazinyl fumarate JP-2-196 handle is the best minimal unit identified so far for covalently engaging RNF126.

To further map the targets of this optimized fumarate handle, we synthesized an alkyne-functionalized probe JP-2-196-alkyne (Figure 2.3f). We first demonstrated covalent and dose-responsive labeling of pure RNF126 protein with JP-2- 196-alkyne by gel-based ABPP and that this labeling was attenuated upon pretreatment with JP-2-196 (Figure 2.3g,h). To assess the targets of this JP-2-196-alkyne probe, we next treated HEK293T cells with either the JP-2-196-alkyne probe or vehicle and subsequently appended an azide-functionalized biotin enrichment handle through copper-catalyzed “click-chemistry” followed by avidin enrichment of probe-modified peptides to assess probe-enriched proteins by quantitative proteomics (Figure 2.3i and Table S3). We identified 23 distinct protein targets that were significantly ($p < 0.001$) enriched by the JP-2-196-alkyne probe over vehicle control by >2-fold, of which RNF126 was the only E3 ligase among these 23 targets (Figure 2.3i). Using a less stringent filter, an additional 87 proteins were significantly ($p < 0.01$) enriched by the JP-2-196-alkyne probe by >2-fold,

which included five additional E3 ligases - RNF40, MID2, RNF219, RNF14, and LRSAM1 (Figure 2.3i). Interestingly, all six of these belong to the RING family of E3 ligases. While all six of these RING E3 ligases are potentially involved in the mechanism underlying degradation, we sought to investigate the interactions of our fumarate handle with the most significantly enriched E3 ligase RNF126, which had already been a hit in the isoDTB-ABPP experiment.

To further characterize the binding of JP-2-196 to RNF126, we recorded the ^{1}H-1D and ^{1}H,^{15}N-HMQC spectra of the uniformly ^{15}N-enriched first 40 amino acids of RNF126 (RNF126(1−40)) in the absence and presence of JP-2-196. The apo spectrum of RNF126 showed the expected number of peaks. Signals were dispersed, with some peaks located downfield of 8.5 ppm, indicating the presence of a well-behaved and folded protein (Figure S5a; black peaks). While our spectrum was not entirely identical to a previously recorded spectrum due to the usage of different buffer conditions, we could transfer most of the published peak assignments with high confidence.[29] Upon addition of JP-2-196 to apo-RNF126, we observed several residue-dependent chemical shift perturbations (CSPs), whereas the spectral dispersion and the overall signal intensities were unchanged (Figure S5a; red peaks). These results strongly suggested that our fumarate handle interacted with the protein without altering its fold or stability. Upon qualitatively clustering and mapping all spectral changes - CSPs and line broadening - onto a recently disclosed three-dimensional structure of RNF126(1−40),[29] we found that the ligand specifically bound at or close to the zinc binding site and that the rest of the protein remained unaffected (Figure S5b).

2.3.5 Transplanting a Fumarate-Based Covalent Handle onto Protein-Targeting Ligands that Already Possess Piperazines or Morpholines at the Exit Vector

Having identified a minimal motif required to potently engage RNF126, we next sought to transplant this handle onto other protein-targeting ligands to test if this module could be widely used to degrade the ligands' respective protein targets. We first focused on ligands that, like ribociclib, already possessed piperazine moieties at the solvent-exposed exit vector. Incorporation of our fumarate motif onto the clinically approved BCR-ABL and c-ABL kinase inhibitor dasatinib, the phosphodiesterase 5 (PDE5) inhibitor sildenafil, the SMARCA2-bromodain ligand 1 used in a previously developed SMARCA2 PROTAC ABCI1 developed by the Ciulli group,[32] and the LRRK2 inhibitor HG-10-102-01 that is currently under evaluation for Parkinson's disease that bears a morpholine exit vector led to the generation of JP-2-227, JP-2-201, JP-2-249, and JP-2-244. All four of these derivatives showed potent labeling of RNF126 and led to the degradation of their targets BCR-ABL and c-ABL, PDE5, SMARCA2 and SMARCA4, and LRRK2, respectively (Figures 2.4a−h and S6a−j). Collectively, our data demonstrated that this fumarate chemical handle could be used to extend several protein-targeting ligands already bearing piperazine exit vectors to degrade their respective targets across several protein classes from kinases, phosphodiesterases, and transcriptional activators.

2.3.6 Transplanting a Covalent Chemical Handle onto Protein-targeting Ligands from Unrelated Chemical and Protein Classes

We next sought to transplant this handle onto protein-targeting ligands that did not already possess a piperazine toward the exit vector of the compound. We first

incorporated the JP-2-196 handle onto the BET family bromodomain inhibitor JQ1, forming JP-2-197 (Figure 2.5a). This compound still potently labeled pure RNF126 protein and led to highly potent mid-nanomolar degradation of both long and short isoforms of BRD4 in HEK293T cells in a dose-responsive, time-dependent, and proteasome-dependent manner (Figures 2.5b−d and S7a−c). JQ1 also inhibits other BET family proteins; however, we did not observe degradation of BRD2 or BRD3 (Figure S7d,e).[33] Similar to our observation of RNF126 loss with EST1027, we also observed RNF126 loss at the highest concentration of JP-2-197 (Figure 2.5b). Pretreatment of cells with excess JQ1 completely attenuated JP-2-197-mediated BRD4 degradation (Figure S7f). Quantitative proteomic profiling of JP-2-197 also demonstrated selective degradation of BRD4 with two other targets also showing >4-fold reduced protein levels across >5000 proteins quantified (Figure 2.5e and Table S4). A nonreactive derivative of JP-2-197, JP-2-232, still showed binding to RNF126, albeit less potently compared to JP-2-197, but did not result in BRD4 degradation (Figure S7g−i). The chemical handle JP-2-196 itself does not alter BRD4 levels compared to the BRD4 degrader JP-2-197 (Figure S7j).

Next, we studied the interaction of JP-2-197 with RNF126(1−40) and BRD4(44−168) by proton-observed NMR. Our BRD4 construct showed two heavily up-field shifted methyl signals that were well-resolved (Figure S8a; black spectrum). Upon mixing BRD4(44−168) with JP-2-197, we observed strong signal perturbations of one of the methyl peaks ($\delta \approx -0.19$ ppm) and the appearance of new resonances (red spectrum) (Figure S8a). BRD4 remained soluble and folded when JP-2-197 was bound as indicated by an almost unchanged signal intensity of the unperturbed methyl resonance ($\delta \approx -0.46$ ppm) and the unaffected overall methyl group signal dispersion (Figure S8a). Combining RNF126(1− 40), BRD4(44−168), and JP-2-197 together resulted in a ^{1}H-1D spectrum with highly similar perturbations but with small additional chemical shift changes (e.g., for the peak at −0.38 ppm) and clear line broadening (green spectrum) (Figure S8a). We did not detect any comparable changes when the two proteins were combined without JP-2-197 (blue spectrum) or when treated with JQ1 or the fumarate handle JP-2-196 alone (magenta spectrum) (Figure S8a). Overall, these results support our premise that JP-2-197 induced a ternary complex formation between BRD4 and RNF126.

We generated a derivative of JP-2-197 that replaced its piperazine moiety with an ethyl diamine linker, JP-2-219 (Figure S8b). JP-2-219 was still able to degrade BRD4 but substantially less potently compared to JP-2-197, again demonstrating a tunable SAR for these covalent glue degraders (Figure S8c). We next assessed whether the maleic Z-isomer of our covalent handle was still capable of binding to RNF126 and whether this cis-isomer, when appended to JQ1, would affect BRD4 degradation. We found that both the trans- and cis-isomers of our covalent handle, both as tert-butyloxycarbonyl-protected handles - JP-2-190 and LE-21-PX17, respectively - were capable of binding to RNF126 (Figure S9a,b). We further demonstrated that the cis-isomer maleic handle appended onto JQ1 also potently bound to RNF126 and degraded BRD4 with equivalent potency compared to its trans-isomer JP-2-197 (Figure S9c−e).

BRD4 is a protein which is relatively easy to degrade and has been used as a test case for many different types of degraders.[27,34−36] Thus, we next sought to expand the scope of ligand and target classes to understand the diversity of targets that our chemical handle could access for targeted protein degradation applications. First, we incorporated our fumarate handle into the pan-histone deacetylase (HDAC) inhibitor vorinostat to

generate DD-1-073 (Figure S10a). We observed potent binding to RNF126 and degradation of HDAC1 and HDAC3 but not HDAC2 or HDAC6 in MDA-MB-231 cells (Figure S10b,c). Next, we incorporated our fumarate handle into the BTK inhibitor ibrutinib, replacing the BTK C481-targeting cysteine-reactive acrylamide warhead to generate JP-2-247 (Figure S10d). This molecule still potently labeled RNF126 and also showed BTK degradation in MINO lymphoma cancer cells (Figure S10e−g).

We next tackled a more challenging target, the truncated and constitutively active mutant of androgen receptor (AR), AR-V7, that drives the pathogenesis of androgen-resistant prostate cancers.[37] AR-V7 is a relatively undruggable target, given that the ligand binding domain that is the target of most AR-targeting drugs is missing from AR-V7. We linked our fumarate derivative JP-2-196 onto a previously discovered DNA-binding domain ligand, VPC-14228, for the androgen receptor that had recently been used in several VHL-based PROTACs to degrade AR-V7, through two different types of linkages to yield JP-2-217 and JP-2-224 (Figure 2.5f).[38−40] Both compounds showed potent binding to pure RNF126 protein (Figure S11a,b). Given that VPC-14228 binds to the DNA binding domain shared between wild-type full-length AR as well as its truncation mutants, we first tested this degrader for wild-type AR degradation in AR-sensitive LNCaP prostate cancer cells. JP-2-217 degraded AR in LNCaP cells in a dose-responsive manner (Figures 2.5g and S11c). We next tested both degraders in the androgen-resistant prostate cancer cell line 22Rv1 that expresses wild-type AR and AR-V7 and demonstrated that both JP-2-217 and JP-2-224, but not VPC-14228 or a previously reported VHL-based AR-V7 PROTAC (compound 6),[40] degraded both wild-type AR and AR-V7 (Figures 2.5h and S11d−h). Overall, we demonstrated that the minimal covalent handle JP-2-196 could be used to convert protein-targeting ligands into degraders of several proteins from different protein classes.

2.4 Discussion/Conclusion

While our chemical handle likely still requires significant optimization to improve potency, selectivity, and its versatility as a general motif for degrader design, we demonstrated proof-of-concept to convert protein-targeting ligands in a more rational manner into monovalent degraders of their targets without the need for long linkers and resultant high molecular weight PROTACs. We note that the molecular weights of all our degraders are lower than traditional PROTAC molecules, which may ease the burden of future medicinal chemistry efforts to generate compounds that show optimal pharmacokinetic parameters.

There are still many open questions that we hope to address in future studies. These questions include further understanding the mechanism underlying the versatile degradation observed with our chemical motif once appended to numerous ligands across so many different protein and ligand classes, the contribution of RNF126 and the role of BAG6 in RNF126-mediated responses, and the likely contribution of additional components of the ubiquitin-proteasome system beyond RNF126. We would also like to determine in future studies whether we are disrupting RNF126 endogenous function and whether this may pose any toxicity. While we were able to obtain a sufficient proteome to perform the described studies at the 24 h time points, many of the degraders reported here showed differing degrees of cytotoxicity at 24 h. We note though that many of the

covalent derivatives that we generated in our original SAR showed similar cytotoxicity, but differential CDK4 degradation, supporting the premise that the degradation we observe is not through nonspecific toxicity-mediated mechanisms. Given that JP-2-196 targets a zinc-coordinating cysteine within RNF126 that is also found across many other RING E3 ligases, we conjecture that as we optimized for RNF126 binding, we likely also optimized binding toward similar motifs that may be conserved across other RING E3 ligases. This is supported by our chemoproteomic data demonstrating that our covalent handle also engages additional RING E3 ligases RNF40, MID2, RNF219, RNF14, and LRSAM1. We believe that these E3 ligases, alongside RNF126, may also play a role in the mechanism underlying target degradation observed in our study. Additional areas of investigation will be to further optimize the potency and selectivity while reducing the reactivity of our covalent handles so that this strategy can be more broadly applied in future drug discovery applications.

Overall, our study identifies a potential starting point for developing chemical rational design principles for converting protein-targeting ligands into monovalent molecular glue degraders through appending a minimal linker-less covalent handle that can recruit RNF126 and additional RING E3 ligases. We recognize that with the optimization of the RNF126-recognizing ligand, our resulting covalent handle linked to protein-targeting ligands could also be considered linker-less PROTACs, but we anticipate that as molecular glue and PROTAC design evolves, the definition between PROTACs and molecular glue degraders will likely begin to merge and that our study represents a step toward that direction.

2.5 Figures

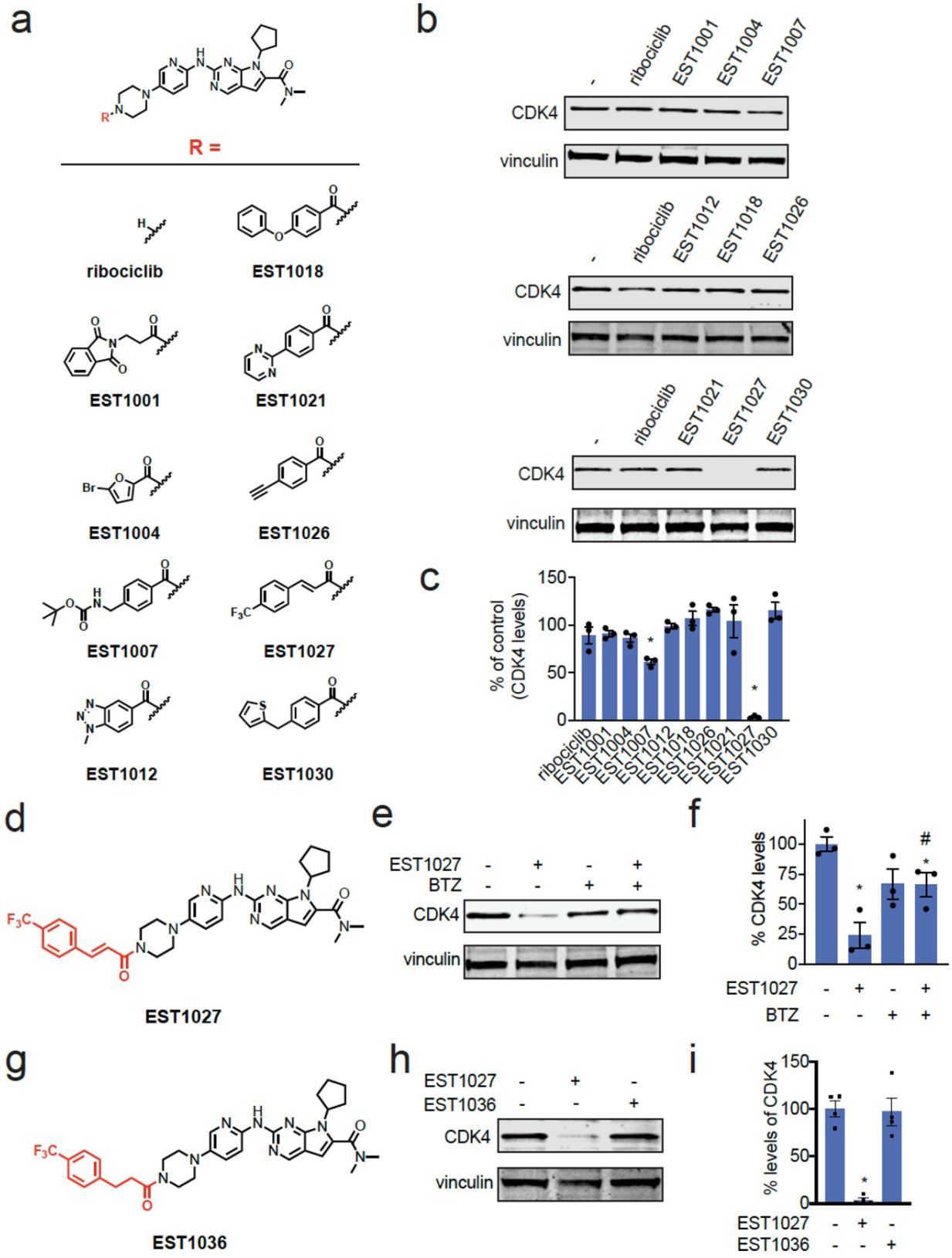
a
R =
ribociclib
EST1018
EST1001
EST1021
EST1004
EST1026
EST1007
EST1027
EST1012
EST1030
b
-
ribociclib
EST1001
EST1004
EST1007
CDK4
vinculin
ribociclib
EST1012
EST1018
EST1026
CDK4
vinculin
ribociclib
EST1021
EST1027
EST1030
CDK4
vinculin
c
% of control (CDK4 levels)
150
100
50
0
ribociclib
EST1001
EST1004
EST1007
EST1012
EST1018
EST1026
EST1021
EST1027
EST1030
d
EST1027
e
EST1027 - + - +
BTZ - - + +
CDK4
vinculin
f
% CDK4 levels
100
75
50
25
0
#
*
EST1027 - + - +
BTZ - - + +
g
EST1036
h
EST1027 - + -
EST1036 - - +
CDK4
vinculin
i
% levels of CDK4
150
100
50
0
*
EST1027 - + -
EST1036 - - +

Figure 2.1 Synthesis and testing of analogs with chemical handles appended to the exit vector of the CDK4/6 inhibitor ribociclib. (a) Structures of ribociclib analogs wherein various chemical handles were appended onto the solvent-exposed end of ribociclib. (b) Testing ribociclib analogs in C33A cervical cancer cells to identify compounds that reduce CDK4 levels. C33A cells were treated with DMSO vehicle or compounds (3 μM) for 24 h. CDK4 and loading control vinculin levels were assessed by Western blotting. (c) Quantification of the data shown in (b). (d) Full structure of hit compound EST1027 that showed >50% loss of CDK4 in (b,c) with the appended chemical handle shown in red. (e) Proteasome-dependent degradation of CDK4 by EST1027. C33A cells were pretreated with DMSO vehicle or the proteasome inhibitor bortezomib (BTZ) (10 μM) 1 h prior to treatment of cells with DMSO vehicle or EST1027 (5 μM), and CDK4 and loading control vinculin levels were assessed by Western blotting. (f) Quantification of the experiment described in (e). (g) Structure of EST1036, a nonreactive derivative of EST1027. (h) EST1036 does not degrade CDK4. C33A cells were treated with DMSO vehicle or compounds (5 μM) for 24 h, and CDK4 and loading control vinculin levels were assessed by Western blotting. (i) Quantification of experiment in (h). Blots shown in (b,e,h) are representative of n = 3 biologically independent replicates/group. Bar graphs in (c,f,i) show individual replicate values and average ± sem. Statistical significance is calculated as *$p < 0.05$ compared to DMSO vehicle in (c,f,i) and #$p < 0.05$ compared to the EST1027-treated group in (f).

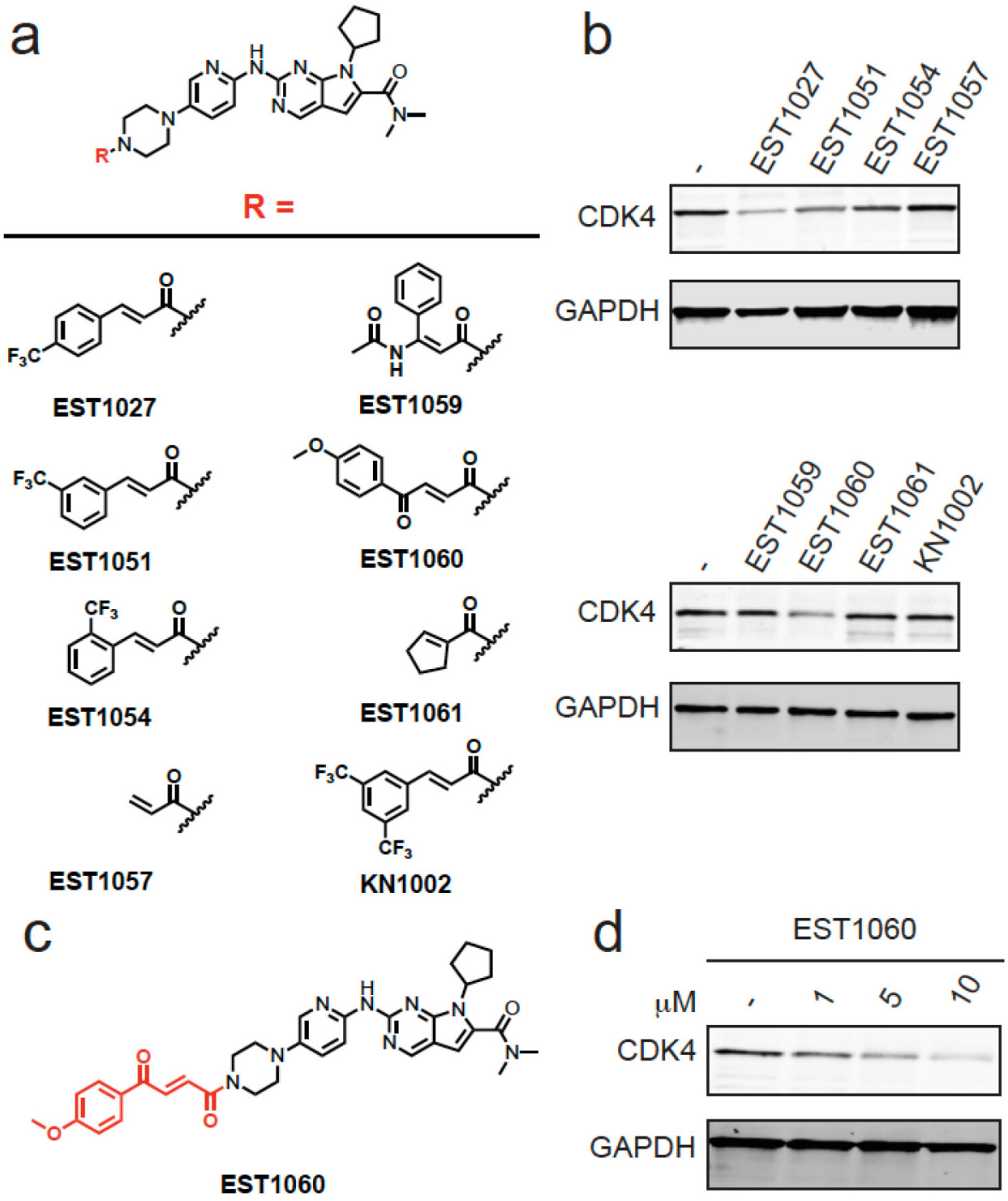
a
R =
EST1027
EST1059
EST1051
EST1060
EST1054
EST1061
EST1057
KN1002
b
-
EST1027
EST1051
EST1054
EST1057
CDK4
GAPDH
-
EST1059
EST1060
EST1061
KN1002
CDK4
GAPDH
c
EST1060
d
EST1060
μM
-
1
5
10
CDK4
GAPDH

Figure 2.2 Structure−activity relationship of CDK4 degrader. (a) Structures of EST1027 analogs assessing structure−activity relationships. (b) Testing EST1027 analogs in C33A cervical cancer cells to identify compounds that reduce CDK4 levels. C33A cells were treated with DMSO vehicle or compounds (5 μM) for 24 h. CDK4 and loading control GAPDH levels were assessed by Western blotting. (c) Full structure of hit compound EST1060. (d) Dose−response of EST1060 CDK4 degradation. C33A cells were treated with DMSO vehicle or EST1060 for 24 h. CDK4 and loading control GAPDH levels were assessed by Western blotting. Gels and blots in (b,d) are representative images from n = 3 biologically independent replicates/group.

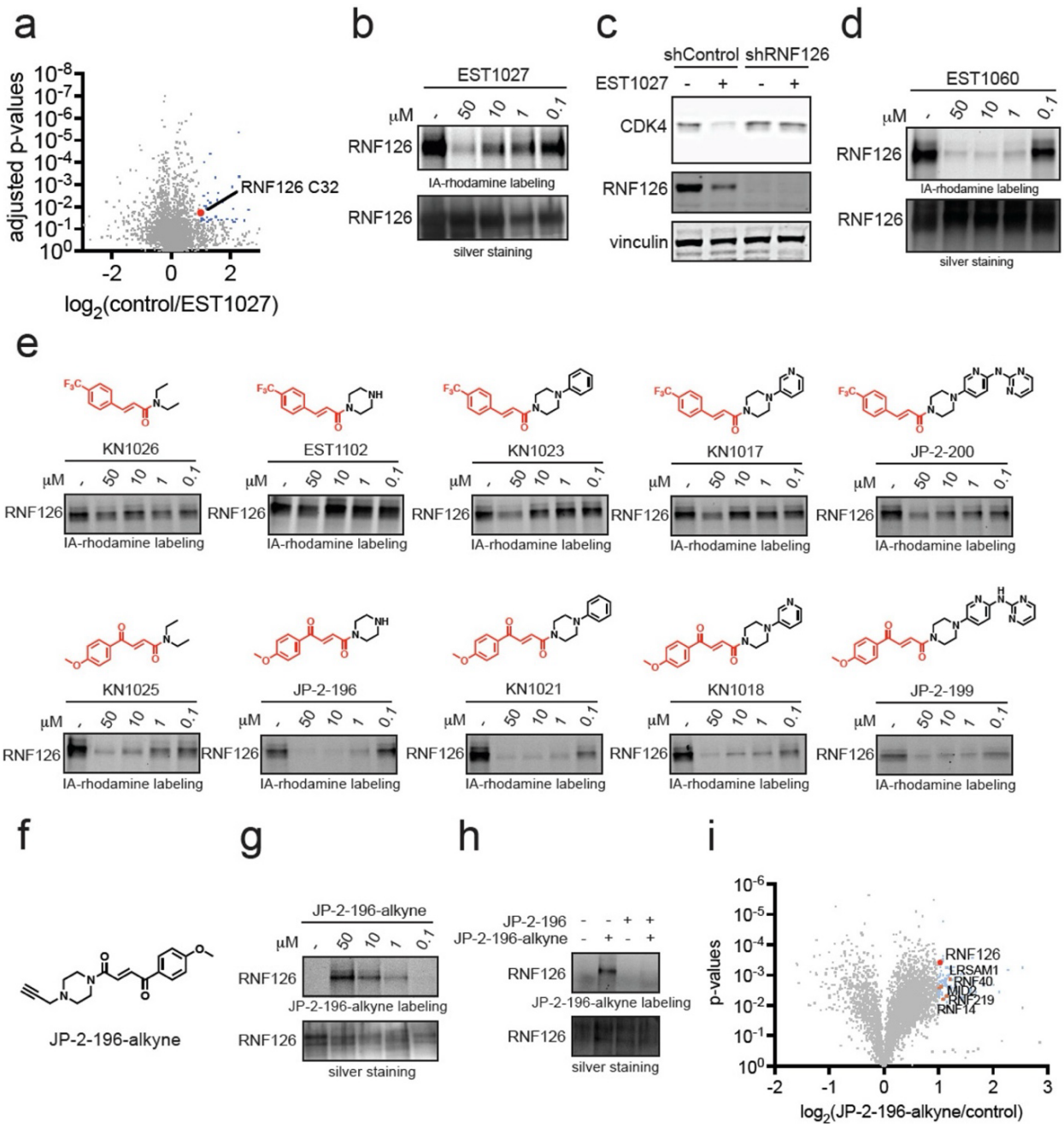

Figure 2.3 Mapping proteome-wide interactions of the fumarate handle. (a) Cysteine chemoproteomic profiling of EST1027 in C33A cervical cancer cells using isoDTB-ABPP. C33A cells were treated with DMSO vehicle or EST1027 (20 μM) for 2 h. Resulting lysates were labeled with an alkyne-functionalized iodoacetamide probe (IA-alkyne) (200 μM) for 1 h, after which isotopic desthiobiotin tags were appended by copper-catalyzed azide−alkyne cycloaddition (CuAAC) and taken through the isoDTB-ABPP procedure. Shown in blue and red are probe-modified cysteines that showed control/EST1027 ratios >2 with $p < 0.05$ from n = 3 biologically independent replicates. Shown in red is RNF126 C32. (b) Gel-based ABPP of EST1027 against RNF126. Recombinant RNF126 was

preincubated with DMSO vehicle or EST1027 for 30 min prior to labeling of RNF126 with IA-rhodamine (250 nM) for 1 h. Gels were visualized by in-gel fluorescence, and protein loading was assessed by silver staining. (c) RNF126 knockdown attenuates EST1027-mediated CDK4 degradation. RNF126 was stably knocked down in C33A cells using short hairpin oligonucleotides (shRNF126) compared to nontargeting shControl oligonucleotides. C33A shControl and shRNF126 cells were treated with DMSO vehicle or EST1027 (5 μM) for 24 h. CDK4, RNF126, and loading control vinculin levels were assessed by Western blotting. (d) Gel-based ABPP of EST1060 against RNF126 performed as described in (b). (e) Gel-based ABPP of covalent chemical handles against RNF126 performed as described in (b). (f) Structure of JP-2-196-alkyne probe. (g) JP-2-196-alkyne labeling of pure RNF126 protein. RNF126 was labeled with DMSO vehicle or JP-2-196-alkyne for 30 min. Probe-modified RNF126 was subjected to CuAAC with a rhodamine-functionalized azide handle and visualized by SDS/PAGE and in-gel fluorescence. (h) Competition of JP-2-196-alkyne labeling of RNF126 by JP-2-196. RNF126 pure protein was preincubated with JP-2-196 (50 μM) for 30 min at 37 °C prior to JP-2-196-alkyne labeling (50 μM) for 30 min at room temperature. Probe-modified RNF126 was subjected to CuAAC with a rhodamine-functionalized azide handle and visualized by SDS/PAGE and in-gel fluorescence. (i) JP-2-196-alkyne pulldown proteomics showing significant and moderately selective engagement of RNF126 and five additional E3 ubiquitin ligases LRSAM1, RNF40, MID2, RNF219, and RNF14. HEK293T cells were treated with DMSO vehicle or JP-2-196-alkyne (10 μM) for 6 h. Subsequent lysates were subjected to CuAAC with an azide-functionalized biotin handle, after which probe-modified proteins were avidin-enriched, eluted, and digested, and analyzed by TMT-based quantitative proteomics. Data shown are ratios of JP-2-196-alkyne vs DMSO-control-enriched proteins and p-values from n = 3 biologically independent replicates/group. Gels and blots from (b−e,g,h) are representative of n = 3 biologically independent replicates/group.

a

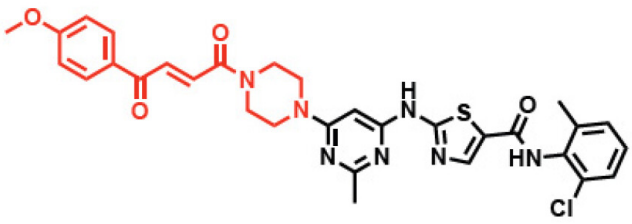

JP-2-227
BCR-ABL/c-ABL kinase degrader

b

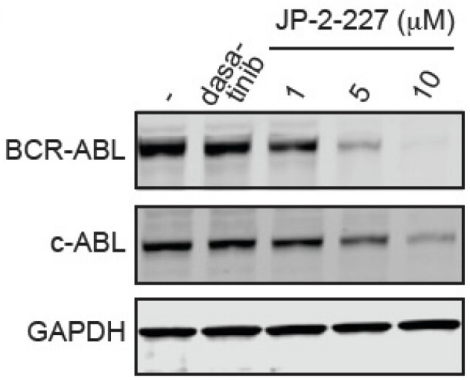

K562 leukemia cancer cells

c

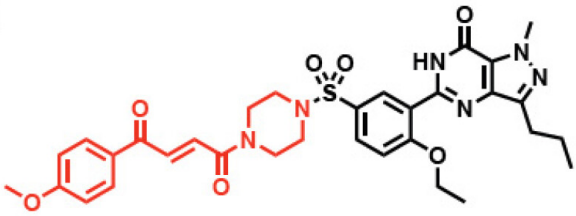

JP-2-201
PDE5 degrader

d

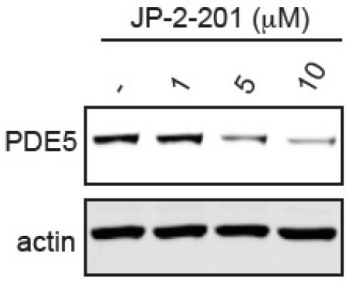

HEK293T cells

e

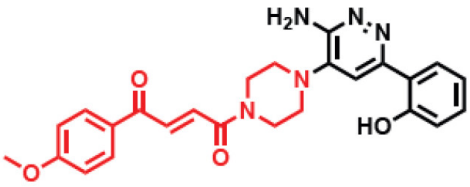

JP-2-249
SMARCA2 degrader

f

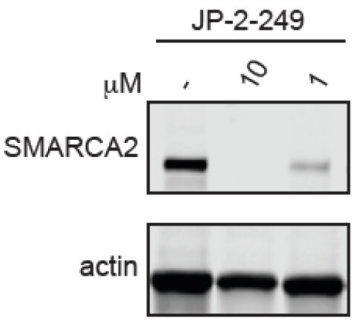

MV-4-11 leukemia cancer cells

g

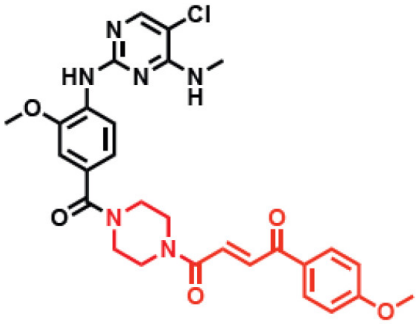

JP-2-244
LRRK2 degrader

h

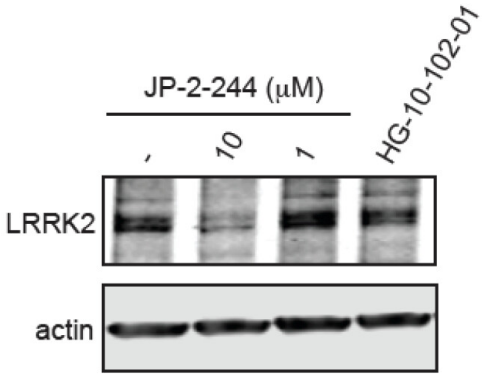

A549 lung cancer cells

Figure 2.4 Transplanting a covalent chemical handle onto protein-targeting ligands that already possess piperazines at the exit vector. (a) Structure of JP-2-227 with the optimized covalent handle shown in red that was appended onto the BCR-ABL and c-ABL kinase inhibitor dasatinib. (b) JP-2-227 degrades BCR-ABL and c-ABL in K562 leukemia cancer cells. K562 cells were treated with DMSO vehicle or JP-2-227 for 24 h, and BCR-ABL, c-ABL, and loading control GAPDH levels were assessed by Western blotting. (c) Structure of JP-2-201 with the optimized covalent handle shown in red that was appended onto the PDE5 inhibitor sildenafil. (d) JP-2-201 degrades PDE5 in HEK293T cells. HEK293T cells were treated with DMSO vehicle or JP-2-201 for 24 h, and PDE5 and loading control actin levels were assessed by Western blotting. (e) Structure of SMARCA2 degrader JP-2-249 consisting of the optimized covalent handle incorporated into a previously reported protein-targeting ligand for SMARCA2. (f) MV-4-11 leukemia cancer cells were treated with DMSO vehicle or JP-2-249 for 24 h, and SMARCA2 and actin loading control levels were assessed by Western blotting. (g) Structure of LRRK2 degrader JP-2-244 consisting of the optimized covalent handle incorporated into a previously reported LRRK2 inhibitor. (h) A549 lung cancer cells were treated with DMSO vehicle or JP-2-244 for 24 h, and LRRK2 and actin loading control levels were assessed by Western blotting. Blots in (b,d,f,h) are representative of n = 3 biologically independent replicates/group.

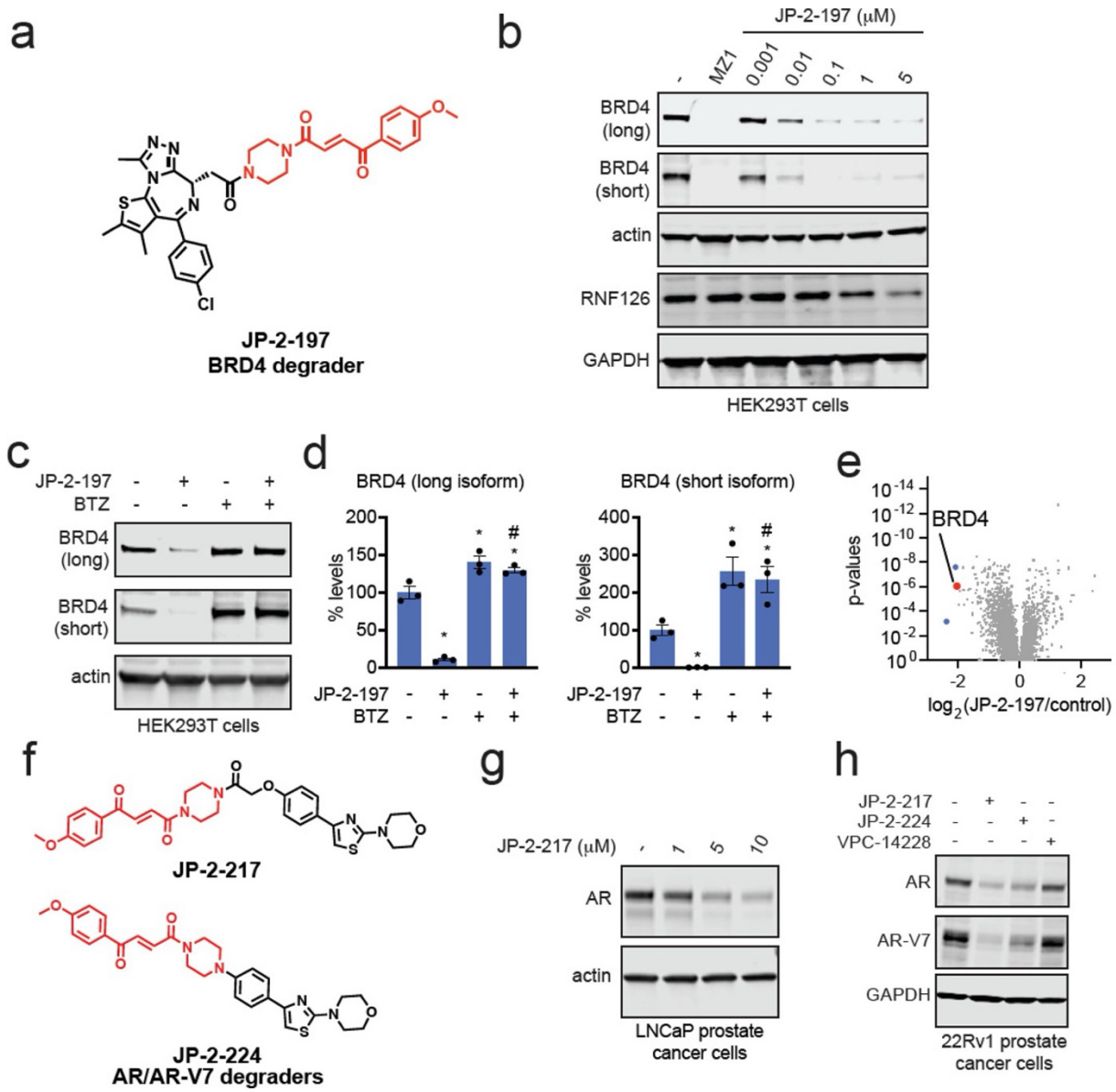

Figure 2.5 Transplanting a covalent chemical handle onto BET family inhibitor JQ1 and AR/AR-V7 targeting ligand to degrade BRD4 and AR/AR-V7. (a) Structure of JP-2-197 with the optimized covalent handle shown in red that was appended onto the BET family bromodomain inhibitor JQ1. (b) JP-2-197 degrades BRD4 in HEK293T cells. HEK293T cells were treated with DMSO vehicle, positive control BRD4 PROTAC MZ1 (1 μM), or JP-2-197 for 24 h. BRD4 long and short isoforms, RNF126, and loading controls actin and GAPDH levels were assessed by Western blotting. (c) Proteasome-dependent degradation of BRD4 by JP-2-197. HEK293T cells were pretreated with DMSO vehicle or the proteasome inhibitor BTZ (10 μM) for 1 h prior to treatment of cells with DMSO vehicle or JP-2-197 (1 μM), and BRD4 and loading control actin levels were assessed by Western blotting. (d) Quantification of the experiment described in (c). (e) TMT-based quantitative proteomic profiling of JP-2-197 in HEK293T cells. HEK293T cells were treated with

DMSO vehicle or JP-2-197 (1 μM) for 24 h. Data are from n = 2 biological replicates per group. (f) Structures of two AR-V7 degraders consisting of the fumarate handle linked to an AR DNA-binding domain ligand VPC-14228−JP-2-217 and JP-2-224. (g) LNCaP prostate cancer cells were treated with JP-2-217 for 24 h, and AR and loading control actin levels were detected by Western blotting. (h) 22Rv1 prostate cancer cells were treated with DMSO vehicle, JP-2-217, JP-2-224, or VPC-14228 (10 μM) for 24 h, and AR, AR-V7, and loading control GAPDH levels were assessed by Western blotting. Blots and gels shown in (b,c,g,h) are representative images from n = 3 biologically independent replicates. Bar graphs in (d) show individual replicate values and average ± sem. Statistical significance is calculated as *$p < 0.05$ compared to DMSO vehicle and #$p < 0.05$ compared to cells treated with JP-2-197 alone.

2.6 Methods

2.6.1 Cell Culture

C33A cells were purchased from the American Type Culture Collection (ATCC) and were cultured in Dulbecco's Modified Eagle Medium (DMEM) containing 10% (v/v) fetal bovine serum (FBS) and maintained at 37 °C with 5% CO_2. 22RV1 cells were purchased from the ATCC and were cultured in RPMI-1640 Medium containing 10% (v/v) FBS and maintained at 37 °C with 5% CO_2. HEK293T cells were obtained from the UC Berkeley Cell Culture Facility and were cultured in DMEM containing 10% (v/v) FBS and maintained at 37 °C with 5% CO_2. K562 cells were obtained from the UC Berkeley Cell Culture Facility and were cultured in Iscove's Modified Dulbecco's Medium (IMDM) containing 10% (v/v) FBS and maintained at 37 °C with 5% CO_2. MV-4-11 cells were obtained from the ATCC and were cultured in IMDM containing 10% (v/v) FBS and maintained at 37 °C with 5% CO_2. A549 cells were obtained from the ATCC and were cultured in F-12K Medium containing 10% (v/v) FBS and maintained at 37 °C with 5% CO_2. Mino cells were obtained from the ATCC and were cultured in RPMI-1640 Medium containing 10% (v/v) FBS and maintained at 37 °C with 5% CO_2. LNCaP cells were obtained from the UC Berkeley Cell Culture Facility and were cultured in RPMI-1640 Medium containing 10% (v/v) FBS and maintained at 37 °C with 5% CO_2. Unless otherwise specified, all cell culture materials were purchased from Gibco. It is not known whether HEK293T cells are from male or female origin.

2.6.2 Expression and Purification of Recombinant RNF126 Protein

RNF126 mammalian expression plasmid with a C-terminal FLAG tag was purchased from Origene (Origene Technologies Inc., RC204986). The plasmid was transformed into NEB 5-alpha Competent E. coli (DH5α) cells (NEB product no. C2987H). The following day, a single transformed colony was used to inoculate 50 mL of nutrient rich LB medium containing kanamycin (50 µg/mL) and was incubated at 37 °C overnight, with agitation (250 rpm). A Miniprep (Qiagen) kit was used to isolate the plasmid before sequence verification with appropriate primers.

HEK293T cells were grown to 30-50% confluency in DMEM supplemented with 10% FBS (Corning) and maintained at 37 °C with 5% CO_2. Immediately before transfection, media was replaced with DMEM containing 10% FBS. Each plate was transfected with 24 µg of overexpression plasmid with 24 µL Lipofectamine 2000 (Invitrogen) in Opti-MEM. After 48 h cells were collected in PBS, lysed by sonication, and batch bound with anti-DYKDDDDK resin (GenScript, L00432) for 2 hours. Lysate and resin were washed with PBS and eluted with 133.33 µg/mL 3X FLAG peptide (ApexBio, A6001) in PBS. Five elutions were performed for 15 minutes each. Elutions were concentrated and the protein was stored in PBS. Concentration and purity was determined using the BCA assay and Western blotting.

2.6.3 Preparation of Cell Lysates

Cells were washed twice with cold PBS, scraped, and pelleted by centrifugation (700 g, 5 min, 4 °C). Pellets were resuspended in PBS, lysed by sonication or RIPA lysis buffer (Thermo Scientific), clarified by centrifugation (12,000 g, 10 min, 4 °C), and lysate was transferred to new low-adhesion microcentrifuge tubes. Proteome concentrations

were determined using the BCA assay and lysate was diluted to appropriate working concentrations.

2.6.4 Western Blotting

Proteins were resolved by SDS/PAGE and transferred to nitrocellulose membranes using the Trans-Blot Turbo transfer system (Bio-Rad). Membranes were blocked with 5% BSA in Tris-buffered saline containing Tween 20 (TBS-T) solution for 1 h at RT, washed in TBS-T, and probed with primary antibody diluted in recommended diluent per manufacturer overnight at 4 °C. After 3 washes with TBS-T, the membranes were incubated in the dark with IR680- or IR800-conjugated secondary antibodies at 1:10,000 dilution in 5 % BSA in TBS-T at RT for 1 h. After 3 additional washes with TBST, blots were visualized using an Odyssey Li-Cor fluorescent scanner. The membranes were stripped using ReBlot Plus Strong Antibody Stripping Solution (EMD Millipore, 2504) when additional primary antibody incubations were performed. Antibodies used in this study were CDK4 (Abcam ab108357), CDK6 (Cell Signaling Technology DCS83), Vinculin (Abcam ab129002), GAPDH (Cell Signaling Technology 14C10), RNF126 (Santa Cruz Biotechnology sc-376005), BRD4 (Abcam ab128874), BRD2 (Cell Signaling Technology D89B4), BRD3 (Abcam ab300106), Beta Actin (Cell Signaling Technology 13E5), PDE5 (Abcam ab259945), AR-V7 (Abcam ab273500), c-Abl (Santa Cruz Biotechnology sc-23), SMARCA2 (Abcam ab240648), BRG1 (SMARCA4) (Cell Signaling Technology D1Q7F), LRRK2 (Abcam ab133474), BTK (Cell Signaling Technology D3H5), Androgen Receptor (Cell Signaling Technology D6F11), HDAC1 (Cell Signaling Technology 10E2), HDAC2 (Cell Signaling Technology 3F3), HDAC3 (Cell Signaling Technology 7G6C5), and HDAC6 (Cell Signaling Technology D2E5).

2.6.5 Knockdown Studies

Short-hairpin oligonucleotides were used to knock down the expression of RNF126 in C33A cells. For lentivirus production, lentiviral plasmids and packaging plasmids (pMD2.G, Addgene catalog no. 12259 and psPAX2, Addgene catalog no. 12260) were transfected into HEK293T cells using Lipofectamine 2000 (Invitrogen). Lentivirus was collected from filtered cultured medium and used to infect the target cell line with 1:1000 dilution of polybrene. Target cells were selected over 3 d with 1 µg/mL of puromycin for C33A cells. The short-hairpin sequences which were used for generation of the knockdown lines were:
RNF126: TGCCATCATCACACAGCTCCT (Sigma RNF126 MISSION shRNA Bacterial Glycerol Stock, TRCN0000368954). MISSION TRC1.5 pLKO.1- or TRC2 pLKO.5-puro Non-Mammalian shRNA Control (Sigma) was used as a control shRNA.

2.6.6 IsoDTB-ABPP Cysteine Chemoproteomic Profiling of EST1027

C33A cells were treated with either EST1027 (20 µM) or DMSO for 2 h before cell collection and lysis. The proteome concentrations were determined using BCA assay and adjusted to 2 mg/mL. For each biological replicate, 2 aliquots of 1 mL of 2 mg/mL were used (i.e. 4 mg per condition). Each aliquot was treated with 20 µL of IA-alkyne (26.6 mg/mL in DMSO, 200 µM final concentration) for 1 h at RT. Two master mixes of the click reagents were prepared in the meanwhile, each containing 510 µL TBTA (0.9 mg/mL in 4:1 tBuOH/DMSO), 165 µL $CuSO_4$ (12.5 mg/mL in H_2O), 165 µL TCEP (14.0 mg/mL in

H_2O) and 160 µL of either heavy or light isoDTB tags (4 mg in DMSO, Click Chemistry Tools, 1565). The samples were then treated with 120 µL of the heavy (DMSO treated) or light (compound treated) master mix for 1 h at RT. After incubation, one light and one heavy-labeled samples were combined and acetone-precipitated overnight at -20 °C. The samples were then centrifuged at 3,500 rpm for 10 min, acetone was removed, and the protein pellets resuspended in cold MeOH by sonication. The samples were centrifuged at 3,500 rpm for 10 min and MeOH was removed (repeated 3× in total). The pellets were dissolved in 600 µL urea (8 M in 0.1 M TEAB) by sonication and the urea concentration was then adjusted to 2 M by adding 1800 µL of TEAB (0.1 M). Two tubes containing solubilized proteins were combined, further diluted with 2400 µL 0.2% NP40 in PBS, and bound to high-capacity streptavidin agarose beads (200 µL/sample, ThermoFisher, 20357) for 1 h at RT with mixing. The beads were then centrifuged for 1 min at 1,000 g, the supernatant was removed, and the beads were washed 3 times with 0.1% NP40 in PBS, 3 times with PBS and 3 times with H_2O. The samples were then resuspended in 8 M urea (600 µL in 0.1 M TEAB) and treated with DTT (30 µL, 31 mg/mL in H_2O) for 45 min at 37 °C. They were then reacted with iodoacetamide (30 µL, 74 mg/mL in H_2O) for 30 min at RT, followed by DTT (30 µL, 31 mg/mL in H_2O) for 30 min at RT. The samples were diluted with 1800 µL TEAB (0.1 M), centrifuged for 1 min at 1,000 g, and the supernatant was removed. The beads were resuspended in 400 µL urea (2M in 0.1 M TEAB), and trypsin (8 µL, 0.5 mg/mL) was added and incubated for 20 h at 37 °C. The samples were then diluted with 800 µL 0.1% NP40 in PBS and the beads were washed 3 times with 0.1% NP40 in PBS, 3 times with PBS, and 3 times with H_2O. Peptides were then eluted with 0.1% formic acid in 50% acetonitrile (3 × 400 µL). The samples were then dried using a vacuum concentrator at 30 °C, resuspended in 300 µL 0.1% TFA in H_2O, and fractionated using high pH reversed-phase peptide fractionation kits (ThermoFisher, 84868) according to the manufacturer's protocol.

2.6.7 IsoDTB-ABPP Mass Spectrometry Analysis

Mass spectrometry analysis was performed on an Orbitrap Eclipse Tribrid Mass Spectrometer with a High Field Asymmetric Waveform Ion Mobility (FAIMS Pro) Interface (Thermo Scientific) with an UltiMate 3000 Nano Flow Rapid Separation LCnano System (Thermo Scientific). Off-line fractionated samples (5 µL aliquot of 15 µL sample) were injected via an autosampler (Thermo Scientific) onto a 5 µL sample loop which was subsequently eluted onto an Acclaim PepMap 100 C18 HPLC column (75 µm x 50 cm, nanoViper). Peptides were separated at a flow rate of 0.3 µL/min using the following gradient: 2% buffer B (100% acetonitrile with 0.1% formic acid) in buffer A (95:5 water:acetonitrile, 0.1% formic acid) for 5 min, followed by a gradient from 2 to 40% buffer B from 5 to 159 min, 40 to 95% buffer B from 159 to 160 minutes, holding at 95% B from 160 to 179 min, 95% to 2% buffer B from 179 to 180 min, and then 2% buffer B from 180 to 200 min. Voltage applied to the nano-LC electrospray ionization source was 2.1 kV. Data was acquired through an MS1 master scan (Orbitrap analysis, resolution 120,000, 400-1800 m/z, RF lens 30%, heated capillary temperature 250 °C) with dynamic exclusion enabled (repeat count 1, duration 60 s). Data-dependent data acquisition comprised a full MS1 scan followed by sequential MS2 scans based on 2 s cycle times. FAIMS compensation voltages (CV) of -35, -45, and -55 were applied. MS2 analysis consisted

of: quadrupole isolation window of 0.7 m/z of precursor ion followed by higher energy collision dissociation (HCD) energy of 38% with a orbitrap resolution of 50,000.

Data were extracted in the form of MS1 and MS2 files using Raw Converter (Scripps Research Institute) and searched against the Uniprot human database using ProLuCID search methodology in IP2 v.3-v.5 (Integrated Proteomics Applications, Inc.).[1] Cysteine residues were searched with a static modification for carboxyaminomethylation (+57.02146) and up to two differential modifications for methionine oxidation and either the light or heavy isoDTB tags (+561.33872 or +567.34621, respectively). Peptides were required to be fully tryptic peptides. ProLuCID data were filtered through DTASelect to achieve a peptide false-positive rate below 5%. Only those probe-modified peptides that were evident across two out of three biological replicates were interpreted for their isotopic light to heavy ratios. Light versus heavy isotopic probe-modified peptide ratios are calculated by taking the mean of the ratios of each replicate paired light versus heavy precursor abundance for all peptide-spectral matches associated with a peptide. The paired abundances were also used to calculate a paired sample t-test P value in an effort to estimate constancy in paired abundances and significance in change between treatment and control. P values were corrected using the Benjamini–Hochberg method.

2.6.8 Gel-Based ABPP

Recombinant RNF126 (0.1 µg/sample) was pre-treated with either DMSO vehicle or covalent ligand at 37 ^{o}C for 30 min in 25 µL of PBS, and subsequently treated with of IA-Rhodamine (concentrations designated in figure legends) (Setareh Biotech) at room temperature for 1 h in the dark. The reaction was stopped by addition of 4×reducing Laemmli SDS sample loading buffer (Alfa Aesar). After boiling at 95 ^{o}C for 5 min, the samples were separated on precast 4−20% Criterion TGX gels (Bio-Rad). Probe-labeled proteins were analyzed by in-gel fluorescence using a ChemiDoc MP (Bio-Rad).

2.6.9 NMR Spectroscopy

We recorded all NMR spectra on Bruker Avance III 600 MHz (using 3 mm tubes filled with 160 µL sample) and Bruker Neo 600 MHz (using 1.7 mm tubes filled with 40 µL of sample) spectrometers, equipped with either a 5 mm QCI-F cryo probe with z-gradient or a 1.7 mm TCI cryo probe, and kept the temperature constant at 298K during our experiments. Standard Bruker ^{1}H-1D (with excitation sculpting water suppression) and ^{1}H,^{15}N-SOFAST-HMQC experiments were conducted while using traditional or 50% non-uniform sampling.[2] Our samples contained 50 µM or 100 µM human wt-(U}-^{15}N-RNF126(1-40), unlabeled 50 µM BRD4(44-168) (for protein-protein binding experiments only), 5% (3 mm tubes) or 10% (1.7 mm tubes) D_2O, 25 mM Hepes pH 7.5, 150 mM NaCl, 11.1 µM DSS, 2% d_6-DMSO, 0-50 µM d-TCEP, and 100 µM or 200 µM of compounds (for samples with compound; DMSO-matched). All spectra were recorded at two time points (incubation times of 30 min and 24 h) to detect time-dependent ligand binding effects.

We assigned most peaks by transferring the published resonance assignments onto our amide spectrum.[3] To localize the ligand-interaction site, we clustered compound-induced chemical shift perturbations and line broadening effects in groups with very strong, strong, medium, weak and no residue-specific spectral changes. Clusters were

subsequently mapped onto the three-dimensional structure of RNF126(1-40) (PDB code: 2N9O).[3]

2.6.10 Protein Expression for NMR Studies

Plasmid construct 8xHis-Thioredoxin-TEV-RNF126(1-40) was transformed into BL21(DE3) competent cells and grown overnight on LB-agar plates. A single colony was used to inoculate a 3 mL LB + kanamycin starter culture, which was grown shaking at 37 °C for 4-6 h. For each liter of culture, 50 mL of expression media (per liter: 50 mL 20X M9 salts dissolved in sterile water, 2 mM $MgSO_4$, 1 mL vitamin solution [Sigma R7256], 0.1 mL 1000X trace elements [made in-house], 1 g ^{15}N-NH_4Cl, 3 g glucose, 50 mg kanamycin, 0.05 mM $ZnCl_2$, 0.25 g ISOGRO-^{15}N [Sigma 606871], sterile water to volume) was inoculated with 0.5 mL of the starter culture and grown overnight shaking at 37 °C. The 50 mL culture was used to inoculate 950 mL of expression media until the OD_{600} reached 0.7-0.8, at which point the culture was induced with 0.5 mM IPTG and the temperature reduced to 18 °C. The culture was grown overnight (~18 h) and harvested via centrifugation. Pellets were stored at -80 °C.

A pET vector containing 6xHis-TEV-BRD4(44-168) was used to transform BL21(DE3) E. coli using standard techniques. 1 L cultures were grown in Terrific Broth supplemented with 50 mM Sodium Phosphate pH 7.0 and 50 µg/mL kanamycin. Cells were induced when the OD_{600} reached 1.0-1.5 and were left to continue to grow overnight at 19 °C. Cells were harvested by centrifugation and lysed via cell homogenizer (Lysis Buffer: 50 mM Tris pH 8.0, 400 mM NaCl, 1 mM TCEP).

2.6.11 Protein Purification for NMR Studies

RNF126(1-40) cell pellets were thawed and resuspended in cold lysis buffer (20 mM HEPES, pH 8.0, 500 mM NaCl, 30 mM Imidazole) at a ratio of 1 g cells to 5 mL buffer. Cells were disrupted via sonication and separated from the supernatant via centrifugation. 1 mL of loose Ni Sepharose 6 Fast Flow resin per 50 mL of supernatant was washed three times in lysis buffer, then incubated with the supernatant for 2-3 h, rotating at 4 °C. The slurry was washed with lysis buffer in a drip column until the flow-though no longer contained protein (measured via NanoDrop). The protein was eluted in 10 x 4 mL steps with the imidazole concentration increasing by 30 mM each step. Cleavage with TEV protease was performed via overnight dialysis in a 1000 MWCO dialysis cassette against dialysis buffer (20 mM HEPES, pH 8.0, 500 mM NaCl) spinning at 4 °C. The protein solution was run through a HisTrap FF 5 mL on AKTA to separate the tag. 0.05 mM $ZnCl_2$ was added to the eluate which was concentrated using an Amicon 1K centrifugal filter. The sample was run on a Superdex 30 size exclusion column with SEC buffer (20 mM HEPES, pH 7.5, 150 mM NaCl). Protein yield was estimated to be between 0.5 and ~1 mg/L according to a NanoDrop readout.

BRD4 cell lysate was clarified via centrifugation (45,000 g for 30 min) prior to IMAC purification using 5 mL Ni-NTA bulk resin pre-equilibrated with Lysis Buffer. The resin was then washed with 5 CV of Lysis Buffer followed by Lysis Buffer supplemented with increasing concentrations of imidazole (20 mM and 40 mM). The protein was eluted with 5 CV of Elution Buffer (50 mM Tris pH 8.0, 400 mM NaCl, 1 mM TCEP, 500 mM imidazole) and subsequently treated with TEV protease while dialyzing against 3 L of Lysis Buffer at 4 °C overnight. Cleaved protein was subject to reverse IMAC purification with 5 mL of Ni-

NTA bulk resin pre-equilibrated with Lysis Buffer. The flow-through was collected, concentrated, and subjected to size exclusion chromatography using a Superdex 200 16/60 column attached to an AKTA FPLC. The column was pre-equilibrated with SEC Buffer (25 mM HEPES pH 7.5, 150 mM NaCl, 1 mM TCEP). Fractions containing protein were pooled, concentrated, and aliquoted. Correct mass was confirmed by ESI-LC/MS and purity was confirmed by SDS-PAGE.

2.6.12 JP-2-196-Alkyne Pulldown Quantitative Proteomics

Cells were treated with either DMSO vehicle or compound (JP-2-196-alkyne, 10 μM) for 6 h. Cells were harvested and lysed by probe sonication in PBS. The proteome concentrations were determined using the BCA assay and adjusted to 5 mg/mL in a volume of 500 μL PBS. For each biological replicate, 4 aliquots were used (i.e. 10 mg per condition). Copper-catalyzed azide-alkyne cycloaddition (CuAAC) was performed by sequential addition of 10 μL TCEP (14.4 mg/mL in H_2O), 30 μL TBTA (0.9 mg/mL in 4:1 tBuOH/DMSO), 10 μL $CuSO_4$ (12.5 mg/mL in H_2O) and 10 μL biotin picolyl azide (10 mM in DMSO). After 1 h, proteomes were precipitated by centrifugation at 6,500 g, washed in ice-cold methanol, combined to attain 10 mg per sample, washed again, then denatured and resolubilized by heating in 1.2% SDS–PBS (1 mL) to 90 °C for 5 min. The soluble proteome was diluted with 4 mL of PBS and labeled proteins were bound to high-capacity streptavidin-agarose beads (170 μL/sample, Thermo Fisher Scientific, 20357) while rotating overnight at 4 °C. Bead-linked proteins were enriched by washing once with 0.2% SDS-PBS and 3 times each in PBS and water, then resuspended in 6 M urea/PBS (500 μL), reduced in DTT (25 μL, 30 mg/mL in H_2O), and alkylated with iodoacetamide (74 mg/mL in H_2O), before being washed and resuspended in 50 mM Triethylammonium bicarbonate (TEAB) (100 μL) and trypsinized overnight with sequencing grade trypsin (4 μL, 0.5 mg/mL). Tryptic peptides were eluted off through centrifugation. Individual samples were then labeled with isobaric tags using commercially available TMTsixplex (Thermo Fisher Scientific, P/N 90061) kits, in accordance with the manufacturer's protocols. Tagged samples (20 μg per sample) were combined, dried using a vacuum concentrator at 30 °C, resuspended with 300 μL 0.1% TFA in H_2O, and fractionated using high pH reversed-phase peptide fractionation kits (Thermo Fisher Scientific, P/N 84868) according to the manufacturer's protocol. Fractions were dried with using a vacuum concentrator at 30 °C, resuspended with 50 μL 0.1% FA in H_2O, and analyzed by LC-MS/MS as described below.

Quantitative TMT-based proteomic analysis was performed as previously described using a Thermo Eclipse with FAIMS LC-MS/MS.[4] Acquired MS data was processed using ProLuCID search methodology in IP2 v.3-v.5 (Integrated Proteomics Applications, Inc.).[1] Trypsin cleavage specificity (cleavage at K, R except if followed by P) allowed for up to 2 missed cleavages. Carbamidomethylation of cysteine was set as a fixed modification, methionine oxidation, and TMT-modification of N-termini and lysine residues were set as variable modifications. Reporter ion ratio calculations were performed using summed abundances with most confident centroid selected from 20 ppm window. Only peptide-to-spectrum matches that are unique assignments to a given identified protein within the total dataset are considered for protein quantitation. High confidence protein identifications were reported with a <1% false discovery rate (FDR)

cut-off. Differential abundance significance was estimated using ANOVA with Benjamini-Hochberg correction to determine p-values.

2.6.13 Quantitative TMT Proteomics Analysis

Cells were treated with either DMSO vehicle or compound (EST1027, 5 μM, or JP-2-197, 1 μM) for 24 h and lysate was prepared as described above. Briefly, 25-100 μg protein from each sample was reduced, alkylated and tryptically digested overnight. Individual samples were then labeled with isobaric tags using commercially available TMTsixplex (Thermo Fisher Scientific, P/N 90061) kits, in accordance with the the manufacturer's protocols. Tagged samples (20 μg per sample) were combined, dried using a vacuum concentrator at 30 °C, resuspended with 300 μL 0.1% TFA in H_2O, and fractionated using high pH reversed-phase peptide fractionation kits (Thermo Fisher Scientific, P/N 84868) according to the manufacturer's protocol. Fractions were dried using a vacuum concentrator at 30 °C, resuspended with 50 μL 0.1% FA in H_2O, and analyzed by LC-MS/MS as described below.

Quantitative TMT-based proteomic analysis was performed as previously described using a Thermo Eclipse with FAIMS LC-MS/MS.[4] Acquired MS data was processed using ProLuCID search methodology in IP2 v.3-v.5 (Integrated Proteomics Applications, Inc.).[1] Trypsin cleavage specificity (cleavage at K, R except if followed by P) allowed for up to 2 missed cleavages. Carbamidomethylation of cysteine was set as a fixed modification, methionine oxidation, and TMT-modification of N-termini and lysine residues were set as variable modifications. Reporter ion ratio calculations were performed using summed abundances with most confident centroid selected from 20 ppm window. Only peptide-to-spectrum matches that are unique assignments to a given identified protein within the total dataset are considered for protein quantitation. High confidence protein identifications were reported with a <1% false discovery rate (FDR) cut-off. Differential abundance significance was estimated using ANOVA with Benjamini-Hochberg correction to determine p-values.

CONCLUDING REMARKS

The study covered in this dissertation illustrates the potential in using minimal covalent chemical handles to convert protein-targeting ligands into molecular glue degraders to induce the degradation of their respective protein targets. Discoveries of molecular glue degraders made prior to this study had occurred through serendipitous means, such as phenotypic screening. There have been one-off, independent examples of monovalent degraders being discovered through small structural changes to protein-binding ligands, but these findings were also non-intentional. This work showcases a first-in-class, transplantable covalent moiety, a fumarate-based chemical handle, that can convert protein-targeting ligands into monovalent molecular glue degraders across a wide array of chemical and protein classes. This handle also serves as the first reported RNF126 recruiter for novel glue degrader design. Through the appending of this moiety to various FDA approved inhibitors and protein-binding ligands, we have been able to degrade proteins from multiple classes from kinases, phosphodiesterases, deacetylases, and transcription factors. Using this covalent handle, a more systematic and modular synthesis of monovalent degraders can now be achieved.

This work serves as the first “rule” that could be used in rationally designing molecular glue degraders and signifies a potential future where monovalent degraders are not just discovered serendipitously, but purposefully and systematically designed. However, this is likely only the tip of the iceberg, the first step in elucidating a larger list of principles in guiding the synthesis of monovalent degraders. I expect many additional covalent handles to be discovered that confer molecular glue degrader properties to the ligands they are appended to, as several groups have already showcased.[21,22,42] As the covalent handle identified in this study is quite robust wherein it is able to induce the degradation of a host of different protein targets through recruitment of RNF126, we will inevitably find a target that it is unable to degrade. Therefore, the discovery and development of additional chemical moieties that can be used in novel glue degrader synthesis becomes extremely important to further advance the scope of targeted protein degradation. Regardless, the covalent handle discussed in this dissertation has shown wonderful utility in degrading a diverse set of protein targets, and overall demonstrates that the rational design of molecular glue degraders is not only possible but offers great therapeutic promise.

References

1. Bond, M. J.; Crews, C. M. Proteolysis targeting chimeras (PROTACs) come of age: entering the third decade of targeted protein degradation. RSC Chem. Biol. 2021, 2, 725−742.
2. Hughes, S. J.; Ciulli, A. Molecular recognition of ternary complexes: a new dimension in the structure-guided design of chemical degraders. Essays Biochem. 2017, 61, 505−516.
3. Schreiber, S. L. The Rise of Molecular Glues. Cell 2021, 184, 3− 9.
4. Burslem, G. M.; Crews, C. M. Small-Molecule Modulation of Protein Homeostasis. Chem. Rev. 2017, 117, 11269−11301.
5. Chamberlain, P. P.; Hamann, L. G. Development of targeted protein degradation therapeutics. Nat. Chem. Biol. 2019, 15, 937−944.
6. Chamberlain, P. P.; et al. Structure of the human Cereblon-DDB1-lenalidomide complex reveals basis for responsiveness to thalidomide analogs. Nat. Struct. Mol. Biol. 2014, 21, 803−809. doi:10.1007/82_2018_121.
7. Donovan, K. A. Thalidomide promotes degradation of SALL4, a transcription factor implicated in Duane Radial Ray Syndrome. eLife 2018, 7, e38430.
8. Mayor-Ruiz, C.; et al. Rational discovery of molecular glue degraders via scalable chemical profiling. Nat. Chem. Biol. 2020, 16, 1199−1207.
9. Powell, C. E.; et al. Selective Degradation of GSPT1 by Cereblon Modulators Identified via a Focused Combinatorial Library. ACS Chem. Biol. 2020, 15, 2722−2730.
10. Nishiguchi, G.; et al. Identification of Potent, Selective, and Orally Bioavailable Small-Molecule GSPT1/2 Degraders from a Focused Library of Cereblon Modulators. J. Med. Chem. 2021, 64, 7296−7311.
11. Scholes, N. S.; Mayor-Ruiz, C.; Winter, G. E. Identification and selectivity profiling of small-molecule degraders via multi-omics approaches. Cell Chem. Biol. 2021, 28, 1048−1060.
12. Ito, T.; et al. Identification of a primary target of thalidomide teratogenicity. Science 2010, 327, 1345−1350.
13. Matyskiela, M. E.; et al. SALL4 mediates teratogenicity as a thalidomide-dependent cereblon substrate. Nat. Chem. Biol. 2018, 14, 981−987.
14. Lu, G.; et al. The myeloma drug lenalidomide promotes the cereblon-dependent destruction of Ikaros proteins. Science 2014, 343, 305−309.
15. Mayor-Ruiz, C.; et al. Rational discovery of molecular glue degraders via scalable chemical profiling. Nat. Chem. Biol. 2020, 16, 1199−1207.
16. King, E. A.; et al. Chemoproteomics-Enabled Discovery of a Covalent Molecular Glue Degrader Targeting NF-κB. Cell Chem. Biol. 2023, 30 (4), 394-402.
17. Słabicki, M.; et al. The CDK inhibitor CR8 acts as a molecular glue degrader that depletes cyclin K. Nature 2020, 585, 293−297.
18. Słabicki, M.; et al. Small-molecule-induced polymerization triggers degradation of BCL6. Nature 2020, 588, 164−168.
19. Petretich, M.; Demont, E. H.; Grandi, P. Domain-selective targeting of BET proteins in cancer and immunological diseases. Curr. Opin. Chem. Biol. 2020, 57, 184−193.

20. Shergalis, A. G.; et al. CRISPR Screen Reveals BRD2/4 Molecular Glue-like Degrader via Recruitment of DCAF16. ACS Chem. Biol. 2023, 18, 331−339.
21. Hsia, O.; et al. Targeted protein degradation via intramolecular bivalent glues. Nature 2024, 627, 204-211.
22. Li, Y.-D.; et al. Template-assisted covalent modification of DCAF16 underlies activity of BRD4 molecular glue degraders. bioRxiv 2023.02.14.528208. Preprint at DOI: 10.1101/2023.02.14.528208.
23. Poratti, M.; Marzaro, G. Third-generation CDK inhibitors: A review on the synthesis and binding modes of Palbociclib, Ribociclib and Abemaciclib. Eur. J. Med. Chem. 2019, 172, 143−153.
24. Zanon, P. R. A.; Lewald, L.; Hacker, S. M. Isotopically Labeled Desthiobiotin Azide (isoDTB) Tags Enable Global Profiling of the Bacterial Cysteinome. Angew. Chem., Int. Ed. 2020, 59, 2829−2836.
25. Weerapana, E.; et al. Quantitative reactivity profiling predicts functional cysteines in proteomes. Nature 2010, 468, 790−795.
26. Backus, K. M.; et al. Proteome-wide covalent ligand discovery in native biological systems. Nature 2016, 534, 570−574.
27. Spradlin, J. N.; et al. Harnessing the anti-cancer natural product nimbolide for targeted protein degradation. Nat. Chem. Biol. 2019, 15, 747−755.
28. Spradlin, J. N.; Zhang, E.; Nomura, D. K. Reimagining Druggability Using Chemoproteomic Platforms. Acc. Chem. Res. 2021, 54, 1801−1813.
29. Krysztofinska, E. M.; et al. Structural and functional insights into the E3 ligase, RNF126. Sci. Rep. 2016, 6, 26433.
30. Rodrigo-Brenni, M. C.; Gutierrez, E.; Hegde, R. S. Cytosolic quality control of mislocalized proteins requires RNF126 recruitment to Bag6. Mol. Cell 2014, 55, 227−237.
31. Hu, X.; et al. RNF126-Mediated Reubiquitination Is Required for Proteasomal Degradation of p97-Extracted Membrane Proteins. Mol. Cell 2020, 79, 320−331.e9.
32. Farnaby, W.; et al. BAF complex vulnerabilities in cancer demonstrated via structure-based PROTAC design. Nat. Chem. Biol. 2019, 15, 672−680.
33. Filippakopoulos, P.; et al. Selective inhibition of BET bromodomains. Nature 2010, 468, 1067−1073.
34. Ward, C. C.; et al. Covalent Ligand Screening Uncovers a RNF4 E3 Ligase Recruiter for Targeted Protein Degradation Applications. ACS Chem. Biol. 2019, 14, 2430−2440.
35. Zengerle, M.; Chan, K.-H.; Ciulli, A. Selective Small Molecule Induced Degradation of the BET Bromodomain Protein BRD4. ACS Chem. Biol. 2015, 10, 1770−1777.
36. Henning, N. J.; et al. Discovery of a Covalent FEM1B Recruiter for Targeted Protein Degradation Applications. J. Am. Chem. Soc. 2022, 144, 701−708.
37. Uo, T.; Plymate, S. R.; Sprenger, C. C. The potential of AR-V7 as a therapeutic target. Expert Opin. Ther. Targets 2018, 22, 201−216.
38. Dalal, K.; et al. Selectively targeting the DNA-binding domain of the androgen receptor as a prospective therapy for prostate cancer. J. Biol. Chem. 2014, 289, 26417−26429.

39. Lee, G. T.; et al. Effects of MTX-23, a Novel PROTAC of Androgen Receptor Splice Variant-7 and Androgen Receptor, on CRPC Resistant to Second-Line Antiandrogen Therapy. Mol. Cancer Ther. 2021, 20, 490−499.
40. Bhumireddy, A.; et al. Design, synthesis, and biological evaluation of phenyl thiazole-based AR-V7 degraders. Bioorg. Med. Chem. Lett. 2022, 55, 128448.
41. Toriki, E. S. et al. Rational Chemical Design of Molecular Glue Degraders. ACS Cent. Sci. 2023, 9, 915-926.
42. Lim, M. et al. DCAF16-Based Covalent Handle for the Rational Design of Monovalent Degraders. bioRxiv 2024. 2024.02.20.580683. Preprint at DOI: 10.1101/2024.02.20.580683.

APPENDICES

Supplementary Figures

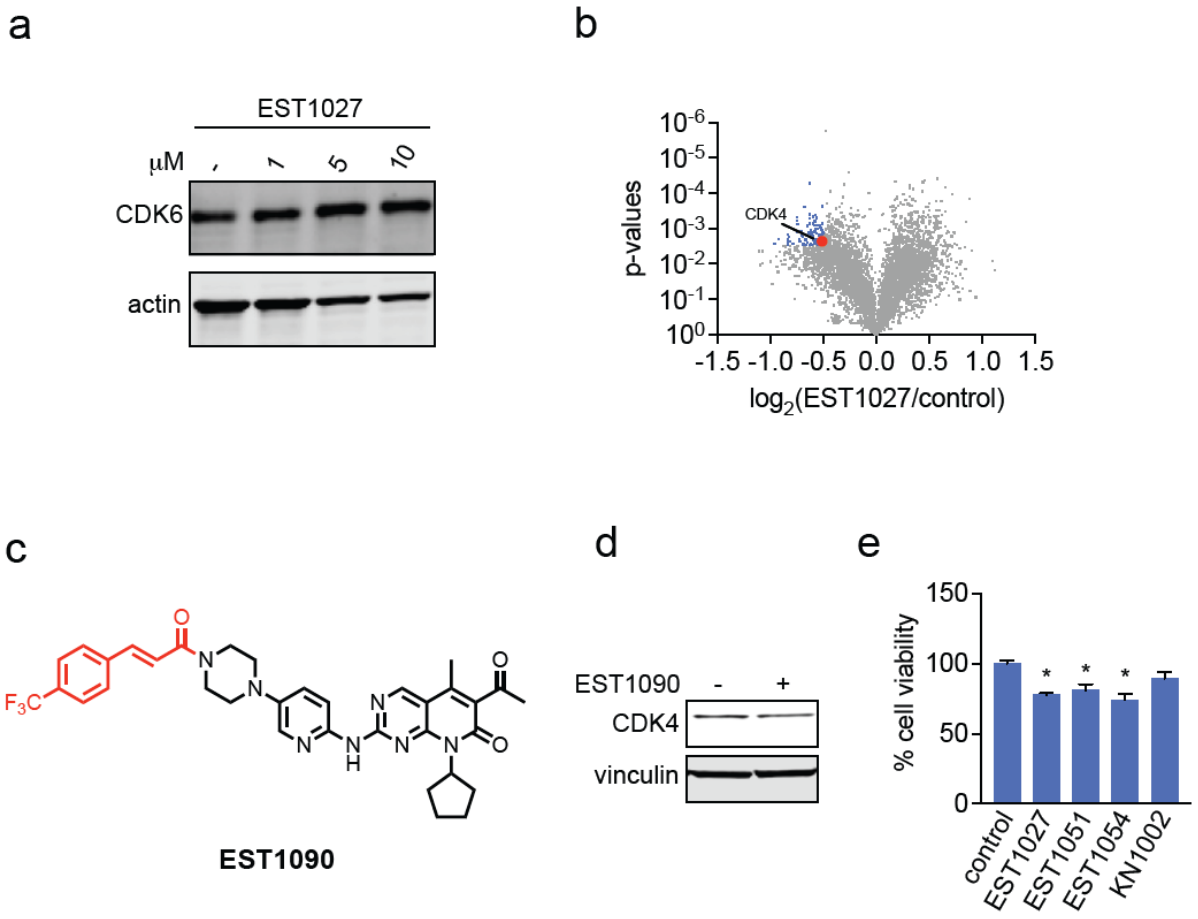

Figure S1. Palbociclib derivatives and their ability to degrade CDK4 and CDK6. (a) CDK6 levels in C33A cells. C33A cells were treated with DMSO vehicle or EST1027 for 24 h and CDK6 and loading control actin levels were detected by Western blotting. (b) TMT-based quantitative proteomic profiling of EST1027 in C33A cells. C33A cells were treated with DMSO vehicle or EST1027 (5 μM) for 24 h and cell lysates were subjected to TMT-based proteomic analyses. Shown are average EST1027/control TMT protein level ratios with points in blue or red noting proteins that showed ratios <0.7 and $p < 0.003$ from n = 3 biologically independent replicates/group. Shown in red is CDK4. (c) Structure of EST1090 with the trifluoromethyl propenamide handle linked to the CDK4/6 inhibitor Palbociclib. (d) CDK4 levels in C33A cells. C33A cells were treated with DMSO vehicle or EST1090 (10 μM) for 24 h and CDK4 and loading control vinculin levels were detected by Western blotting. (e) Cell viability assessed by Cell Titer Glo in C33A cells treated with DMSO vehicle or compounds (5 μM) for 24 h. Gels and blots in (a,d) are representative of n = 3 biologically independent replicates/group. Bar graph in (e) show average ± sem. Statistical significance in (e) is calculated as *$p < 0.05$ compared to DMSO vehicle.

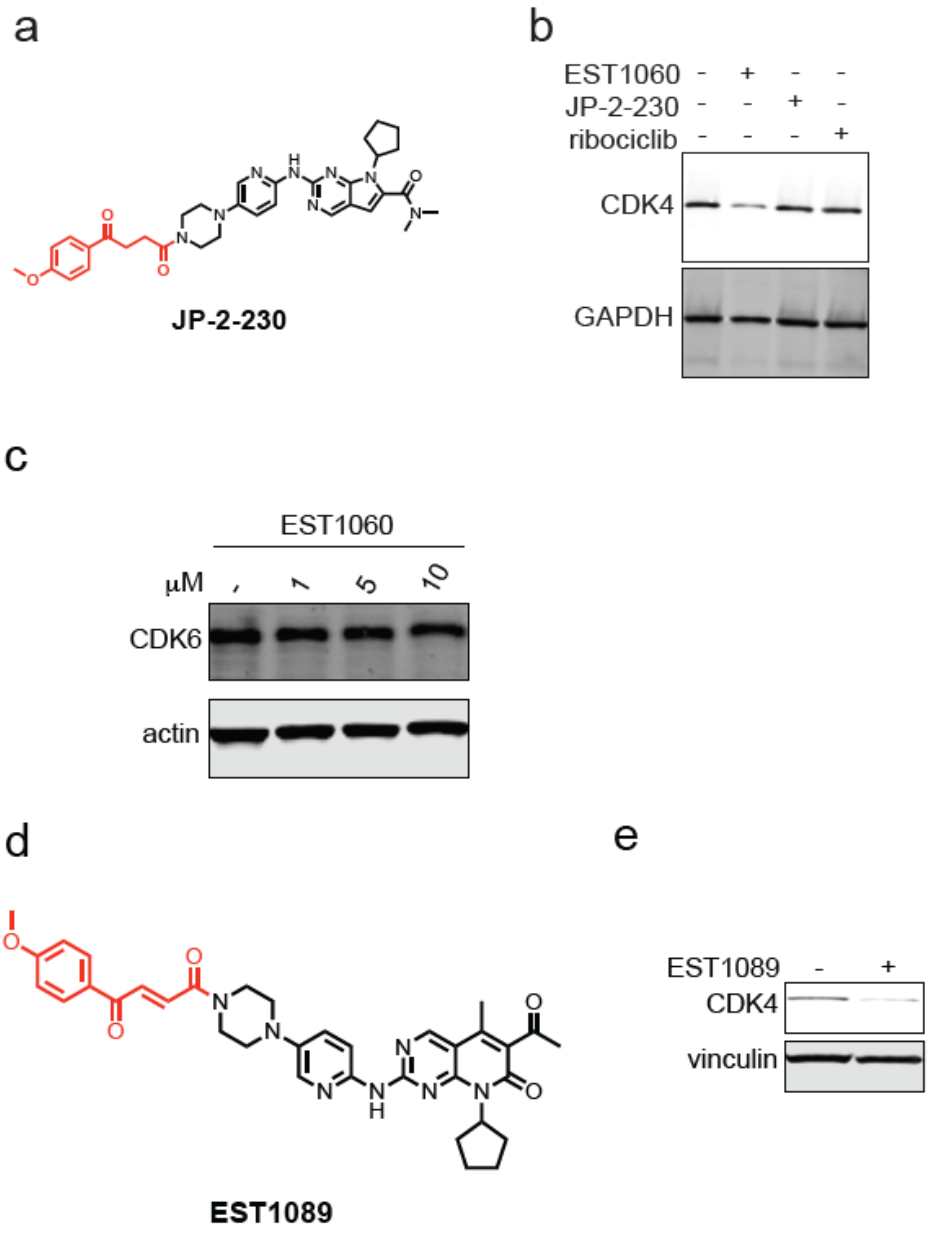

Figure S2. Ribociclib and palbociclib derivatives and their ability to degrade CDK4 and CDK6. (a) Structure of JP-2-230 with non-reactive handle linked to the CDK4/6 inhibitor ribociclib. (b) CDK4 levels in C33A cells. C33A cells were treated with DMSO vehicle, EST1060, or JP-2-230 (10 μM) for 24 h and CDK4 and loading control GAPDH levels were detected by Western blotting. (c) CDK6 levels in C33A cells. C33A cells were treated with DMSO vehicle or EST1060 for 24 h and CDK6 and loading control actin levels were assessed by Western blotting. (d) Structure of EST1089 with fumarate handle linked to the CDK4/6 inhibitor Palbociclib. (e) CDK4 levels in C33A cells. C33A cells were treated with DMSO vehicle or EST1089 (10 μM) for 24 h and CDK4 and loading control vinculin

levels were detected by Western blotting. Gels and blots in (b,c,e) are representative of n = 3 biologically independent replicates/group.

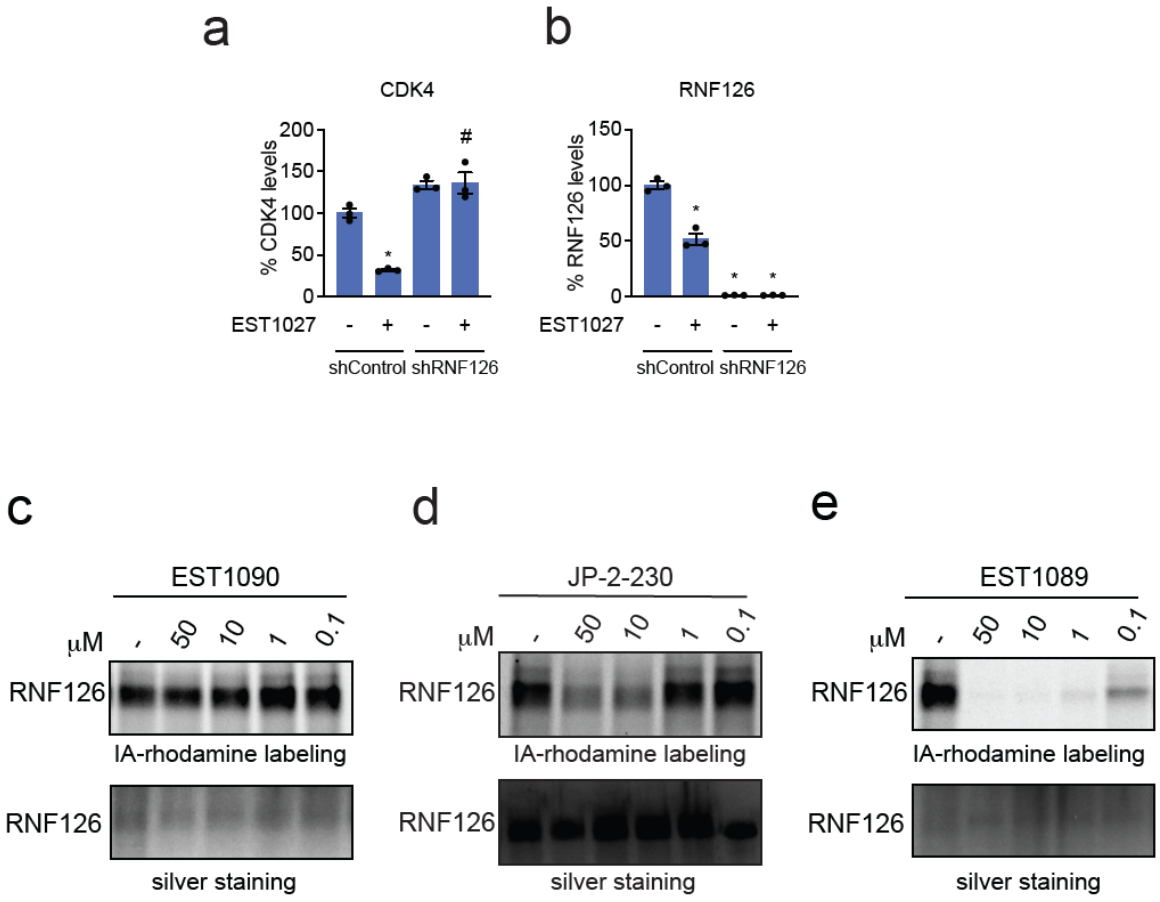

Figure S3. Characterization of CDK4 degraders. (a, b) Quantification of experiment described in Figure 2.3c. (c, d, e) Gel-based ABPP of EST1090, JP-2-230, EST1089 against RNF126. Recombinant RNF126 was pre-incubated with DMSO vehicle or compounds for 30 min prior to labeling of RNF126 with IA-rhodamine (250 nM) for 1 h. Gels were visualized by in-gel fluorescence and protein loading was assessed by silver staining. Shown are representative gels from n = 3 biologically independent replicates/group. Bar graphs in (a,b) show individual replicate values and average ± sem. Statistical significance in (a,b) is calculated as *p < 0.05 compared to DMSO vehicle and #p < 0.05 compared to EST1027-treated group.

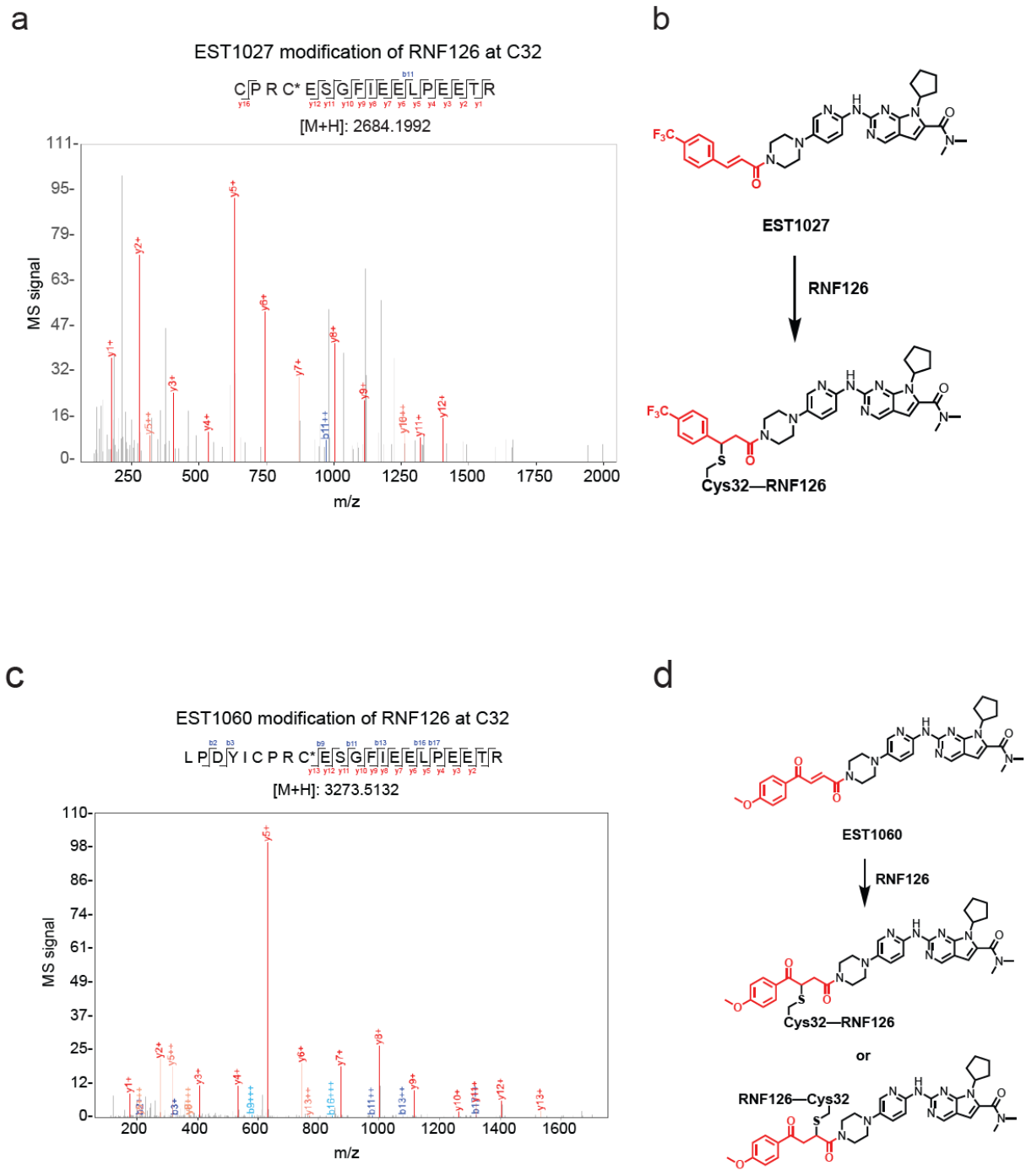

Figure S4. Site of modification analysis of EST1027 and EST1060 with pure RNF126 protein. RNF126 protein (24 µg) was incubated with EST1027 (a, b) or EST1060 (c, d) (50 µM) for 30 min and tryptic digests were analyzed by LC-MS/MS. (b, d) Structure of presumed adduct of EST1027 and EST1060 with C32 of RNF126.

a

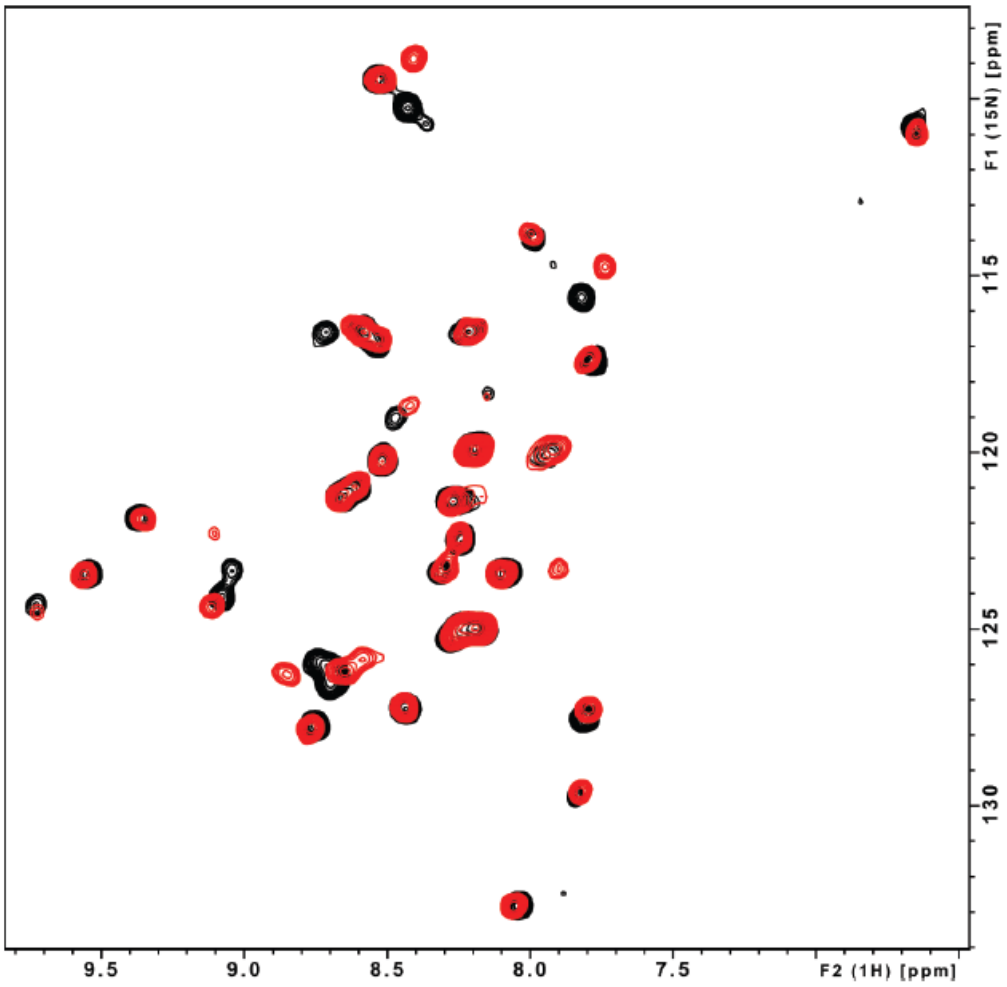
F1 (15N) [ppm]
115
120
125
130
9.5
9.0
8.5
8.0
7.5
F2 (1H) [ppm]

b

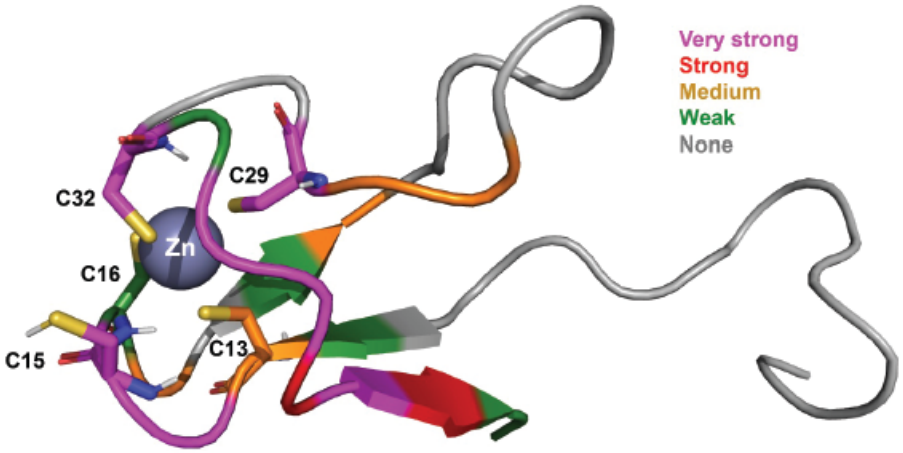
Very strong
Strong
Medium
Weak
None
C29
C32
Zn
C16
C13
C15

Figure S5. Fumarate binding to RNF126(1-40) is specific and does not lead to protein unfolding or aggregation. (a) Overlay of two ^{1}H, ^{15}N-HMQC spectra, with peaks shown in black corresponding to ~75 µM of apo-RNF126 and signals in red representing protein amide groups in the presence of 200 µM of JP-2-196. The compound-induced, peak-dependent chemical shift perturbations are proof of specific binding of the small molecule to RNF126. Overall protein signal intensities and the spectral dispersion are unchanged upon compound addition, indicating that the ligand interactions do not lead to protein unfolding or aggregation. (b) Three-dimensional structure of RNF126(1-40) with color-coded mapping of chemical shift perturbations and residue-specific line broadening. The ligand binds at or close to the zinc ("Zn") coordination site while the other areas of RNF126(1-40) remain unchanged.

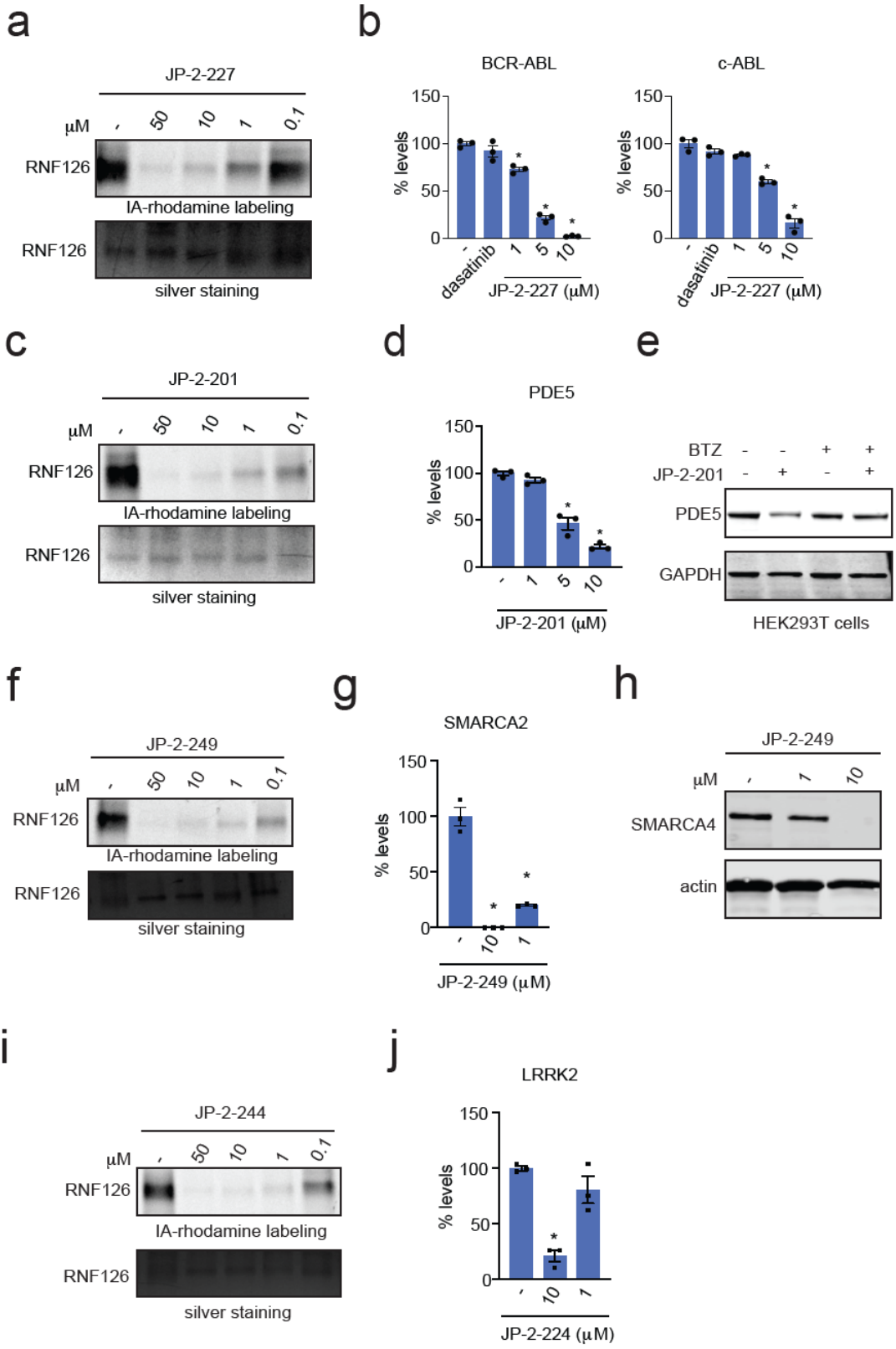
a
JP-2-227
μM
-
50
10
1
0.1
RNF126
IA-rhodamine labeling
RNF126
silver staining
b
BCR-ABL
c-ABL
% levels
150
100
50
0
-
dasatinib
1
5
10
JP-2-227 (μM)
c
JP-2-201
μM
-
50
10
1
0.1
RNF126
IA-rhodamine labeling
RNF126
silver staining
d
PDE5
% levels
150
100
50
0
-
1
5
10
JP-2-201 (μM)
e
BTZ
JP-2-201
PDE5
GAPDH
HEK293T cells
f
JP-2-249
μM
-
50
10
1
0.1
RNF126
IA-rhodamine labeling
RNF126
silver staining
g
SMARCA2
% levels
150
100
50
0
-
10
1
JP-2-249 (μM)
h
JP-2-249
μM
-
1
10
SMARCA4
actin
i
JP-2-244
μM
-
50
10
1
0.1
RNF126
IA-rhodamine labeling
RNF126
silver staining
j
LRRK2
% levels
150
100
50
0
-
10
1
JP-2-224 (μM)

Figure S6. Characterizing degraders against additional targets. (a) Gel-based ABPP analysis of JP-2-227 against RNF126. Recombinant RNF126 was pre-incubated with DMSO vehicle or JP-2-227 for 30 min prior to labeling of RNF126 with IA-rhodamine (250 nM) for 1 h. Gels were visualized by in-gel fluorescence and protein loading was assessed by silver staining. (b) Quantitation of data in Figure 2.4b. (c) Gel-based ABPP analysis of JP-2-201 as described in (a). (d) Quantitation of data in Figure 2.4d. (e) JP-2-201-mediated degradation of PDE5 is proteasome-dependent. HEK293T cells were pre-treated with DMSO vehicle or bortezomib (1 mM) for 1 h prior to treating cells with DMSO or JP-2-201 (10 mM). PDE5 and loading control GAPDH levels were assessed by Western blotting. (f) Gel-based ABPP analysis of JP-2-249 against RNF126 as described in (a). (g) Quantitation of data in Figure 2.4f. (h) MV-4-11 cells were treated with DMSO vehicle or JP-2-249 for 24 h and SMARCA4 and loading control actin levels were assessed by Western blotting. (i) Gel-based ABPP of JP-2-244 against RNF126 as described in (a). (j) Quantitation of data in Figure 2.4h. Gels and blots shown in (a,c,e,f,h,i) are representative images from n = 3 biological replicates. Bar graphs in (b,d,g,j) show individual replicate values and average ± sem. Statistical significance is calculated as *p < 0.05 compared to DMSO vehicle.

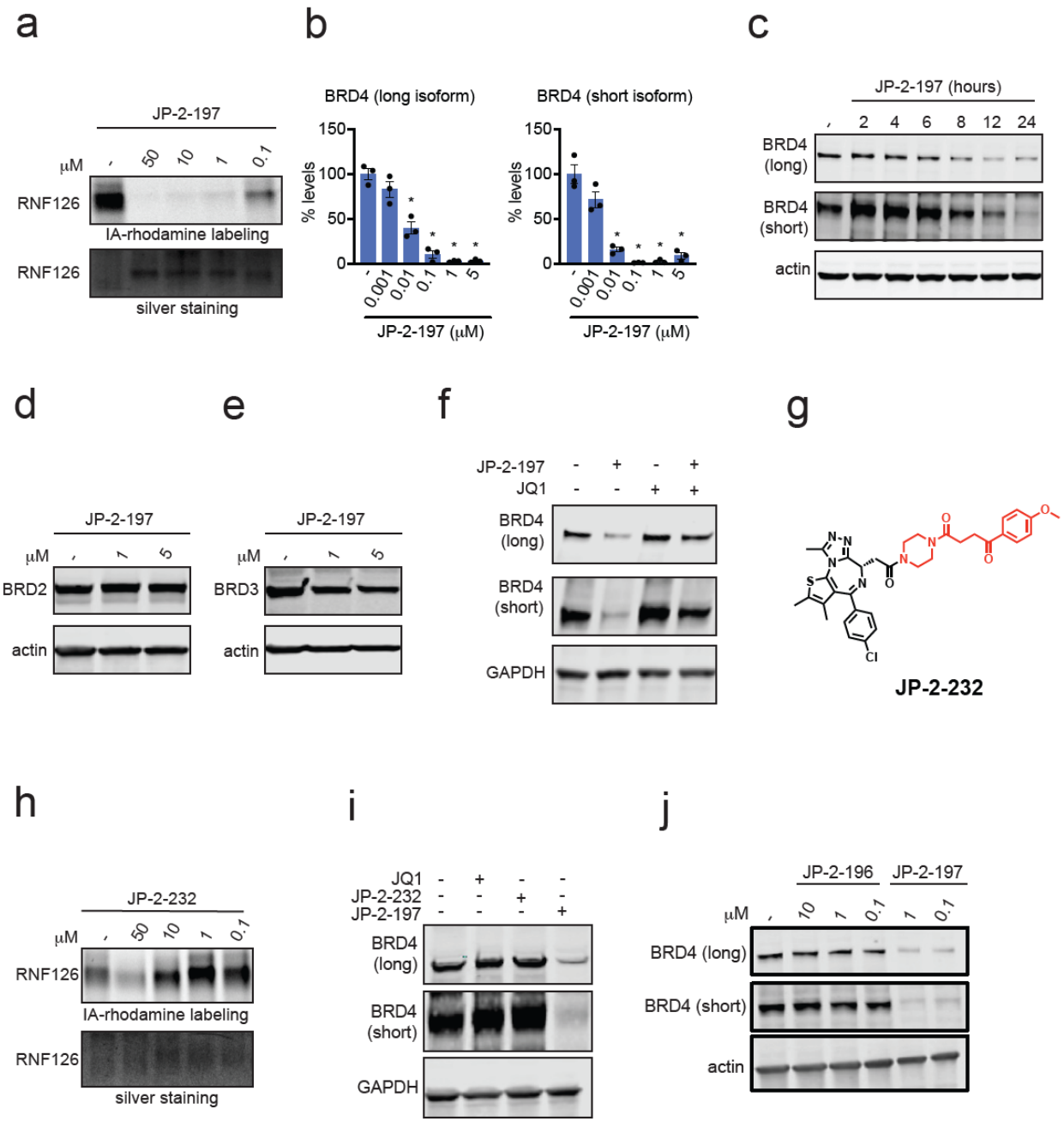

Figure S7. Characterization of BRD4 degraders and their derivatives. (a) Gel-based ABPP analysis of JP-2-197 against RNF126. Recombinant RNF126 was pre-incubated with DMSO vehicle or JP-2-197 for 30 min prior to labeling of RNF126 with IA-rhodamine (250 nM) for 1 h. Gels were visualized by in-gel fluorescence and protein loading was assessed by silver staining. (b) Quantitation of data in Figure 2.5b. (c) Time-course of BRD4 degradation with JP-2-197. HEK293T cells were treated with DMSO vehicle or JP-2-197 (1 μM) and BRD4 and loading control actin levels were assessed by Western

blotting. (d, e) BRD2 (d) and BRD3 (e) levels in HEK293T cells. HEK293T cells were treated with DMSO vehicle or JP-2-197 for 24 h and BRD2, BRD3, and loading control actin levels were assessed by Western blotting. (f) HEK293T cells were pre-treated with either DMSO vehicle or JQ1 (1 mM) for 1 h prior to treating cells with DMSO or JP-2-197 (0.1 mM) for 24 h and BRD4 and loading control GAPDH levels were assessed by Western blotting. (g) Structure of non-reactive derivative of JP-2-197, JP-2-232. (h) Gel-based ABPP of JP-2-232 against RNF126. Recombinant RNF126 was pre-incubated with DMSO vehicle or JP-2-232 for 30 min prior to labeling of RNF126 with IA-rhodamine (250 nM) for 1 h. Gels were visualized by in-gel fluorescence and protein loading was assessed by silver staining. (i) BRD4 levels in HEK293T cells. HEK293T cells were treated with DMSO vehicle, JP-2-197, or JP-2-232 (1 mM) for 24 h and BRD4 and loading control GAPDH levels were detected by Western blotting. (j) HEK293T cells were treated with DMSO vehicle, JP-2-196, or JP-2-197 for 24 h and BRD4 and loading control actin levels were assessed by Western blotting. Gels and blots in (a,c,d,e,f,h,i,j) are representative of n = 3 biologically independent replicates/group. Bar graphs in (b) show individual replicate values and average ± sem. Statistical significance is calculated as *$p < 0.05$ compared to DMSO vehicle.

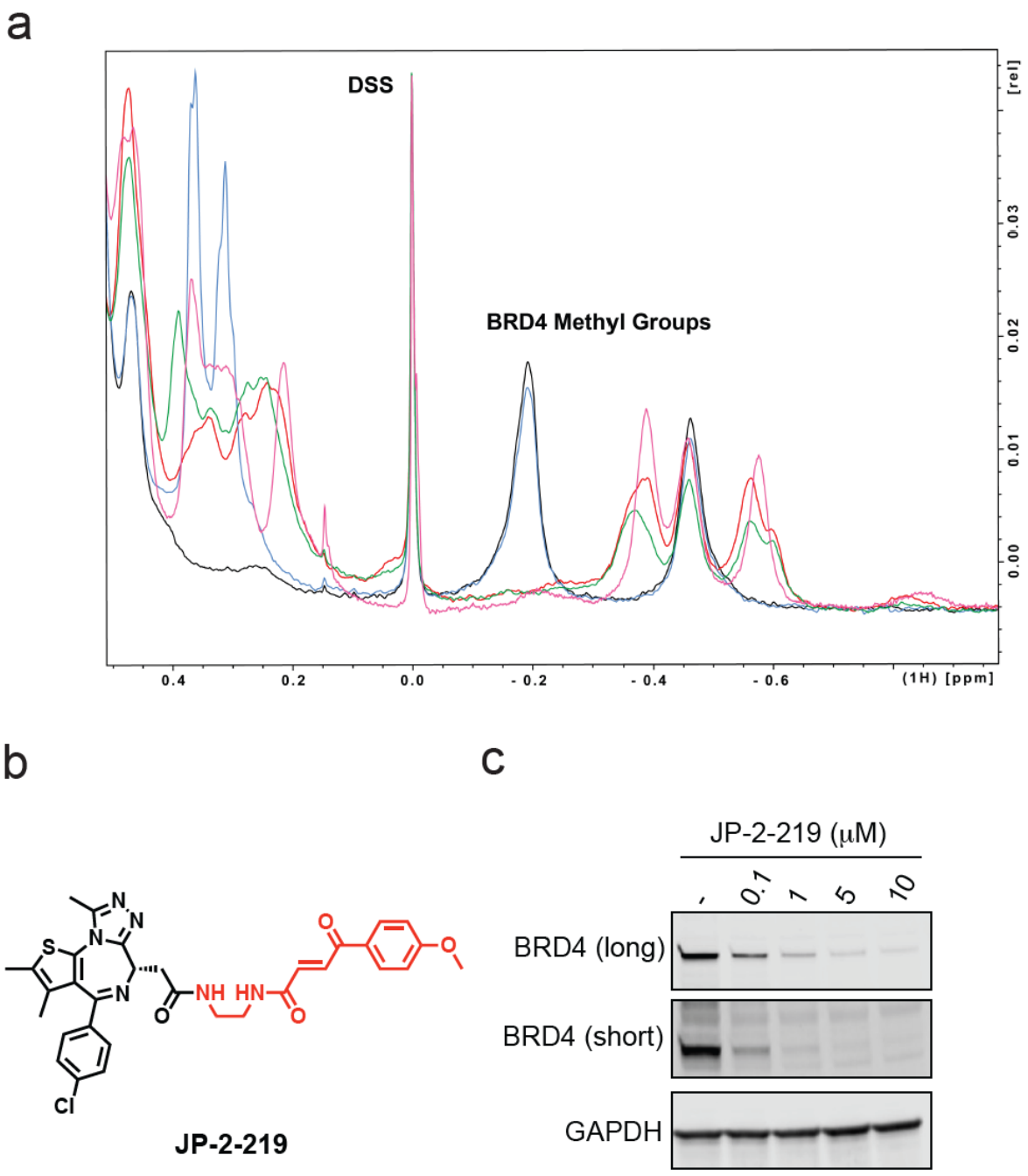

Figure S8. Characterization of BRD4 degraders. (a) Overlay of ^{1}H-1D spectra of the following samples: 50 μM BRD4(44-168) (black); 50 μM BRD4(44-168) + 200 μM JP-2-197 (red); 50 μM BRD4(44-168) + RNF126(1-40) + JP-2-197 (green); 50 μM BRD4(44-168) + RNF126(1-40) (blue); 50 μM BRD4(44-168) + RNF126(1-40) + 100 μM JQ1 + 100 μM JP-2-196 (magenta). BRD4 (black spectrum) and JP-2-197 strongly interact with each other as indicated by the drastic perturbation of one of the upfield shifted BRD4 methyl signals (δ ≈ -0.19 ppm) and the appearance of additional signals (red spectrum). When

RNF126(1-40) is present, the perturbations are further pronounced as small additional chemical shifts and line broadening are detected, suggesting slowed down protein tumbling due to the formation of a ternary protein-protein-glue complex (green spectrum). There is hardly any effect on the BRD4 methyl peaks in the absence of the glue molecule (blue spectrum). No line broadening is observed when the unlinked protein ligands JQ1 (BRD4 ligand) and JP-2-196 (RNF126 ligand) are added to the protein mixture (magenta). (b) Shown is a structure of JP-2-219, a BRD4 degrader with an alkyl linker rather than a piperazine linking the fumarate handle to the BRD4 inhibitor JQ1. (c) BRD4 levels in HEK293T cells. HEK293T cells were treated with DMSO vehicle or JP-2-219 (1 mM) for 24 h and BRD4 and loading control GAPDH levels were detected by Western blotting. Blot is a representative of n = 3 biologically independent replicates/group.

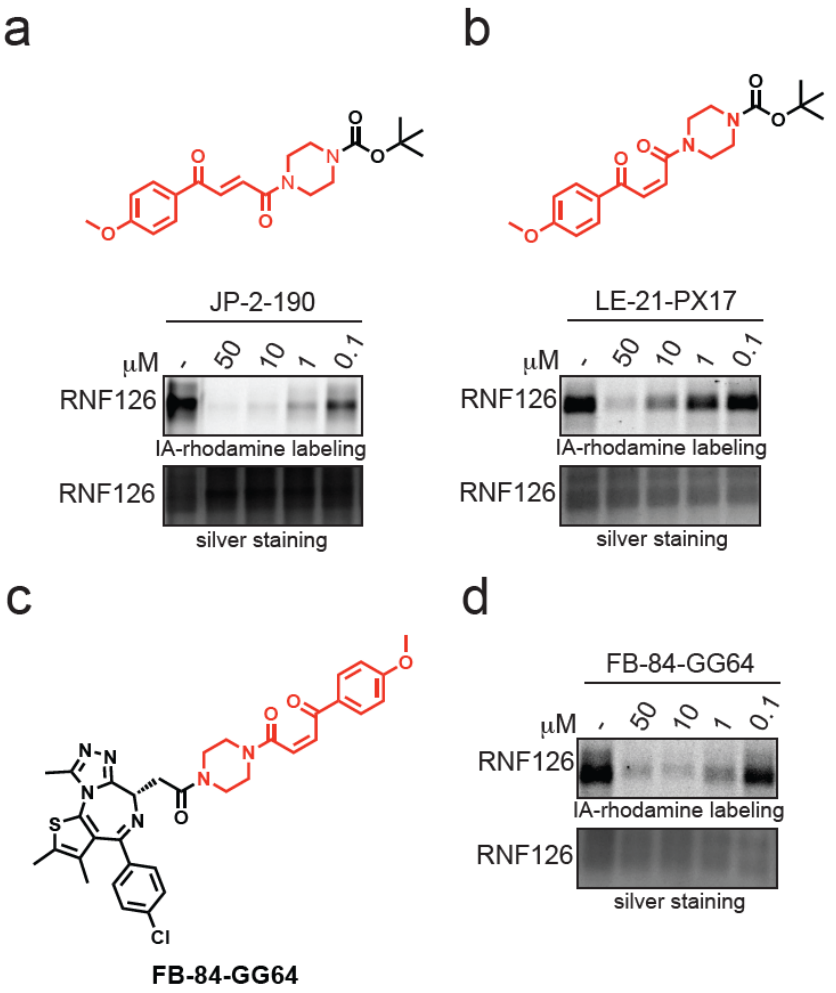

Figure S9. Characterizing the cis-isomer covalent handle and degrader. (a, b) Gel-based ABPP of JP-2-190 and LE-21-PX17 against RNF126. Recombinant RNF126 was pre-incubated with DMSO vehicle or compounds for 30 min prior to labeling of RNF126

with IA-rhodamine (250 nM) for 1 h. Gels were visualized by in-gel fluorescence and protein loading was assessed by silver staining. (c) Structure of the cis isoform of the JP-2-197 BRD4 degrader, FB-84-GG64. (d) Gel-based ABPP of FB-84-GG64 against RNF126. Recombinant RNF126 was pre-incubated with DMSO vehicle or FB-84-GG64 for 30 min prior to labeling of RNF126 with IA-rhodamine (250 nM) for 1 h. Gels were visualized by in-gel fluorescence and protein loading was assessed by silver staining. (e) BRD4 degradation by FB-84-GG64 in HEK293T cells. HEK293T cells were treated with DMSO vehicle or FB-84-GG64 for 24 h and BRD4 and loading control actin levels were assessed by Western blotting. Gels and blots shown in (a,b,d,e) are representative of n = 3 biologically independent replicates/group.

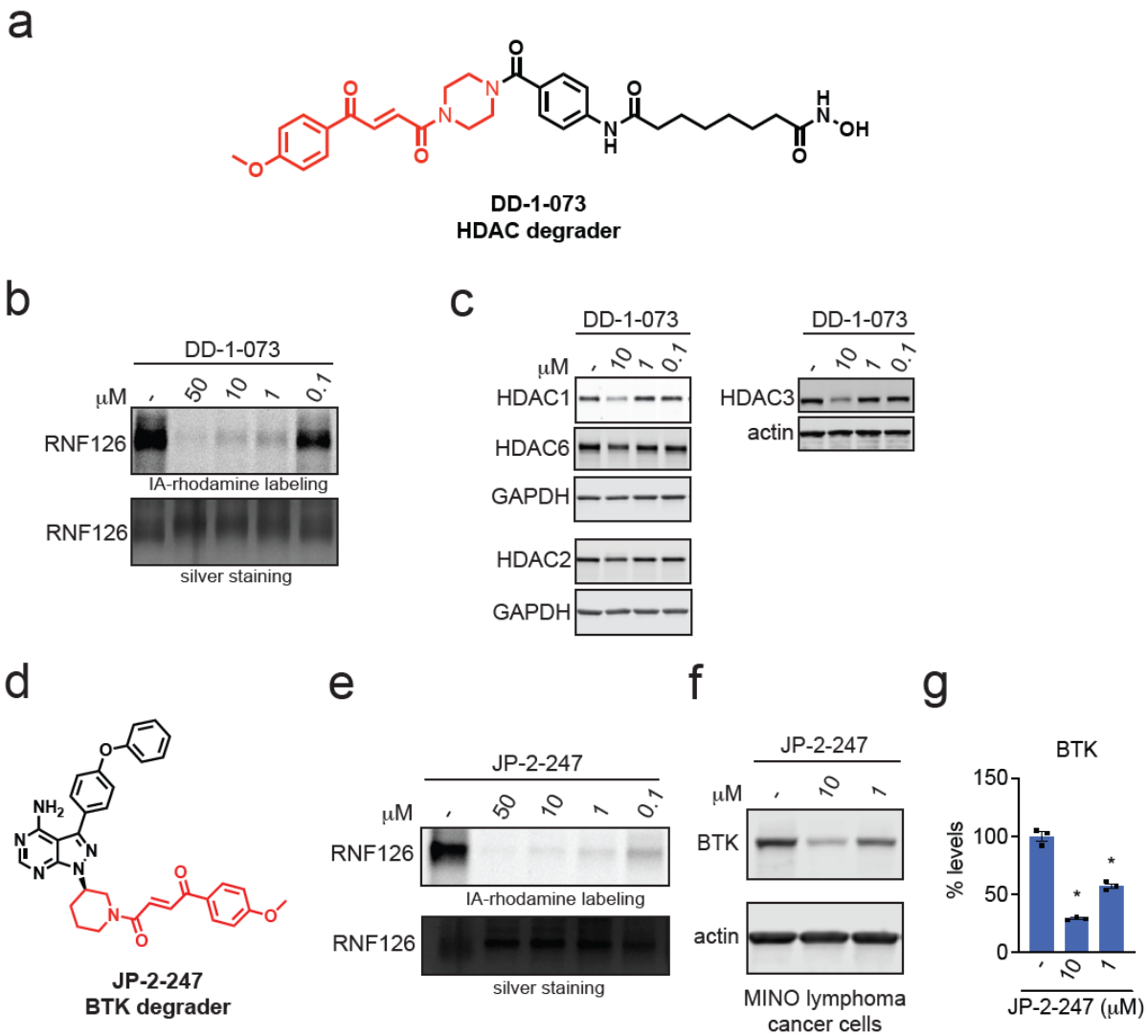

Figure S10. Characterization of HDAC and BTK degraders. (a) Structure of DD-1-073 HDAC degrader linking our fumarate JP-2-196 handle to the HDAC inhibitor vorinostat. (b) Gel-based ABPP of DD-1-073 against RNF126. Recombinant RNF126 was pre-incubated with DMSO vehicle or DD-1-073 for 30 min prior to labeling of RNF126 with IA-rhodamine (250 nM) for 1 h. Gels were visualized by in-gel fluorescence and protein loading was assessed by silver staining. (c) HDAC1, HDAC2, HDAC3, and HDAC6 levels in MDA-MB-231 cells. MDA-MB-231 cells were treated with DMSO vehicle or DD-1-073 for 24 h and HDAC and loading control GAPDH and actin levels were detected by Western blotting. (d) Structure of a BTK degrader JP-2-247 consisting of the fumarate handle incorporated into the BTK inhibitor ibrutinib. (e) Gel-based ABPP analysis of JP-2-247 against RNF126. Recombinant RNF126 was pre-incubated with DMSO vehicle or JP-2-247 for 30 min prior to labeling of RNF126 with IA-rhodamine (250 nM) for 1 h. Gels were visualized by in-gel fluorescence and protein loading was assessed by silver staining. (f) MINO lymphoma cancer cells were treated with DMSO vehicle or JP-2-247 for 24 h and BTK and loading control actin levels were detected by Western blotting. (g) Quantitation of the data shown in (f). Gels and blots shown in (b,c,e,f) are representative of n = 3 biologically independent replicates/group. Bar graph in (g) shows individual replicate values and average ± sem. Statistical significance is calculated as *$p < 0.05$ compared to DMSO vehicle.

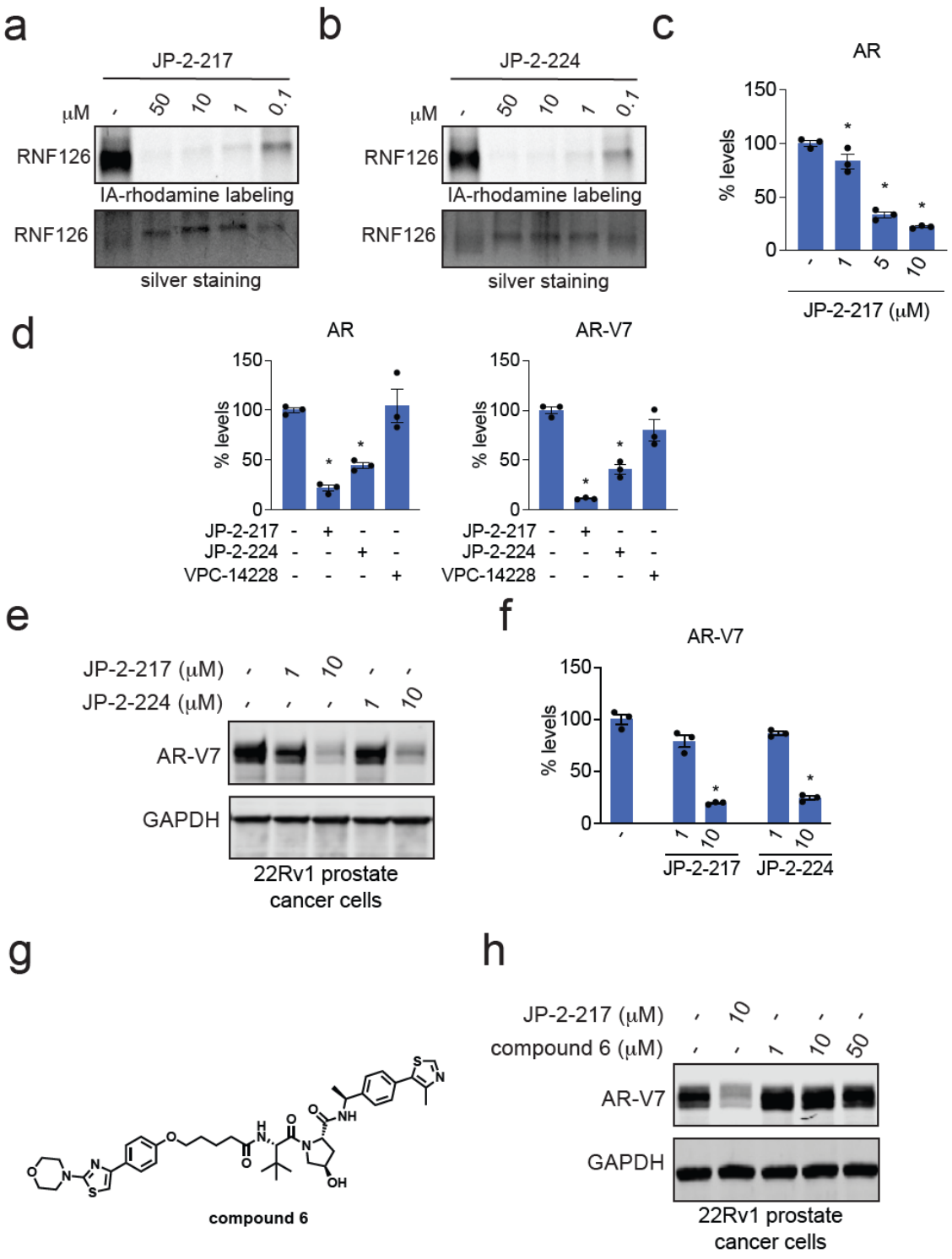

Figure S11. Characterization of AR-V7 degraders. (a, b) Gel-based ABPP analysis of JP-2-217 (a) and JP-2-224 (b) against RNF126. Recombinant RNF126 was pre-

incubated with DMSO vehicle or JP-2-217 or JP-2-224 for 30 min prior to labeling of RNF126 with IA-rhodamine (250 nM) for 1 h. Gels were visualized by in-gel fluorescence and protein loading was assessed by silver staining. (c) Quantitation of data in Figure 2.5g. (d) Quantitation of data in Figure 2.5h. (e) 22Rv1 cells were treated with DMSO vehicle, JP-2-217, or JP-2-224 for 24 h and AR-V7 and loading control GAPDH levels were detected by Western blotting. (f) Quantified AR-V7 levels from experiment described in (e). (g) Structure of a previously reported AR-V7 degrader linking the AR DNA binding domain ligand VPC-14228 to a VHL recruiter, compound 6. (h) AR-V7 levels in 22Rv1 cells. 22Rv1 cells were treated with DMSO vehicle, JP-2-217, or compound 6 for 24 h and AR-V7 and loading control GAPDH levels were detected by Western blotting. Gels and blots in (a,b,e,h) are representative of n = 3 biologically independent replicates/group with individual replicates. Bar graphs in (c,d,f) show individual replicate values and average ± sem. Statistical significance is calculated as *$p < 0.05$ compared to DMSO vehicle.

Supporting Table Legends

The following supplementary datasets have been deposited online with the submission of this dissertation.

Table S1. TMT-based quantitative proteomic profiling of EST1027 in C33A cells. C33A cells were treated with DMSO vehicle or EST1027 (5 μM) for 24 h. Data are from n = 3 biological replicates per group.

Table S2. Cysteine chemoproteomic profiling of EST1027 in C33A cells using isoDTB-ABPP. C33A cells were treated with DMSO vehicle or EST1027 (20 μM) for 2 h**.** Resulting lysates were labeled with an alkyne- functionalized iodoacetamide probe (IA-alkyne) (200 μM) for 1 h, after which isotopic desthiobiotin tags were appended by CuAAC and taken through the isoDTB-ABPP procedure. Experiment was from n = 3 biologically-independent replicates.

Table S3. Quantitative proteomics of JP-2-196-Alkyne pulldown in HEK293T cells. JP-2-196 pulldown proteomics showing significant and moderately selective engagement of RNF126 with less significant engagement of 5 additional E3 ubiquitin ligases LRSAM1, RNF40, MID2, RNF219, and RNF14. HEK293T cells were treated with DMSO vehicle or JP-2-196-alkyne (10 μM) for 6 h. Subsequent lysates were subjected to copper-catalyzed azide-alkyne cycloaddition (CuAAC) with an azide-functionalized biotin handle, after which probe-modified proteins were avidin-enriched, eluted, and digested, and analyzed by TMT-based quantitative proteomics. Data shown are ratios of JP-2-196-alkyne vs DMSO control enriched proteins and p-values from n = 3 biologically independent replicates/group.

Table S4. TMT-based quantitative proteomic profiling of JP-2-197 in HEK293T cells. HEK293T cells were treated with DMSO vehicle, JP-2-196 (1 μM), or JP-2-197 (1 μM) for 24 h. Data are from n = 2 biological replicates per group.

Synthetic Methods and Characterization

All chemical reactions were carried out under a nitrogen atmosphere with dry solvents under anhydrous conditions, unless otherwise noted. Reagents were purchased at the highest commercial quality and used without further purification, unless otherwise stated. The key building block, *trans*-3-(4-methoxybenzoyl)acrylic acid, was acquired from Sigma-Aldrich (Catalog Number: 650765) at a reported purity of 99%, however upon further investigation this purity was found to vary between batches, consisting of anywhere from 0-10% of the *cis*-isomer. Reactions were stirred magnetically and monitored by thin layer chromatography (TLC) carried out on Merck glass silica gel plates (60 F254) using UV light as a visualizing agent and iodine and/or phosphomolybdic acid stain as developing agents. Solvents were removed in vacuo using either a Buchi R-300 Rotavapor (equipped with an I-300 Pro Interface, B-300 Base Heating Bath, Welch 2037B-01 DryFast pump, and VWR AD15R-40-V11B Circulating Bath). Solvents for silica gel chromatography were used as supplied by Sigma-Aldrich. Automated flash chromatography was performed on a Biotage Isolera instrument, equipped with a UV detector. Chromatograms were recorded at 254 and 280 nm. Analytical ultra-performance liquid chromatography (UPLC) was performed on a Waters Acquity UPLC-MS(SQD) with a Phenomenex Kinetix EVO-C18 2.6 µm, 100 Å, 2.1 × 50 mm column. Solvents (water and acetonitrile) containing 0.1% trifluoroacetic acid (TFA) were used. A gradient of 2-88% acetonitrile in water, 0−10 min was used at ambient temperature. Purification was run with a flow rate of 1.2 mL/min with detection at 220 nm. Certain fumarate analogs were sensitive to acidic aqueous purification conditions, and a small fraction was found to isomerize between the E and Z-isomers therefore a neutral, SFC analytical method was also employed using an Amino Phenyl SFC 5 µm, 120 Å, 30 mm × 25 cm column. Solvents (CO_2 and MeOH) were used at a flow rate of 2.5 mL/min with detection at 220 nm. The purity of final compounds was evaluated using the analytical systems described above, characterized by MS and nuclear magnetic resonance (NMR) and ratios of E/Z-isomers were reported as detected in UPLC analysis. Isomerization rates were analyzed for key final compounds by preparing small amounts of material in a 1:1 mixture of water:acetonitrile, filtering through a 0.2 µm syringe filter for UPLC analysis at days 1 and 6. Low-resolution mass spectra were obtained using Agilent 6460 Triple Quad LC/MS instrument. High-resolution mass spectra (HRMS) were obtained at the Catalysis Center at the College of Chemistry, University of California, Berkeley. ^{1}H and ^{13}C nuclear magnetic resonance (NMR) spectra were recorded on BRUKER AV (600 MHz and 700 MHz), AVB (400 MHz), AVQ (400 MHz) and NEO (500 MHz) spectrometers. Measurements were carried out at ambient temperature. Chemical shifts (δ) are reported in ppm with the residual solvent signal as internal standard (chloroform at 7.26 and 77.00 ppm for ^{1}H NMR and ^{13}C NMR spectroscopy, respectively). The data is reported as (s = singlet, d = doublet, t = triplet, q = quartet, p = quintet, m = multiplet or unresolved, br = broad signal, coupling constant(s) in Hz, integration). 13C NMR spectra were recorded with broadband 1H decoupling.

General Procedures

Amide Couplings

General Procedure A

A mixture of the corresponding carboxylic acid (1.1 equiv.) and HATU (1.2 equiv.) was purged with N_2 for 5 minutes. The mixture was dissolved in N,N-dimethylformamide (DMF) (0.1 M), N,N-diisopropylethylamine (DIPEA) (3 equiv.) was added and the reaction mixture was allowed to stir at ambient temperature for 30 minutes. The corresponding amine (1 equiv.) was dissolved in DMF (0.1 M) then added dropwise and the reaction mixture was stirred at ambient temperature overnight. The reaction was quenched with 5 times the reaction volume of 5% $LiCl_{(aq)}$ and extracted 3 times with dichloromethane (DCM) or ethyl acetate (EtOAc). The organic extracts were dried over Na_2SO_4, vacuum filtered, and concentrated *in vacuo*. The resultant residue was purified by silica gel flash chromatography to afford the title compound.

General Procedure B

The corresponding carboxylic acid (1.1 equiv.) was added to a vessel and purged with N_2 for 5 minutes. The acid was then dissolved in DCM (0.1 M) and cooled to 0 °C in an ice bath. Oxalyl chloride (1.2 equiv.) was added dropwise at 0 °C. A few drops of DMF were added and the reaction mixture was allowed to stir and come to ambient temperature over 2 hours. The volatiles were removed *in vacuo* and the resultant residue was redissolved in DCM (0.1 M) and cooled to 0 °C in an ice bath. The corresponding amine (1.1 equiv.) was dissolved in DCM (0.1M). DIPEA (3 equiv.) was added, and the mixture was stirred for 5 minutes at ambient temperature before being added to the acyl chloride dropwise at 0 °C. The reaction mixture was allowed to stir and come to ambient temperature overnight. The reaction was quenched with water and extracted 3 times with EtOAc. The organic extracts were dried over Na_2SO_4, vacuum filtered, and concentrated in vacuo. The resultant residue was purified by silica gel flash chromatography to afford the title compound.

General Procedure C

The corresponding carboxylic acid (1.1 equiv.) was added to a vessel and purged with N_2 for 5 minutes. The acid was dissolved in acetonitrile (0.1 M) and DIPEA (2 equiv.) was added. Pentafluoropyridine (1.1 equiv.) was added dropwise, and the reaction mixture was stirred at ambient temperature for 30 minutes. The corresponding amine was dissolved in acetonitrile (0.1 M) and added to acyl fluoride. The reaction mixture was stirred at 100 °C overnight. The volatiles were removed in vacuo, and the resultant residue was purified by silica gel flash chromatography to afford the title compound.

General Procedure D

The corresponding carboxylic acid (1.0 equiv.) was added to a vessel and purged with N_2 for 5 minutes. The acid was dissolved in DMF (0.1 M) and DIPEA (3 equiv.) was added. A >50% wt. solution of propylphosphonic anhydride (T3P) in EtOAc (1.5 equiv.) was added dropwise, and the reaction mixture was stirred at ambient temperature for 30 minutes. The corresponding amine (1.2 equiv.) was dissolved in DMF (0.1 M) then added dropwise and the reaction mixture was stirred at ambient temperature overnight. The reaction was quenched with 5 times the reaction volume of 5% $LiCl_{(aq)}$ and extracted 3

times with EtOAc. The organic extracts were washed once with 5% $LiCl_{(aq)}$, dried over Na_2SO_4, vacuum filtered, and concentrated in vacuo. The resultant residue was purified by silica gel flash chromatography to afford the title compound.

Tert-butyloxycarbonyl Deprotection

General Procedure E

The corresponding tert-butyloxycarbonyl protected amine (1 equiv.) was dissolved in DCM (0.1 M). Trifluoroacetic acid (32 equiv.) was added, and the reaction mixture was stirred at ambient temperature for 30 minutes to overnight. The volatiles were removed in vacuo and the crude residue was used without further purification, unless otherwise noted.

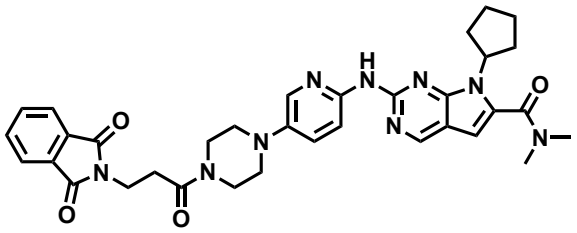

EST1001

General Procedure A was followed with 3-phthalimidopropionic acid (21.6 mg, 0.06 mmol), HATU (43.8 mg, 0.12 mmol), DIPEA (0.04 mL, 0.23 mmol), and ribociclib (25.0 mg, 0.06 mmol). The crude residue was purified by silica gel chromatography (0-10% MeOH in DCM) to afford 14.9 mg (41%) of the title compound as a yellow film.

^{1}H NMR (500 MHz, $CDCl_3$) δ 8.70 (s, 1H), 8.37 (d, *J* = 9.0 Hz, 1H), 8.03 – 7.95 (m, 2H), 7.89 – 7.81 (m, 2H), 7.75 – 7.68 (m, 2H), 7.32 (dd, *J* = 9.1, 3.0 Hz, 1H), 6.44 (s, 1H), 4.79 (p, *J* = 9.0 Hz, 1H), 4.09 – 4.03 (m, 2H), 3.80 (t, *J* = 5.2 Hz, 2H), 3.64 (t, *J* = 5.1 Hz, 2H), 3.15 (s, 6H), 3.14 – 3.08 (m, 4H), 2.85 – 2.78 (m, 2H), 2.65 – 2.52 (m, 2H), 2.06 (m 4H), 1.77 – 1.70 (m, 2H).

^{13}C NMR (151 MHz, $CDCl_3$) δ 168.4, 168.2, 164.1, 154.5, 151.9, 151.8, 147.6, 142.1, 137.6, 134.0, 132.1, 132.1, 127.4, 123.3, 112.7, 112.4, 101.0, 57.9, 50.6, 50.3, 45.4, 41.5, 34.3, 31.6, 30.2, 24.7.

LRMS (ESI) *m/z* calcd for $[C_{34}H_{37}N_9O_4 + H]^+$ = 636.3, found 636.4.

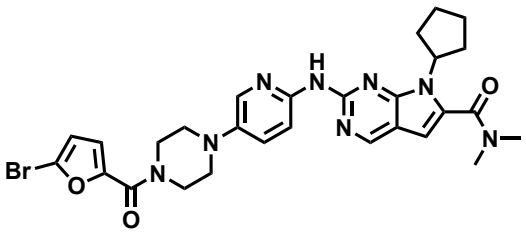

EST1004

General Procedure A was followed with 5-Bromo-2-furoic acid (11.0 mg, 0.06 mmol), HATU (43.8 mg, 0.12 mmol), DIPEA (0.04 mL, 0.23 mmol), and ribociclib (25.0mg, 0.06 mmol). The crude residue was purified by silica gel chromatography (0-15% MeOH in DCM) to afford 23.9 mg (63%) of the title compound as a yellow film.

^{1}H NMR (500 MHz, $CDCl_3$) δ 8.72 (s, 1H), 8.39 (d, *J* = 9.0 Hz, 1H), 8.25 (s, 1H), 8.06 (d, *J* = 3.0 Hz, 1H), 7.34 (dd, *J* = 9.1, 3.0 Hz, 1H), 7.03 (d, *J* = 3.5 Hz, 1H), 6.48 – 6.42 (m, 2H), 4.79 (p, *J* = 8.9 Hz, 1H), 3.98 (s, 4H), 3.24 – 3.18 (m, 4H), 3.15 (s, 6H), 2.58 (m, 2H), 2.11 – 2.01 (m, 4H), 1.76 – 1.68 (m, 2H).
^{13}C NMR (151 MHz, $CDCl_3$) δ 164.1, 157.8, 154.6, 151.9, 151.9, 149.5, 147.7, 142.0, 137.5, 132.0, 127.3, 124.4, 119.3, 113.5, 112.6, 112.5, 101.0, 57.9, 50.6, 30.2, 24.7.
LRMS (ESI) *m/z* calcd for $[C_{28}H_{31}BrN_8O_3 + H]^+$ = 607.3, found 607.2.

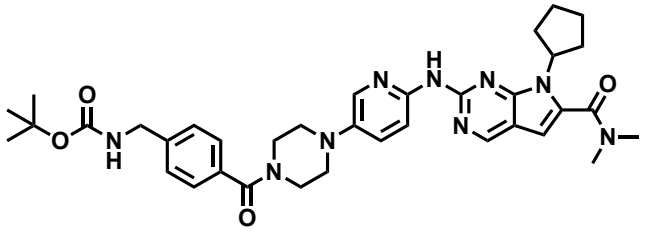

EST1007

General Procedure A was followed with 4-(Boc-aminomethyl)benzoic acid (14.5 mg, 0.06 mmol), HATU (43.8 mg, 0.12 mmol), DIPEA (0.04 mL, 0.23 mmol), and ribociclib (25.0 mg, 0.06 mmol). The crude residue was purified by silica gel chromatography (0-15% MeOH in DCM) to afford 29.5 mg (77%) of the title compound as a yellow film.
^{1}H NMR (500 MHz, $CDCl_3$) δ 8.72 (s, 1H), 8.37 (d, *J* = 9.1 Hz, 1H), 8.26 (s, 1H), 8.04 (d, *J* = 2.9 Hz, 1H), 7.41 (d, *J* = 7.9 Hz, 2H), 7.36 – 7.30 (m, 3H), 6.44 (s, 1H), 4.99 (d, *J* = 6.5 Hz, 1H), 4.79 (p, *J* = 9.0 Hz, 1H), 4.35 (d, *J* = 6.1 Hz, 2H), 3.94 (s, 2H), 3.62 (s, 2H), 3.20 (br s, 2H), 3.15 (s, 6H), 3.09 (br s, 2H), 2.58 (m, 2H), 2.11 – 2.00 (m, 4H), 1.76 – 1.67 (m, 2H), 1.46 (s, 9H).
^{13}C NMR (151 MHz, $CDCl_3$) δ 170.2, 164.1, 156.0, 154.6, 151.9, 151.9, 147.7, 142.0, 141.1, 137.6, 134.4, 132.0, 127.5, 127.4, 112.7, 112.5, 101.0, 79.7, 57.9, 50.6, 44.3, 39.4, 35.2, 30.2, 28.4, 24.7.
LRMS (ESI) *m/z* calcd for $[C_{36}H_{45}N_9O_4 + H]^+$ += 668.4, found 668.5.

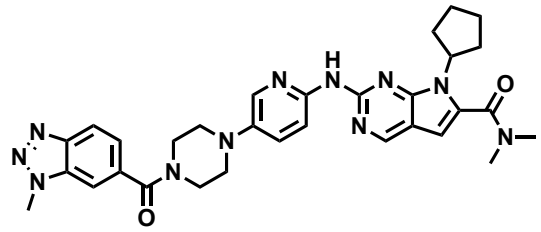

EST1012

General Procedure A was followed with 1-Methyl-1h-1,2,3-benzotriazole-6-carboxylic acid (10.2 mg, 0.06 mmol), HATU (43.8 mg, 0.12 mmol), DIPEA (0.04 mL, 0.23 mmol), and ribociclib (25.0 mg, 0.06 mmol). The crude residue was purified by silica gel chromatography (0-15% MeOH in DCM) to afford 23.7 mg (69%) of the title compound as a yellow film.
^{1}H NMR (500 MHz, $CDCl_3$) δ 8.72 (s, 1H), 8.34 (s, 1H), 8.21 (s, 1H), 8.15 (d, *J* = 1.1 Hz, 1H), 8.04 (d, *J* = 2.9 Hz, 1H), 7.68 – 7.58 (m, 2H), 7.35 (dd, *J* = 9.0, 2.9 Hz, 1H), 6.44 (s, 1H), 4.79 (p, *J* = 8.9 Hz, 1H), 4.34 (s, 3H), 3.94 (br s, 2H), 3.70 (br s, 2H), 3.15 (m, 10H), 2.57 (m, 2H), 2.12 – 1.99 (m, 4H), 1.71 (d, *J* = 4.1 Hz, 2H).

^{13}C NMR (126 MHz, $CDCl_3$) δ 169.7, 164.0, 151.9, 145.3, 142.0, 134.1, 131.3, 127.1, 119.2, 112.9, 112.6, 109.9, 101.0, 57.9, 50.6, 34.5, 30.2, 24.7.
LRMS (ESI) *m/z* calcd for $[C_{31}H_{35}N_{11}O_2 + H]^+$ = 594.3, found 594.3.

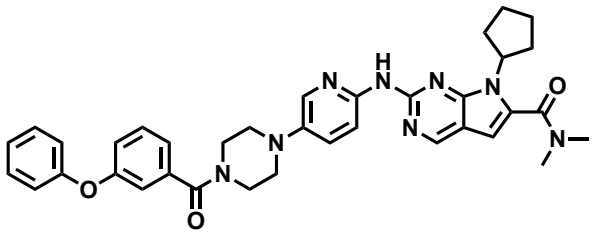

EST1018

General Procedure A was followed with 3-phenoxybenzoic acid (12.3 mg, 0.06 mmol), HATU (43.8 mg, 0.12 mmol), DIPEA (0.04 mL, 0.23 mmol), and ribociclib (25.0 mg, 0.06 mmol). The crude residue was purified by silica gel chromatography (0-15% MeOH in DCM) to afford 30.1 mg (83%) of the title compound as a yellow film.
^{1}H NMR (500 MHz, $CDCl_3$) δ 8.72 (s, 1H), 8.39 (d, *J* = 9.0 Hz, 1H), 8.30 (s, 1H), 8.05 (d, *J* = 2.9 Hz, 1H), 7.47 – 7.42 (m, 2H), 7.42 – 7.31 (m, 3H), 7.19 – 7.12 (m, 1H), 7.04 (ddd, *J* = 13.1, 7.6, 1.6 Hz, 4H), 6.44 (s, 1H), 4.79 (p, *J* = 8.9 Hz, 1H), 3.96 – 3.62 (m, 4H), 3.15 (m, 10H), 2.64 – 2.53 (m, 2H), 2.11 – 2.00 (m, 4H), 1.76 – 1.65 (m, 2H).
^{13}C NMR (126 MHz, $CDCl_3$) δ 170.1, 164.1, 159.1, 156.2, 154.5, 151.9, 151.8, 147.6, 142.1, 137.3, 132.1, 130.0, 129.8, 129.3, 127.5, 124.1, 119.7, 118.1, 112.7, 112.5, 101.0, 57.9, 50.7, 39.5, 35.2, 30.2, 24.7. (Mixture of rotamers)
LRMS (ESI) *m/z* calcd for $[C_{36}H_{38}N_8O_3 + H]^+$ = 631.3, found 631.3.

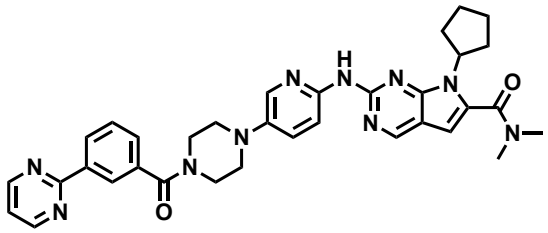

EST1021

General Procedure A was followed with 3-(2-pyrimidinyl)benzoic acid (11.5 mg, 0.06 mmol), HATU (43.8 mg, 0.12 mmol), DIPEA (0.04 mL, 0.23 mmol), and ribociclib (25.0 mg, 0.06 mmol). The crude residue was purified by silica gel chromatography (0-15% MeOH in DCM) to afford 12.2 mg (34%) of the title compound as a yellow film.
^{1}H NMR (500 MHz, $CDCl_3$) δ 8.83 (d, *J* = 4.8 Hz, 2H), 8.69 (s, 1H), 8.54 (dt, *J* = 8.9, 1.7 Hz, 2H), 8.38 (d, *J* = 9.1 Hz, 1H), 8.01 (d, *J* = 2.9 Hz, 1H), 7.92 (s, 1H), 7.63 – 7.54 (m, 2H), 7.35 (dd, *J* = 9.1, 2.9 Hz, 1H), 7.23 (t, *J* = 4.8 Hz, 1H), 6.44 (s, 1H), 4.79 (p, *J* = 8.9 Hz, 1H), 4.01 (br s, 2H), 3.69 (br s, 2H), 3.25 (br s, 2H), 3.15 (s, 6H), 3.13 (br s, 2H), 2.64 – 2.52 (m, 2H), 2.12 – 1.99 (m, 4H), 1.77 – 1.69 (m, 2H).
^{13}C NMR (151 MHz, $CDCl_3$) δ 170.1, 164.1, 163.9, 157.4, 154.4, 152.0, 151.8, 147.5, 142.2, 137.9, 135.9, 132.2, 129.5, 129.5, 129.1, 127.6, 126.8, 119.5, 112.8, 112.6, 101.0, 57.9, 42.1, 39.5, 35.2, 30.2, 24.7.
LRMS (ESI) *m/z* calcd for $[C_{34}H_{36}N_{10}O_2 + H]^+$ = 617.3, found 617.3.

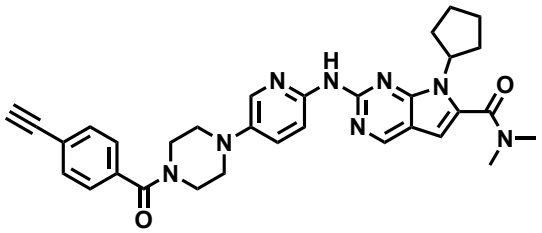

EST1026

General Procedure A was followed with 4-Ethynylbenzoic acid (8.4 mg, 0.06 mmol), HATU (43.8 mg, 0.12 mmol), DIPEA (0.04 mL, 0.23 mmol), and ribociclib (25.0 mg, 0.06 mmol). The crude residue was purified by silica gel chromatography (0-15% MeOH in DCM) to afford 13.6 mg (42%) of the title compound as a yellow film.

^{1}H NMR (500 MHz, CDCl3) δ 8.70 (s, 1H), 8.35 (d, J = 9.1 Hz, 1H), 8.16 (s, 1H), 7.99 (d, J = 2.9 Hz, 1H), 7.58 - 7.53 (m, 2H), 7.44 - 7.39 (m, 2H), 7.35 (dd, J = 9.1, 3.0 Hz, 1H), 6.45 (s, 1H), 4.79 (p, J = 9.0, 9.0, 9.0, 9.0 Hz, 1H), 3.93 (s, 2H), 3.61 (s, 2H), 3.16 (d, J = 3.9 Hz, 10H), 2.61 (s, 1H), 2.56 (dt, J = 16.4, 8.3, 8.3 Hz, 2H), 2.11 - 2.01 (m, 4H), 1.74 - 1.68 (m, 2H).

^{13}C NMR (151 MHz, $CDCl_3$) δ 169.7, 164.0, 154.2, 151.9, 151.6, 147.4, 142.1, 135.6, 132.3, 128.9, 127.2, 123.9, 112.9, 112.7, 101.0, 82.8, 78.8, 57.9, 47.6, 39.4, 35.2, 31.1, 30.2, 29.7, 24.8.

LRMS (ESI) *m/z* calcd for $[C_{32}H_{34}N_8O_2 + H]^+$ = 563.3, found 563.3.

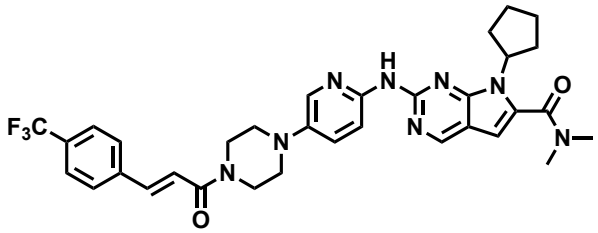

EST1027

General Procedure A was followed with *trans*-4-(trifluoromethyl)cinnamic acid (12.4 mg, 0.06 mmol), HATU (43.8 mg, 0.12 mmol), DIPEA (0.04 mL, 0.23 mmol), and ribociclib (25.0 mg, 0.06 mmol). The crude residue was purified by silica gel chromatography (0-15% MeOH in DCM) to afford 24.7 mg (68%) of the title compound as a yellow film.

^{1}H NMR (500 MHz, $CDCl_3$) δ 8.73 (s, 1H), 8.17 (s, 1H), 8.00 (d, *J* = 2.9 Hz, 1H), 7.71 (d, *J* = 15.4 Hz, 1H), 7.64 (s, 4H), 7.44 – 7.37 (m, 1H), 7.01 (d, *J* = 15.5 Hz, 1H), 6.46 (s, 1H), 4.77 (q, *J* = 8.9 Hz, 1H), 3.99 – 3.78 (m, 4H), 3.19 (br s, 4H), 3.15 (s, 6H), 2.53 (m, 2H), 2.10 – 1.97 (m, 4H), 1.69 (m, 2H).

^{13}C NMR (126 MHz, $CDCl_3$) δ 164.9, 164.1, 154.8, 152.1, 152.0, 148.0, 141.9, 141.3, 138.6, 137.7, 131.9, 131.2 (q, $^4J_{CF}$ = 32.5 Hz), 127.9, 127.3, 125.8 (q, $^3J_{CF}$ = 3.7 Hz), 125.0, 122.8 (q, $^1J_{CF}$ = 272.2 Hz), 119.4, 112.5, 101.1, 57.9, 50.9, 50.3, 45.9, 42.2, 39.4, 35.2, 30.1, 24.7.

HRMS (ESI) *m/z* calcd for $[C_{33}H_{35}F_3N_8O_2 + H]^+$ = 633.2835, found 633.2906.

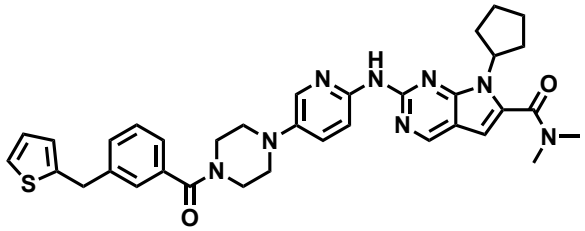

EST1030

General Procedure A was followed with 4-(2-thienylmethyl)benzoic acid (12.6 mg, 0.06 mmol), HATU (43.8 mg, 0.12 mmol), DIPEA (0.04 mL, 0.23 mmol), and ribociclib (25.0 mg, 0.06 mmol). The crude residue was purified by silica gel chromatography (0-15% MeOH in DCM) to afford 32.3 mg (88%) of the title compound as a yellow film.

^{1}H NMR (500 MHz, $CDCl_3$) δ 8.65 (s, 1H), 8.35 (d, *J* = 9.1 Hz, 1H), 8.30 (s, 1H), 7.89 (d, *J* = 2.9 Hz, 1H), 7.35 – 7.28 (m, 3H), 7.27 – 7.21 (m, 2H), 7.10 (dd, *J* = 5.2, 1.2 Hz, 1H), 6.87 (dd, *J* = 5.2, 3.4 Hz, 1H), 6.75 (dd, *J* = 3.3, 1.2 Hz, 1H), 6.38 (s, 1H), 4.73 (p, *J* = 8.8 Hz, 1H), 4.12 (s, 2H), 3.94 – 3.50 (m, 4H), 3.08 (s, 10H), 2.54 – 2.43 (m, 2H), 2.06 – 1.91 (m, 4H), 1.70 – 1.60 (m, 2H).

^{13}C NMR (126 MHz, $CDCl_3$) δ 170.4, 164.0, 154.4, 151.9, 151.7, 147.5, 143.0, 142.5, 142.1, 133.6, 132.3, 128.8, 127.8, 127.6, 126.9, 125.5, 124.2, 112.8, 112.7, 101.0, 57.9, 50.6, 39.5, 35.8, 30.2, 24.7.

LRMS (ESI) *m/z* calcd for $[C_{35}H_{38}N_8O_2S + H]^+$ = 635.3, found 635.4.

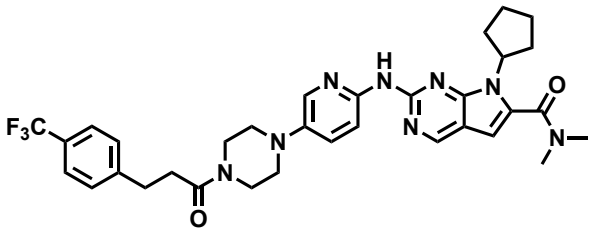

EST1036

General Procedure A was followed with 4-(trifluoromethyl)hydrocinnamic acid (99,5 mg, 0.46 mmol), HATU (350.2 mg, 0.92 mmol), DIPEA (0.32 mL, 1.4 mmol), and ribociclib (200.1 mg, 0.46 mmol). The crude residue was purified by reverse phase silica gel chromatography (5-95% MeCN in H_2O) to afford 133.0 mg (46%) of the title compound as a yellow film.

^{1}H NMR (500 MHz, $CDCl_3$) δ 9.93 (s, 1H), 8.76 (s, 1H), 7.79 (s, 1H), 7.54 (d, *J* = 8.2 Hz, 2H), 7.47 (d, *J* = 7.9 Hz, 2H), 7.32 (d, *J* = 7.9 Hz, 2H), 6.48 (s, 1H), 4.73 (p, *J* = 8.8 Hz, 1H), 3.74 (t, *J* = 5.0 Hz, 2H), 3.58 (t, *J* = 4.6 Hz, 2H), 3.12 (d, *J* = 13.6 Hz, 6H), 3.08 – 3.00 (m, 6H), 2.71 (t, *J* = 7.5 Hz, 2H), 2.38 (m, 2H), 2.05 – 1.91 (m, 4H), 1.64 – 1.56 (m, 2H).

^{13}C NMR (126 MHz, $CDCl_3$) δ 170.1, 164.1, 154.7, 152.0, 151.9, 147.9, 145.4, 141.9, 137.4, 132.0, 128.9, 128.4 (q, $^2J_{CF}$ = 32.2 Hz), 127.5, 127.4, 125.4 (q, $^3J_{CF}$ = 3.7 Hz), 124.3 (q, $^1J_{CF}$ = 271.8 Hz), 112.5, 101.1, 57.9, 50.6, 50.3, 45.4, 41.6, 39.4, 35.2, 34.4, 31.0, 30.1, 24.7.

HRMS (ESI) *m/z* calcd for $[C_{33}H_{37}F_3N_8O_2 + H]^+$ = 635.2992, found 635.3061.

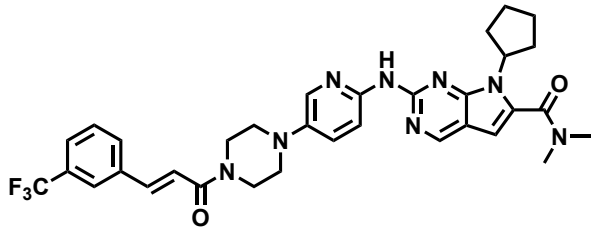

EST1051

General Procedure A was followed with 3-(trifluoromethyl)cinnamic acid (12.4 mg, 0.06 mmol), HATU (43.8 mg, 0.12 mmol), DIPEA (0.04 mL, 0.23 mmol), and ribociclib (25.0 mg, 0.06 mmol). The crude residue was purified by silica gel chromatography (0-10% MeOH in DCM) to afford 30.3 mg (83%) of the title compound as a yellow film.

^{1}H NMR (500 MHz, CDCl3) δ 8.65 (s, 1H), 8.32 (d, J = 9.0 Hz, 1H), 8.31 (s, 1H), 8.12 (s, 1H), 7.97 (d, J = 2.9 Hz, 1H), 7.72 (d, J = 2.1 Hz, 1H), 7.66 (d, J = 15.4 Hz, 1H), 7.62 (d, J = 7.7 Hz, 1H), 7.55 (d, J = 7.8 Hz, 1H), 7.45 (t, J = 7.8, 7.8 Hz, 1H), 7.29 (dd, J = 9.1, 3.0 Hz, 1H), 6.92 (d, J = 15.4 Hz, 1H), 6.38 (s, 1H), 4.73 (p, J = 9.0, 9.0, 8.9, 8.9 Hz, 1H), 3.91 - 3.76 (m, 4H), 3.13 (t, J = 5.0, 5.0 Hz, 4H), 3.09 (s, 6H), 2.57 - 2.46 (m, 2H), 2.05 - 1.95 (m, 4H), 1.69 - 1.62 (m, 2H).

^{13}C NMR (126 MHz, $CDCl_3$) δ 164.9, 164.0, 154.2, 151.9, 151.6, 147.3, 142.0, 141.6, 136.0, 132.5, 131.4 (q, $^2J_{CF}$ = 31.7 Hz), 131.3, 129.5, 126.2 (q, $^3J_{CF}$ = 3.7 Hz), 123.9 (q, $^3J_{CF}$ = 3.8 Hz), 122.8 (q, $^1J_{CF}$ = 272.6 Hz), 118.7, 113.0, 113.0, 101.0, 57.9, 50.3, 45.9, 42.2, 39.5, 35.2, 30.3, 24.8.

HRMS (ESI) *m/z* calcd for $[C_{33}H_{35}F_3N_8O_2 + H]^+$ = 633.2835, found 633.2906.

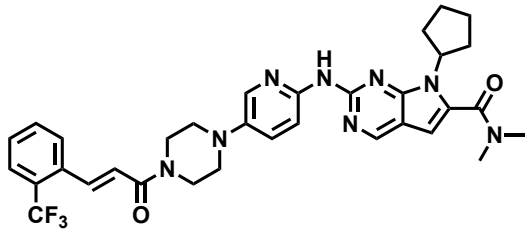

EST1054

General Procedure A was followed with *trans*-2-(trifluoromethyl)cinnamic acid (12.4 mg, 0.06 mmol), HATU (43.8 mg, 0.12 mmol), DIPEA (0.04 mL, 0.23 mmol), and ribociclib (25.0 mg, 0.06 mmol). The crude residue was purified by silica gel chromatography (0-10% MeOH in DCM) to afford 26.1 mg (72%) of the title compound as a yellow film.

^{1}H NMR (500 MHz, $CDCl_3$) δ 8.65 (s, 1H), 8.36 (d, *J* = 9.2 Hz, 1H), 8.30 (s, 1H), 7.96 – 7.87 (m, 2H), 7.66 – 7.60 (m, 2H), 7.50 (t, *J* = 7.6 Hz, 1H), 7.43 – 7.32 (m, 2H), 6.76 (d, *J* = 15.3 Hz, 1H), 6.39 (s, 1H), 4.73 (p, *J* = 8.7 Hz, 1H), 3.92 – 3.71 (m, 4H), 3.12 (t, *J* = 5.1 Hz, 4H), 3.08 (s, 6H), 2.48 (m, 2H), 2.06 – 1.95 (m, 4H), 1.71 – 1.59 (m, 2H).

^{13}C NMR (126 MHz, $CDCl_3$) δ 165.0, 164.0, 154.2, 151.9, 151.6, 147.4, 142.0, 138.4, 134.4, 132.4, 132.0, 129.1, 128.5 (q, $^2J_{CF}$ = 30.3 Hz), 128.0, 126.2 (q, $^3J_{CF}$ = 5.5 Hz), 122.9 (d, $^1J_{CF}$ = 274.0 Hz), 121.9, 112.9, 112.9, 101.0, 57.9, 50.2, 46.0, 42.1, 39.5, 35.2, 30.3, 24.8.

HRMS (ESI) *m/z* calcd for $[C_{33}H_{35}F_3N_8O_2 + H]^+$ = 633.2835, found 633.2906.

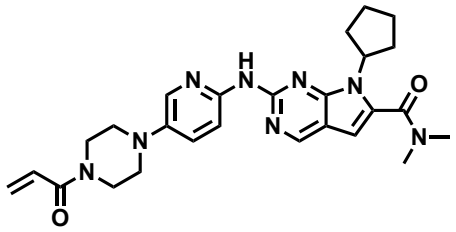

EST1057

General Procedure A was followed with acrylic acid (0.004 mL, 0.06 mmol), HATU (43.8 mg, 0.12 mmol), DIPEA (0.04 mL, 0.23 mmol), and ribociclib (25.0 mg, 0.06 mmol). The crude residue was purified by silica gel chromatography (0-10% MeOH in DCM) to afford 15.2 mg (54%) of the title compound as a yellow film.

^{1}H NMR (500 MHz, $CDCl_3$) δ 8.7 (s, 1H), 7.9 (br s, 2H), 7.6 – 7.4 (m, 1H), 6.6 (dd, *J* = 16.8, 10.6 Hz, 1H), 6.5 (s, 1H), 6.2 (d, *J* = 16.8 Hz, 1H), 5.7 (d, *J* = 10.6 Hz, 1H), 4.7 (p, *J* = 9.0 Hz, 1H), 3.8 (t, *J* = 5.2 Hz, 2H), 3.7 (q, *J* = 9.4 Hz, 2H), 3.1 – 3.1 (m, 8H), 3.0 – 2.9 (m, 2H), 2.4 (p, *J* = 8.3 Hz, 2H), 2.0 – 2.0 (m, 2H), 2.0 (q, *J* = 7.7 Hz, 2H), 1.6 (h, *J* = 8.0 Hz, 2H).

^{13}C NMR (126 MHz, $CDCl_3$) δ 165.4, 164.0, 154.4, 151.9, 151.8, 147.5, 142.1, 132.2, 128.3, 127.8, 127.3, 112.8, 112.7, 101.0, 57.9, 50.8, 50.3, 45.8, 41.9, 39.5, 30.2, 24.8.

LRMS (ESI) *m/z* calcd for $[C_{26}H_{32}N_8O_2 + H]^+$ = 489.3, found 489.4.

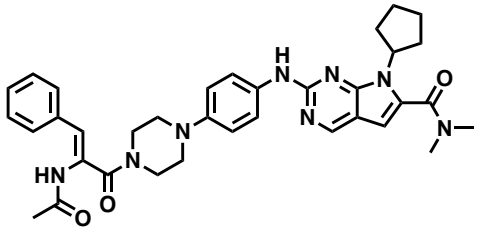

EST1059

General Procedure A was followed with 2-(acetylamino)-3-phenyl-2-propenoic acid (12.7 mg, 0.06 mmol), HATU (43.8 mg, 0.12 mmol), DIPEA (0.04 mL, 0.23 mmol), and ribociclib (25.0 mg, 0.06 mmol). The crude residue was purified by silica gel chromatography (0-10% MeOH in DCM) to afford 34.2 mg (96%) of the title compound as a yellow film.

^{1}H NMR (700 MHz, DMSO) δ 10.84 (s, 1H), 10.11 (s, 1H), 8.93 (s, 1H), 7.95 (d, *J* = 2.6 Hz, 2H), 7.75 (d, *J* = 8.9 Hz, 1H), 7.68 (d, *J* = 8.4 Hz, 2H), 7.63 (d, *J* = 8.3 Hz, 2H), 7.49 (d, *J* = 15.2 Hz, 1H), 7.23 (d, *J* = 15.3 Hz, 1H), 6.76 (s, 1H), 4.80 (p, *J* = 8.9 Hz, 1H), 3.91 (s, 2H), 3.77 (s, 2H), 3.22 (s, 4H), 3.06 (s, 6H), 2.40 – 2.31 (m, 2H), 2.07 (s, 3H), 2.05 – 2.00 (m, 2H), 1.99 – 1.93 (m, 2H), 1.66 (m, 2H).

^{13}C NMR (151 MHz, DMSO) δ 169.0, 165.2, 162.9, 153.0, 152.0, 149.7, 145.1, 142.4, 142.1, 141.1, 134.9, 130.2, 129.3, 119.3, 116.5, 115.0, 113.9, 101.4, 79.6, 57.5, 49.5, 49.1, 48.8, 45.1, 41.7, 39.2, 35.0, 30.5, 24.7, 24.5.

LRMS (ESI) *m/z* calcd for $[C_{35}H_{40}N_8O_3 + H]^+$ = 621.8, found 622.3.

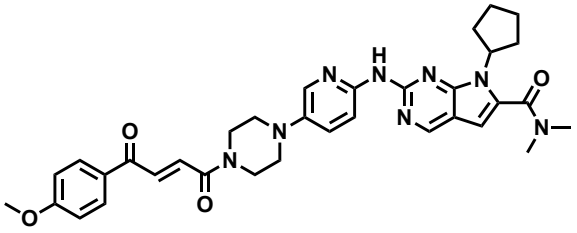

EST1060

General Procedure D was followed with *trans*-3-(4-methoxybenzoyl)acrylic acid (99.6 mg, 0.48 mmol), T3P (0.46 mL, 0.72 mmol), DIPEA (0.25 mL, 1.5 mmol), and ribociclib (216.0 mg, 0.57 mmol). The crude residue was purified by silica gel chromatography (0-10% MeOH in DCM). The resultant dark yellow oil was triturated in diethyl ether to afford 199.3 mg (83% - *E:Z* = >99:<1) of the title compound as an orange powder.

^{1}H NMR (500 MHz, $CDCl_3$) δ 8.75 (s, 2H), 8.28 (d, *J* = 8.1 Hz, 1H), 8.06 – 8.01 (m, 3H), 7.98 (d, *J* = 14.9 Hz, 1H), 7.50 (d, *J* = 15.0 Hz, 1H), 7.36 (dd, *J* = 9.1, 2.9 Hz, 1H), 7.00 – 6.93 (m, 2H), 6.45 (s, 1H), 4.78 (p, *J* = 8.9 Hz, 1H), 3.92 (t, *J* = 5.2 Hz, 2H), 3.88 (s, 3H), 3.82 (t, *J* = 5.1 Hz, 2H), 3.17 (t, *J* = 5.2 Hz, 4H), 3.14 (s, 6H), 2.60 – 2.49 (m, 2H), 2.11 – 1.97 (m, 4H), 1.73 – 1.63 (m, 2H).

^{13}C NMR (126 MHz, $CDCl_3$) δ 187.7, 164.2, 164.1, 164.1, 154.5, 151.9, 151.8, 147.7, 141.9, 134.7, 132.1, 131.3, 131.3, 130.0, 127.6, 114.1, 112.7, 112.5, 101.0, 57.9, 55.6, 50.9, 50.3, 46.0, 42.2, 39.5, 35.2 30.2, 24.7.

HRMS (ESI) *m/z* calcd for $[C_{34}H_{38}N_8O_4 + H]^+$ = 623.3016, found 623.3086.

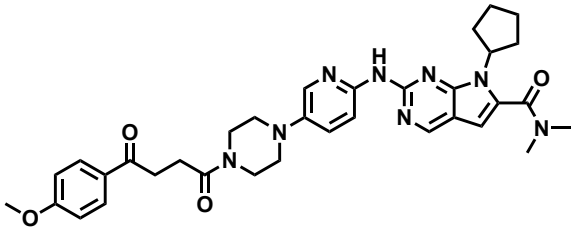

JP-2-230

A modified **General Procedure A** was followed with 3-(4-Methoxybenzoyl)propionic acid (15.9 mg, 0.08 mmol), HATU (25.5 mg, 0.07 mmol), DIPEA (0.04 mL, 0.23 mmol), and ribociclib (27.6 mg, 0.06 mmol). A precipitate had formed during the reaction which was vacuum filtered and washed with hexanes. The yellow precipitate was dissolved in DCM and dry loaded onto silica gel and was purified by silica gel chromatography (0-7% MeOH in DCM) to afford 28.9 mg (73%) of the title compound as a yellow-white powder.

^{1}H NMR (700 MHz, $CDCl_3$) δ 8.74 (s, 1H), 8.43 (s, 1H), 8.38 (d, *J* = 9.0 Hz, 1H), 8.07 (d, *J* = 2.9 Hz, 1H), 8.02 – 7.98 (m, 2H), 7.33 (dd, *J* = 9.1, 2.9 Hz, 1H), 6.95 – 6.91 (m, 2H), 6.44 (s, 1H), 4.79 (p, *J* = 8.9 Hz, 1H), 3.86 (s, 3H), 3.81 (t, *J* = 5.1 Hz, 2H), 3.76 (t, *J* = 5.1 Hz, 2H), 3.34 (t, *J* = 6.6 Hz, 2H), 3.18 (t, *J* = 5.1 Hz, 2H), 3.15 (s, 6H), 3.11 (t, *J* = 5.2 Hz, 2H), 2.82 (t, *J* = 6.6 Hz, 2H), 2.62 – 2.54 (m, 2H), 2.11 – 2.00 (m, 4H), 1.75 – 1.67 (m, 2H).

^{13}C NMR (151 MHz, $CDCl_3$) δ 197.6, 170.4, 164.1, 163.5, 154.6, 152.0, 151.9, 147.6, 142.1, 137.5, 132.0, 130.4, 129.9, 127.3, 113.7, 112.6, 112.4, 101.0, 57.9, 55.5, 50.6, 50.3, 45.4, 41.7, 39.5, 35.2, 33.2, 30.2, 27.1, 24.7.

HRMS (ESI) *m/z* calcd for $[C_{34}H_{40}N_8O_4 + H]^+$ = 625.3173, found 625.3242.

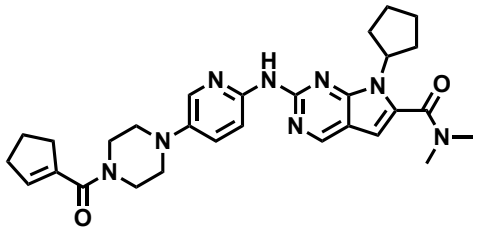

EST1061

General Procedure A was followed with 1-cyclopentenecarboxylic acid (6.5 mg, 0.06 mmol), HATU (43.8 mg, 0.12 mmol), DIPEA (0.04 mL, 0.23 mmol), and ribociclib (25.0 mg, 0.06 mmol). The crude residue was purified by silica gel chromatography (0-10% MeOH in DCM) to afford 23.3 mg (77%) of the title compound as a yellow powder.

^{1}H NMR (500 MHz, $CDCl_3$) δ 8.75 (s, 1H), 8.02 (s, 1H), 7.94 (d, *J* = 2.9 Hz, 1H), 7.50 – 7.42 (m, 1H), 6.47 (s, 1H), 5.93 (p, *J* = 2.2 Hz, 1H), 4.77 (p, *J* = 8.9 Hz, 1H), 3.78 (s, 4H), 3.21 – 3.08 (m, 10H), 2.63 (tq, *J* = 7.5, 2.4 Hz, 2H), 2.54 – 2.42 (m, 4H), 2.12 – 1.99 (m, 4H), 1.96 (p, *J* = 7.6 Hz, 2H), 1.67 (h, *J* = 8.4 Hz, 2H).

^{13}C NMR (151 MHz, $CDCl_3$) δ 168.6, 163.9, 154.1, 152.0, 151.4, 147.1, 142.2, 138.1, 133.1, 132.7, 113.0, 101.0, 58.0, 53.8, 50.5, 39.5, 35.2, 34.5, 33.3, 30.3, 24.8, 22.9, 18.7, 17.5.

LRMS (ESI) *m/z* calcd for $[C_{29}H_{36}N_8O_2 + H]^+$ = 529.3, found 529.4.

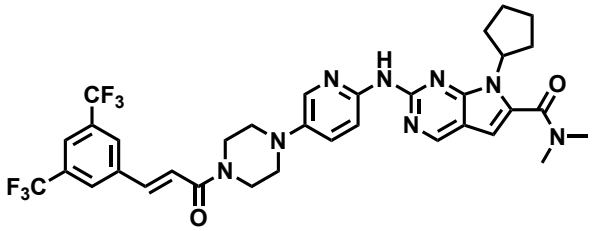

KN1002

General Procedure A was followed with *trans*-3,5-bis(trifluoromethyl)cinnamic acid (14.6 mg, 0.06 mmol), HATU (43.8 mg, 0.12 mmol), DIPEA (0.04 mL, 0.23 mmol), and ribociclib (25.0 mg, 0.06 mmol). The crude residue was purified by silica gel chromatography (0-10% MeOH in DCM) to afford 14.5 mg (40%) of the title compound as a yellow film.

^{1}H NMR (500 MHz, $CDCl_3$) δ 8.65 (s, 1H), 8.28 (s, 1H), 7.97 (d, *J* = 3.0 Hz, 2H), 7.87 (s, 2H), 7.79 (s, 1H), 7.68 (d, *J* = 15.4 Hz, 1H), 7.30 (dd, *J* = 9.2, 2.9 Hz, 1H), 6.99 (d, *J* = 15.4 Hz, 1H), 6.38 (s, 1H), 4.73 (t, *J* = 8.9 Hz, 1H), 3.88 (s, 2H), 3.82 (d, *J* = 13.7 Hz, 2H), 3.13 (d, *J* = 8.6 Hz, 4H), 3.09 (s, 6H), 2.50 (dq, *J* = 15.6, 7.3 Hz, 2H), 2.06 – 1.92 (m, 4H), 1.65 (dt, *J* = 12.6, 5.1 Hz, 2H).

^{13}C NMR (126 MHz, $CDCl_3$) δ 164.4, 164.2, 154.4, 151.9, 151.8, 147.6, 142.0, 139.9, 137.5, 137.2, 132.4 (q, $^{2}J_{CF}$ = 33.4 Hz), 132.1, 127.5, 126.3, 124.1, 122.9 (q, $^{1}J_{CF}$ = 273.0 Hz), 122.0, 120.7, 119.8, 112.7, 112.6, 112.6, 101.1, 57.9, 50.8, 50.3, 49.9, 49.8, 49.6, 49.4, 49.3, 45.9, 42.3, 39.5, 35.2, 30.1, 24.7.

LRMS (ESI) *m/z* calcd for $[C_{34}H_{34}F_6N_8O_2 + H]^+$ = 701.3, found 701.4.

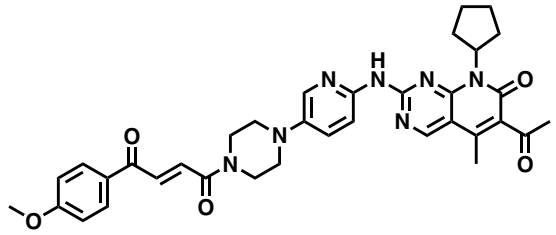

EST1089

General Procedure A was followed with 4-methoxycinnamic acid (13.8 mg, 0.06 mmol), HATU (42.5 mg, 0.11 mmol), DIPEA (0.04 mL, 0.23 mmol), and palbociclib (25.0 mg, 0.06 mmol). The crude residue was purified by silica gel chromatography (0-10% MeOH in DCM) to afford 26.1 mg (74% - *E:Z* = >99:<1) of the title compound as a yellow film.

^{1}H NMR (500 MHz, $CDCl_3$) δ 8.86 (s, 1H), 8.22 (d, *J* = 9.0 Hz, 1H), 8.09 (d, *J* = 2.9 Hz, 1H), 8.08 – 8.02 (m, 2H), 8.00 (d, *J* = 14.9 Hz, 1H), 7.52 (d, *J* = 14.8 Hz, 1H), 7.35 (dd, *J* = 9.1, 3.0 Hz, 1H), 7.01 – 6.95 (m, 2H), 5.88 (p, *J* = 8.9 Hz, 1H), 3.94 (t, *J* = 5.2 Hz, 2H), 3.89 (s, 3H), 3.85 (t, *J* = 5.1 Hz, 2H), 3.22 (t, *J* = 5.2 Hz, 4H), 2.54 (s, 3H), 2.38 (s, 3H), 2.36 – 2.30 (m, 1H), 2.12 – 2.01 (m, 2H), 1.89 (dddd, *J* = 15.4, 13.0, 7.6, 4.7 Hz, 2H), 1.75 – 1.64 (m, 3H).

^{13}C NMR (151 MHz, $CDCl_3$) δ 202.6, 187.6, 164.3, 164.1, 161.4, 158.0, 157.2, 155.5, 145.8, 143.0, 141.7, 137.3, 134.9, 131.3, 131.1, 130.9, 129.9, 126.9, 114.2, 113.6, 107.9, 55.6, 54.1, 53.4, 50.4, 49.8, 45.8, 42.1, 31.5, 28.1, 25.8, 22.7, 14.0.

HRMS (ESI) *m/z* calcd for $[C_{35}H_{37}N_7O_5 + H]^+$ = 636.2929, found 636.2935.

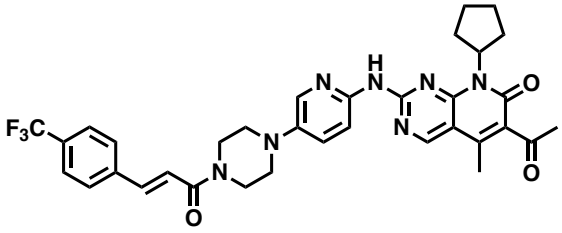

EST1090

General Procedure A was followed with *trans*-4-(trifluoromethyl)cinnamic acid (14.5 mg, 0.07 mmol), HATU (42.5 mg, 0.11 mmol), DIPEA (0.04 mL, 0.23 mmol), and palbociclib (0.25, 0.06 mmol). The crude residue was purified by silica gel chromatography (0-100% EtOAc in Hexanes) to afford 22.8 mg (63%) of the title compound as a yellow film.

^{1}H NMR (500 MHz, $CDCl_3$) δ 8.87 (s, 1H), 8.74 (s, 1H), 8.22 (d, *J* = 9.1 Hz, 1H), 8.09 (d, *J* = 2.9 Hz, 1H), 7.72 (d, *J* = 15.4 Hz, 1H), 7.64 (s, 4H), 7.37 (dd, *J* = 9.1, 3.0 Hz, 1H), 7.00 (d, *J* = 15.5 Hz, 1H), 5.88 (p, *J* = 8.9 Hz, 1H), 4.01 – 3.81 (m, 4H), 3.23 (t, *J* = 5.1 Hz, 4H), 2.54 (s, 3H), 2.38 (s, 3H), 2.37 – 2.31 (m, 2H), 2.07 (tdd, *J* = 11.9, 9.9, 5.2 Hz, 2H), 1.92 – 1.84 (m, 2H), 1.69 (tdd, *J* = 10.9, 6.6, 4.0 Hz, 2H).

^{13}C NMR (126 MHz, $CDCl_3$) δ 202.6, 164.9, 161.4, 158.0, 157.2, 155.6, 145.8, 143.1, 141.8, 141.6, 138.5 (d, $^5J_{CF}$ = 1.4 Hz) , 137.1, 131.4 (q, $^2J_{CF}$ = 32.7 Hz), 130.9, 128.0, 126.9, 125.8 (q, $^3J_{CF}$ = 3.8 Hz), 123.9 (d, $^1J_{CF}$ = 272.1 Hz), 119.2, 113.7, 107.9, 54.1, 50.3, 49.8, 45.7, 42.1, 31.5, 28.1, 25.8, 14.0.

HRMS (ESI) *m/z* calcd for $[C_{34}H_{34}F_3N_7O_3 + H]^+$ = 646.2748, found 646.2741.

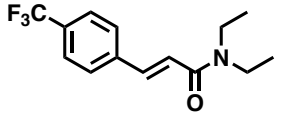

KN1026

General Procedure A was followed with *trans*-4-(trifluoromethyl)cinnamic acid (100.0 mg, 0.06 mmol), HATU (43.8 mg, 0.12 mmol), DIPEA (0.04 mL, 0.23 mmol), and *N,N*-diethylamine (0.05, 0.48 mmol). The crude residue was purified by silica gel chromatography (0-60% EtOAC in Hexanes) to afford 66.0 mg (50%) of the title compound as a yellow film.

^{1}H NMR (500 MHz, $CDCl_3$) δ 7.63 (d, *J* = 15.4 Hz, 1H), 7.54 (s, 4H), 6.83 (d, *J* = 15.4 Hz, 1H), 3.42 (dq, *J* = 9.8, 7.1 Hz, 4H), 1.19 (t, *J* = 7.2 Hz, 3H), 1.12 (t, *J* = 7.1 Hz, 3H).

^{13}C NMR (126 MHz, $CDCl_3$) δ 165.1, 140.5, 138.9 (d, $^5J_{CF}$ = 1.4 Hz), 131.0 (q, $^2J_{CF}$ = 32.5 Hz), 127.9, 125.7 (q, $^3J_{CF}$ = 3.8 Hz), 123.9 (q, $^1J_{CF}$ = 272.1 Hz), 120.3, 42.4, 41.2, 15.1, 13.1.

LRMS (ESI) *m/z* calcd for $[C_{14}H_{16}F_3NO + H]^+$ = 272.1, found 272.2.

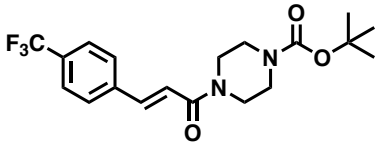

EST1096

General Procedure A was followed with *trans*-4-(trifluoromethyl)cinnamic acid (100.0 mg, 0.46 mmol), HATU (43.8 mg, 0.12 mmol), DIPEA (0.04 mL, 0.23 mmol), and 1-boc-piperazine (94.7 mg, 0.51 mmol). The crude residue was purified by silica gel chromatography (0-70% EtOAc in Hexanes) to afford 72.5 mg (41%) of the title compound as a white powder.

^{1}H NMR (500 MHz, $CDCl_3$) δ 7.62 (d, *J* = 15.4 Hz, 1H), 7.55 (s, 4H), 6.87 (d, *J* = 15.4 Hz, 1H), 3.60 (s, 4H), 3.42 (dd, *J* = 6.6, 3.9 Hz, 4H), 1.41 (s, 9H).

^{13}C NMR (151 MHz, $CDCl_3$) δ 165.0, 154.5, 141.4, 138.5, 131.3 (q, $^2J_{CF}$ = 32.6 Hz), 127.9, 125.8 (q, $^3J_{CF}$ = 3.7 Hz), 123.9 (q, $^1J_{CF}$ = 272.3 Hz), 119.3, 80.4, 45.7, 42.0, 28.4.

LRMS (ESI) *m/z* calcd for $[C_{19}H_{23}F_3N_2O_3 + Na]^+$ = 407.2, found 407.2.

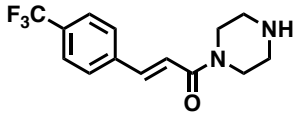

EST1102

General Procedure E was followed with **EST1096** (47.3 mg, 0.12 mmol), and TFA (0.3 mL, 3.94 mmol) for 2 hours. The crude residue was purified by silica gel chromatography (0-17% MeOH in DCM) using a Biotage® Sfär KP-Amino D cartridge to afford 14.5 mg (41%) of the title compound as a white film.

^{1}H NMR (500 MHz, $CDCl_3$) δ 7.64 (d, *J* = 15.5 Hz, 1H), 7.59 (s, 4H), 6.93 (d, *J* = 15.4 Hz, 1H), 3.72 – 3.66 (m, 2H), 3.64 – 3.58 (m, 2H), 2.89 (t, *J* = 5.0, 5.0 Hz, 4H), 1.80 (s, 1H).

^{13}C NMR (126 MHz, $CDCl_3$) δ 164.9, 141.3, 138.6, 131.2 (q, $^2J_{CF}$ = 32.6 Hz), 127.9, 125.8 (q, $^3J_{CF}$ = 3.8 Hz), 125.0, 122.8 (q, $^1J_{CF}$ = 272.0 Hz), 119.4, 46.5, 46.1, 45.5, 42.7.

LRMS (ESI) *m/z* calcd for $[C_{14}H_{15}F_3N_2O + H]+$ = 285.1, found 285.2.

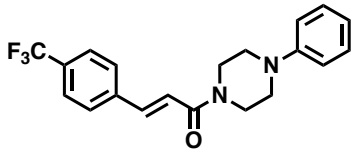

KN1023

General Procedure A was followed with *trans*-4-(trifluoromethyl)cinnamic acid (200.0 mg, 0.93 mmol), HATU (703.6 mg, 1.85 mmol), DIPEA (0.64 mL, 3.7 mmol), and 1-phenylpiperazine (150.1 mg, 0.93 mmol). The crude residue was purified by silica gel chromatography (15-55% EtOAc in Hexanes) to afford 125.0 mg (37%) of the title compound as a yellow powder.

^{1}H NMR (500 MHz, $CDCl_3$) δ 7.62 (d, *J* = 15.4 Hz, 1H), 7.53 (s, 4H), 7.23 – 7.16 (m, 2H), 6.91 (d, *J* = 15.4 Hz, 1H), 6.83 (dd, *J* = 16.5, 7.9 Hz, 3H), 3.80 (br s, 2H), 3.72 (br s, 2H), 3.13 (m, 4H).

^{13}C NMR (126 MHz, $CDCl_3$) δ 164.9, 150.9, 141.3, 138.7, 131.2 (q, $^2J_{CF}$ = 32.5 Hz), 129.3, 128.0, 125.8 (q, $^3J_{CF}$ = 3.8 Hz), 124.0 (q, $^1J_{CF}$ = 272.2 Hz), 120.6, 119.6, 116.7, 49.9, 49.4, 45.9, 42.2.

LRMS (ESI) *m/z* calcd for $[C_{20}H_{19}F_3N_2O + H]^+$ = 361.1, found 361.2.

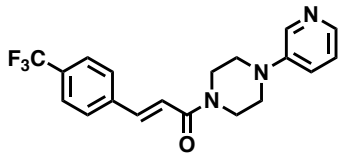

KN1017

General Procedure A was followed with *trans*-4-(trifluoromethyl)cinnamic acid (200.0 mg, 0.93 mmol), HATU (703.6 mg, 1.85 mmol), DIPEA (0.64 mL, 3.7 mmol), and 1-(3-pyridinyl)piperazine (151.1 mg, 0.93 mmol). The crude residue was purified by silica gel chromatography (0-10% MeOH in DCM) to afford 53.1 mg (16%) of the title compound as a yellow powder.

^{1}H NMR (500 MHz, $CDCl_3$) δ 8.34 – 8.29 (m, 1H), 8.14 (dd, *J* = 3.9, 2.1 Hz, 1H), 7.70 (d, *J* = 15.4 Hz, 1H), 7.61 (s, 4H), 7.23 – 7.14 (m, 2H), 6.98 (d, *J* = 15.5 Hz, 1H), 3.90 (br s, 2H), 3.83 (br s, 2H), 3.25 (m, 4H).

^{13}C NMR (126 MHz, $CDCl_3$) δ 164.9, 146.5, 141.7, 141.5, 139.1, 138.5, 131.3 (q, $^2J_{CF}$ = 32.6 Hz), 128.0, 125.8 (q, $^3J_{CF}$ = 3.8 Hz), 123.9 (q, $^1J_{CF}$ = 272.2 Hz), 123.6, 123.1, 119.2, 49.2, 48.7, 45.6, 41.9.

LRMS (ESI) *m/z* calcd for $[C_{19}H_{18}F_3N_3O + H]^+$ = 362.1, found 362.1.

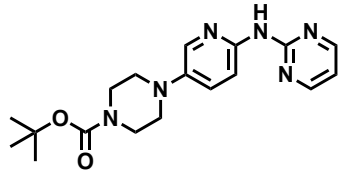

JP-2-195

A combination of 2-chloropyrimidine (100.0 mg, 0.95 mmol), tert-butyl 4-(6-aminopyridin-3-yl)piperazine-1-carboxylate (265.2 mg, 0.95 mmol), palladium (II) acetate (21.4 mg, 0.10 mmol), cesium carbonate (465.6 mg, 1.4 mmol), and Xantphos (82.7 mg, 0.14 mmol) was suspended in dioxane (10 mL) and heated to 120 °C overnight. The volatiles were

removed *in vacuo*, and the crude residue was purified by silica gel chromatography (0-5% MeOH in DCM) to afford 282.1 mg (91%) of the title compound as a beige solid.
^{1}H NMR (700 MHz, $CDCl_3$) δ 8.50 (d, *J* = 4.8 Hz, 2H), 8.30 (d, *J* = 9.0 Hz, 1H), 8.19 (s, 1H), 8.07 (d, *J* = 2.9 Hz, 1H), 7.35 (dd, *J* = 9.1, 3.0 Hz, 1H), 6.78 (t, *J* = 4.8 Hz, 1H), 3.63 (t, *J* = 5.1 Hz, 4H), 3.11 (t, *J* = 5.2 Hz, 4H), 1.51 (s, 9H).
^{13}C NMR (151 MHz, $CDCl_3$) δ 159.3, 158.0, 154.7, 146.6, 143.0, 137.4, 127.2, 113.0, 112.9, 80.0, 50.1, 28.4.
LRMS (ESI) *m/z* calcd for $[C_{18}H_{24}N_6O_2 + H]^+$ = 375.2, found 375.3.

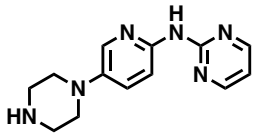

JP-2-198

General Procedure E was followed with **JP-2-195** (152.4 mg, 0.43 mmol), and TFA (1.1 mL, 13.7 mmol) for 2 hours. The crude material was used without further purification.

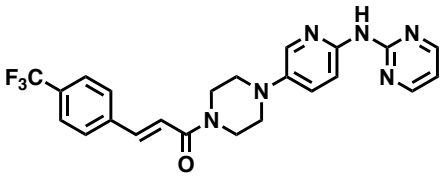

JP-2-200

General Procedure A was followed with *trans*-4-(trifluoromethyl)cinnamic acid (43.0 mg, 0.20 mmol), HATU (82.6 mg, 0.22 mmol), DIPEA (0.09 mL, 0.54 mmol), and **JP-2-198** (46.4 mg, 0.18 mmol). The crude residue was purified by silica gel chromatography (50-100% EtOAc in Hexanes followed by 0-5% MeOH in DCM) to afford 13.3 mg (16%, 2 steps) of the title compound as a yellow residue.
^{1}H NMR (700 MHz, $CDCl_3$) δ 8.48 (dd, *J* = 4.8, 1.6 Hz, 2H), 8.30 (d, *J* = 8.9 Hz, 1H), 8.14 (s, 1H), 8.05 (t, *J* = 2.2 Hz, 1H), 7.72 (dd, *J* = 15.5, 1.7 Hz, 1H), 7.64 (d, *J* = 1.7 Hz, 3H), 7.35 (dt, *J* = 9.1, 2.3 Hz, 1H), 7.00 (dd, *J* = 15.5, 1.6 Hz, 1H), 6.77 (td, *J* = 4.8, 1.7 Hz, 1H), 3.94 (br s, 2H), 3.85 (br s, 2H), 3.19 (m, 3H).
^{13}C NMR (126 MHz, $CDCl_3$) δ 164.9, 159.2, 158.0, 147.0, 142.5, 141.5, 138.6 (d, $^5J_{CF}$ = 1.3 Hz), 137.5, 131.3 (q, $^2J_{CF}$ = 32.8), 127.9, 127.4, 125.8 (q, $^3J_{CF}$ = 3.8 Hz), 123.9 (q, $^1J_{CF}$ = 272.2 Hz), 119.3, 113.1, 113.0, 50.7, 50.1, 45.8, 42.1, 29.7, 28.4.
LRMS (ESI) *m/z* calcd for $[C_{23}H_{21}F_3N_6O + H]^+$ = 455.2, found 455.2.

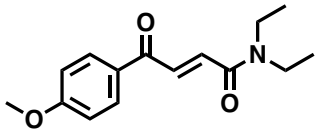

KN1025

General Procedure A was followed with *trans*-3-(4-methoxybenzoyl)acrylic acid (100.1 mg, 0.47 mmol), HATU (175.9 mg, 0.48 mmol), DIPEA (0.08 mL, 0.46 mmol), and *N,N*-diethylamine (25.0 mg, 0.06 mmol). The crude residue was purified by silica gel chromatography (0-55% EtOAc in Hexanes) to afford 16.3 mg (13%) of the title compound as a yellow film.

^{1}H NMR (700 MHz, $CDCl_3$) δ 8.06 – 8.04 (m, 2H), 7.99 (d, *J* = 14.8 Hz, 1H), 7.43 (d, *J* = 14.8 Hz, 1H), 6.99 – 6.95 (m, 2H), 3.89 (s, 3H), 3.52 – 3.45 (m, 4H), 1.24 (t, *J* = 7.2 Hz, 3H), 1.19 (t, *J* = 7.1 Hz, 3H).
^{13}C NMR (126 MHz, $CDCl_3$) δ 187.9, 164.5, 164.1, 134.0, 132.2, 131.3, 131.0, 130.1, 114.1, 55.6, 42.5, 41.2, 15.1, 13.0.
LRMS (ESI) *m/z* calcd for $[C_{15}H_{19}NO_3 + H]^+$ = 262.1, found 262.3.

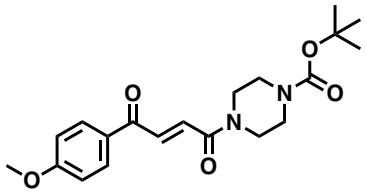

JP-2-190

General Procedure A was followed with *trans*-3-(4-methoxybenzoyl)acrylic acid (977 mg, 7.3 mmol), HATU (3.1 g, 8.1 mmol), DIPEA (3.8 mL, 21.8 mmol), and 1-boc-piperazine (1.5 g, 8.0 mmol). The crude residue was purified by silica gel chromatography (0-50% EtOAc in Hexanes) to afford 1.59 g (58%) of the title compound as a yellow solid.
^{1}H NMR (500 MHz, $CDCl_3$) δ 8.04 (d, *J* = 8.6 Hz, 2H), 7.96 (dd, *J* = 15.4, 3.9 Hz, 1H), 7.46 (d, *J* = 14.9 Hz, 1H), 6.98 (d, *J* = 8.7 Hz, 2H), 3.89 (s, 3H), 3.72 (t, *J* = 5.4, 5.4 Hz, 2H), 3.62 (t, *J* = 5.2, 5.2 Hz, 2H), 3.49 (t, *J* = 5.2, 5.2 Hz, 4H), 1.48 (s, 9H).
^{13}C NMR (126 MHz, $CDCl_3$) δ 187.6, 164.2, 154.5, 134.8, 131.3, 131.2, 131.1, 129.9, 114.1, 114.0, 80.5, 55.6, 45.9, 42.1, 28.4.
LRMS (ESI) *m/z* calcd for $[C_{20}H_{26}N_2O_5 + Na]^+$ = 397.2, found 397.2.

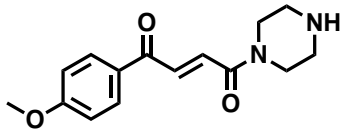

JP-2-196

General Procedure E was followed with **JP-2-190** (78.6 mg, 0.21 mmol), and TFA (0.51 mL, 6.7 mmol) for 1.5 hours. The reaction mixture was concentrated *in vacuo*, redissolved in DCM, and stirred with a saturated solution of $NaHCO_3$ (2 mL) for 30 min. The organic layer was separated, washed with brine, dried over Na_2SO_4, and concentrated *in vacuo*. The crude residue was purified by silica gel chromatography (0-12% MeOH in DCM) to afford 20.8 mg (81% - *E:Z* = 98.5:1.5) of the title compound as a white solid.
^{1}H NMR (700 MHz, $CDCl_3$) δ 7.99 (dd, *J* = 8.9, 1.9 Hz, 2H), 7.93 (dd, *J* = 14.9, 1.8 Hz, 1H), 7.37 (dd, *J* = 14.9, 1.8 Hz, 1H), 6.94 (dd, *J* = 9.0, 2.0 Hz, 2H), 3.97 (t, *J* = 5.4 Hz, 2H), 3.92 (t, *J* = 5.4 Hz, 2H), 3.85 (d, *J* = 1.9 Hz, 3H), 3.22 (t, *J* = 5.2 Hz, 4H), 2.73 (s, 1H).
^{13}C NMR (151 MHz, $CDCl_3$) δ 187.5, 164.5, 136.0, 131.5, 130.0, 129.7, 114.3, 55.7, 43.4, 43.1, 42.8, 38.9.
LRMS (ESI) *m/z* calcd for $[C_{15}H_{18}N_2O_3 + H]^+$ = 275.1, found 275.1.

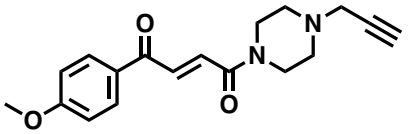

JP-2-253

A combination of **JP-2-196** (25.9 mg, 0.094 mmol) and potassium carbonate (15.7 mg, 0.11 mmol) was suspended in DMF (4 mL) and stirred at ambient temperature for 5 minutes. Propargyl bromide (0.01 mL, 0.13 mmol) was added, and the reaction mixture was heated to 90 °C overnight. The reaction mixture was concentrated *in vacuo*, and the crude residue was purified by silica gel chromatography (0-10% MeOH in DCM) to afford 11.7 mg (40% - *E:Z* = 96:4) of the title compound as a yellow oil.

^{1}H NMR (700 MHz, $CDCl_3$) δ 8.05 – 8.02 (m, 2H), 7.95 (d, *J* = 14.9 Hz, 1H), 7.47 (d, *J* = 14.9 Hz, 1H), 6.99 – 6.95 (m, 2H), 3.89 (s, 3H), 3.79 (t, *J* = 5.1 Hz, 2H), 3.68 (t, *J* = 5.1 Hz, 2H), 3.35 (d, *J* = 2.4 Hz, 2H), 2.60 (q, *J* = 4.6 Hz, 4H), 2.28 (d, *J* = 2.4 Hz, 1H).

^{13}C NMR (151 MHz, $CDCl_3$) δ 187.7, 164.2, 164.0, 134.4, 131.5, 131.3, 130.0, 114.1, 78.0, 73.8, 55.6, 51.9, 51.3, 46.8, 45.9, 42.1.

LRMS (ESI) *m/z* calcd for $[C_{18}H_{20}N_2O_3 + H]^+$ = 213.1, found 213.2.

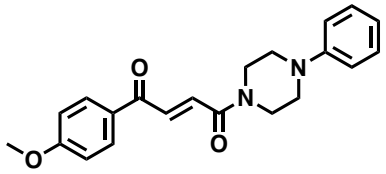

KN1021

General Procedure A was followed with *trans*-3-(4-methoxybenzoyl)acrylic acid (201.2 mg, 0.07 mmol), HATU (737.6 mg, 1.94 mmol), DIPEA (0.68 mL, 3.88 mmol), and 1-phenylpiperazine (25.0 mg, 0.06 mmol). The crude residue was purified by silica gel chromatography (15-55% EtOAc in Hexanes) to afford 255.6 mg (75%) of the title compound as an orange film.

^{1}H NMR (500 MHz, $CDCl_3$) δ 8.05 (d, *J* = 8.6 Hz, 2H), 7.99 (d, *J* = 14.9 Hz, 1H), 7.52 (d, *J* = 14.9 Hz, 1H), 7.30 (t, *J* = 7.7 Hz, 2H), 7.01 – 6.89 (m, 5H), 3.92 (m, 2H), 3.90 (s, 3H), 3.81 (t, *J* = 5.1 Hz, 2H), 3.23 (m, 4H).

^{13}C NMR (126 MHz, $CDCl_3$) δ 187.7, 164.2, 164.1, 150.8, 134.6, 131.4, 131.3, 130.0, 129.3, 120.8, 116.8, 114.1, 55.6, 50.0, 49.4, 46.0, 42.2.

LRMS (ESI) *m/z* calcd for $[C_{21}H_{22}N_2O_3 + H]^+$ = 351.2, found 351.1.

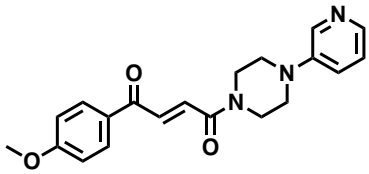

KN1018

General Procedure A was followed with *trans*-3-(4-methoxybenzoyl)acrylic acid (200.2 mg, 0.97 mmol), HATU (740.2 mg, 1.96 mmol), DIPEA (0.68 mL, 3.90 mmol), and 1-(3-pyridinyl)piperazine (158.3 mg, 0.97 mmol). The crude residue was purified by silica gel chromatography (0-8% MeOH in DCM) to afford 40.4 mg (12%) of the title compound as a yellow film.

^{1}H NMR (500 MHz, $CDCl_3$) δ 8.33 – 8.27 (m, 1H), 8.14 (dd, *J* = 3.8, 2.2 Hz, 1H), 8.06 – 8.00 (m, 2H), 7.97 (d, *J* = 14.9 Hz, 1H), 7.49 (d, *J* = 14.8 Hz, 1H), 7.22 – 7.14 (m, 2H), 6.99 – 6.92 (m, 2H), 3.90 (m, 2H), 3.86 (s, 3H), 3.80 (t, *J* = 5.2 Hz, 2H), 3.27 – 3.21 (m, 4H).
^{13}C NMR (126 MHz, $CDCl_3$) δ 187.6, 164.2, 164.1, 146.5, 141.7, 139.2, 134.8, 131.3, 131.1, 129.9, 123.6, 123.1, 114.1, 55.6, 49.2, 48.7, 45.7, 42.0.
LRMS (ESI) *m/z* calcd for $[C_{20}H_{21}N_3O_3 + H]^+$ = 352.2, found 352.1.

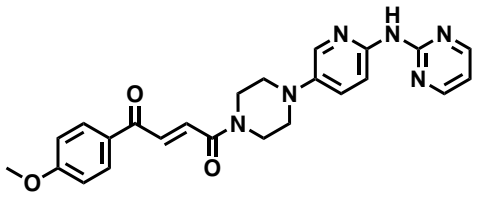

JP-2-199

General Procedure A was followed with *trans*-3-(4-methoxybenzoyl)acrylic acid (39.2 mg, 0.19 mmol), HATU (78.9 mg, 0.21 mmol), DIPEA (0.09 mL, 0.52 mmol), and **JP-2-198** (44.3 mg, 0.17 mmol). The crude residue was purified by silica gel chromatography (50-100% EtOAc in Hexanes followed by 0-5% MeOH in DCM) to afford 37.9 mg (49%) of the title compound as a yellow residue.
^{1}H NMR (700 MHz, $CDCl_3$) δ 8.77 (s, 1H), 8.50 (d, *J* = 4.8 Hz, 2H), 8.31 (d, *J* = 9.1 Hz, 1H), 8.10 (d, *J* = 2.9 Hz, 1H), 8.05 (d, *J* = 8.4 Hz, 2H), 7.99 (d, *J* = 14.8 Hz, 1H), 7.52 (d, *J* = 14.6 Hz, 1H), 7.34 (dd, *J* = 9.0, 2.9 Hz, 1H), 6.98 (d, *J* = 8.4 Hz, 2H), 6.76 (t, *J* = 4.9 Hz, 1H), 3.93 (t, *J* = 5.4 Hz, 2H), 3.89 (s, 3H), 3.83 (t, *J* = 5.1 Hz, 2H), 3.18 (q, *J* = 4.5 Hz, 4H).
^{13}C NMR (126 MHz, $CDCl_3$) δ 187.6, 164.2, 164.1, 159.3, 158.0, 147.2, 142.3, 137.5, 134.7, 131.3, 131.3, 130.0, 127.5, 114.1, 113.2, 112.9, 55.6, 50.7, 50.1, 45.9, 42.2, 29.7, 28.4.
LRMS (ESI) *m/z* calcd for $[C_{24}H_{24}N_6O_3 + H]^+$ = 445.2, found 445.2.

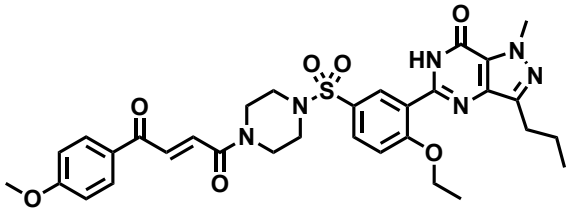

JP-2-201

The secondary amine **JP-2-196** (23.2 mg, 0.08 mmol) was dissolved in DCM (1 mL). DIPEA (0.1 mL, 0.5 mmol) was added, and the reaction mixture was stirred at ambient temperature for 5 minutes. A solution of 5-(5-Chlorosulfonyl-2-ethoxyphenyl)-1-methyl-3-propyl-1,6-dihydro-7H-pyrazolo[4,3-d]pyrimidin-7-one (34.7 mg, 0.08 mmol) in DCM (0.5 mL) was added dropwise to the reaction mixture and allowed to stir at ambient temperature for 2 hours. The volatiles were removed *in vacuo*, and the crude residue was purified by silica gel chromatography (25-100% EtOAc in Hexanes) to afford 49.5 mg (90% - *E:Z* = 90:10) of the title compound as a yellow oil.
^{1}H NMR (500 MHz, $CDCl_3$) δ 10.73 (s, 1H), 8.73 (d, *J* = 2.4 Hz, 1H), 7.92 – 7.89 (m, 2H), 7.82 (d, *J* = 14.9 Hz, 1H), 7.75 (dd, *J* = 8.7, 2.4 Hz, 1H), 7.27 (d, *J* = 14.8 Hz, 1H), 7.09

(d, *J* = 8.8 Hz, 1H), 6.89 – 6.84 (m, 2H), 4.30 (q, *J* = 7.0 Hz, 2H), 4.19 (s, 3H), 3.80 (s, 3H), 3.79 – 3.76 (m, 2H), 3.68 (t, *J* = 5.0 Hz, 2H), 3.05 (q, *J* = 5.4 Hz, 4H), 2.86 (t, *J* = 7.6 Hz, 2H), 1.79 (h, *J* = 7.4 Hz, 2H), 1.57 (t, *J* = 7.0 Hz, 3H), 0.96 (t, *J* = 7.4 Hz, 3H).
^{13}C NMR (126 MHz, $CDCl_3$) δ 187.3, 164.3, 164.0, 159.6, 153.6, 147.0, 146.2, 138.3, 135.2, 131.5, 131.3, 131.1, 130.5, 129.7, 128.5, 124.5, 121.4, 114.1, 113.3, 77.3, 66.2, 55.6, 46.4, 45.8, 45.4, 41.6, 38.2, 27.7, 22.3, 14.5, 14.1.
HRMS (ESI) *m/z* calcd for $[C_{32}H_{36}N_6O_7S + H]^+$ = 649.2366, found 649.2450.

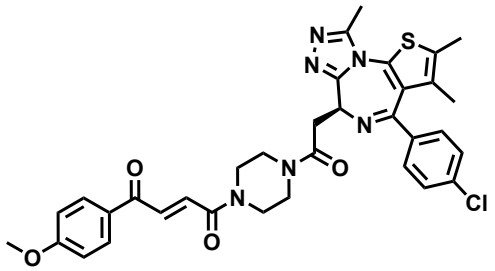

JP-2-197

General Procedure A was followed with (6S)-4-(4-chlorophenyl)-2,3,9-trimethyl-6H-thieno[3,2-f][1,2,4]triazolo[4,3-a][1,4]diazepine-6-acetic acid (JQ1-Acid) (92.5 mg, 0.23 mmol), HATU (93.0 mg, 0.24 mmol), DIPEA (0.1 mL, 0.6 mmol), and **JP-2-196** (55.0 mg, 0.2 mmol). The crude residue was purified by silica gel chromatography (0-5% MeOH in DCM) to afford 108.6 mg (83%, 2 steps - *E:Z* = 89:11) of the title compound as a yellow powder.
^{1}H NMR (700 MHz, $CDCl_3$) δ 8.08 (d, *J* = 8.6 Hz, 2H), 8.02 (dd, *J* = 14.9, 6.5 Hz, 1H), 7.51 (dd, *J* = 14.9, 6.7 Hz, 1H), 7.42 (d, *J* = 7.8 Hz, 2H), 7.39 – 7.34 (m, 2H), 7.01 (d, *J* = 8.5 Hz, 2H), 4.83 (td, *J* = 6.9, 2.9 Hz, 1H), 4.08 – 3.95 (m, 2H), 3.93 (s, 3H), 3.91 – 3.70 (m, 5H), 3.71 – 3.49 (m, 3H), 2.69 (s, 3H), 2.43 (s, 3H), 1.70 (s, 3H).
^{13}C NMR (151 MHz, $CDCl_3$) δ 187.8, 187.7, 169.3, 169.2, 164.5, 164.2, 164.2, 164.1, 155.6, 150.0, 136.7, 136.5, 134.9, 131.9, 131.3, 131.0, 131.0, 131.0, 130.9, 130.5, 129.7, 129.7, 128.6, 114.1, 114.0, 55.5, 54.2, 54.1, 45.8, 45.8, 45.6, 45.2, 42.1, 42.0, 41.8, 41.4, 35.1, 29.6, 14.2, 13.0, 11.6.
HRMS (ESI) *m/z* calcd for $[C_{34}H_{33}ClN_6O_4S + H]^+$ = 657.1973, found 657.2054.

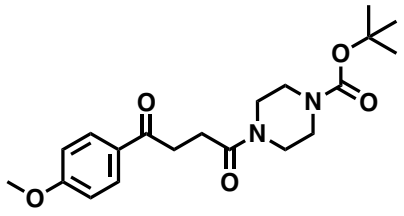

JP-2-229

General Procedure A was followed with 3-(4-methoxybenzoyl)propionic acid (100.7 mg, 0.48 mmol), HATU (206.8 mg, 0.54 mmol), DIPEA (0.25 mL, 1.45 mmol), and 1-boc-piperazine (104.7 mg, 0.56 mmol). The crude residue was purified by silica gel chromatography (0-100% EtOAc in Hexanes) to afford 132.8 mg (73%) of the title compound as a white powder.

^{1}H NMR (700 MHz, $CDCl_3$) δ 7.93 (d, *J* = 8.6 Hz, 2H), 6.87 (d, *J* = 8.5 Hz, 2H), 3.80 (s, 3H), 3.58 – 3.52 (m, 2H), 3.52 – 3.47 (m, 2H), 3.44 (d, *J* = 7.5 Hz, 2H), 3.35 (t, *J* = 5.5 Hz, 2H), 3.26 (t, *J* = 6.5 Hz, 2H), 2.71 (t, *J* = 6.6 Hz, 2H), 1.43 (s, 9H).
^{13}C NMR (151 MHz, $CDCl_3$) δ 197.5, 170.6, 163.5, 154.5, 130.3, 129.8, 113.7, 80.2, 55.4, 45.2, 41.6, 33.1, 29.7, 28.4, 27.1.
LRMS (ESI) *m/z* calcd for $[C_{20}H_{28}N_2O_5 + H]^+$ = 377.5, found 377.2.

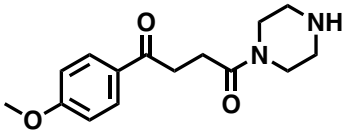

JP-2-231

General Procedure E was followed with **JP-2-229** (23.6 mg, 0.06 mmol), and TFA (0.13 mL, 1.7 mmol) for 2.5 hours. The crude material was used without further purification.

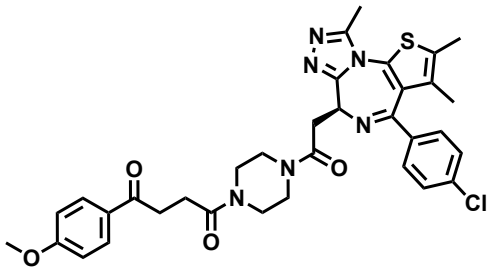

JP-2-232

General Procedure A was followed with (6S)-4-(4-chlorophenyl)-2,3,9-trimethyl-6H-thieno[3,2-f][1,2,4]triazolo[4,3-a][1,4]diazepine-6-acetic acid (JQ1-Acid) (26.1 mg, 0.07 mmol), HATU (27.3 mg, 0.07 mmol), DIPEA (0.4 mL, 0.19 mmol), and **JP-2-231** (17.3 mg, 0.06 mmol). The crude residue was purified by silica gel chromatography (0-7% MeOH in DCM) to afford 38.8 mg (94%, 2 steps) of the title compound as a yellow-white foam.
^{1}H NMR (700 MHz, $CDCl_3$) δ 7.99 (d, *J* = 8.8 Hz, 2H), 7.39 (d, *J* = 8.2 Hz, 2H), 7.32 (dd, *J* = 8.6, 4.2 Hz, 2H), 6.95 – 6.91 (m, 2H), 4.79 (q, *J* = 6.7 Hz, 1H), 4.01 – 3.94 (m, 1H), 3.86 (s, 3H), 3.85 – 3.80 (m, 2H), 3.79 – 3.69 (m, 4H), 3.69 – 3.63 (m, 1H), 3.60 – 3.55 (m, 1H), 3.54 – 3.48 (m, 1H), 3.42 – 3.35 (m, 1H), 3.32 – 3.26 (m, 1H), 2.84 (tt, *J* = 16.0, 6.5 Hz, 1H), 2.78 – 2.73 (m, 1H), 2.65 (d, *J* = 2.8 Hz, 3H), 2.39 (s, 3H), 1.67 (s, 3H).
^{13}C NMR (151 MHz, $CDCl_3$) δ 197.5, 170.7, 169.4, 169.2, 163.9, 163.8, 163.6, 155.8, 149.9, 149.9, 136.8, 136.7, 132.2, 130.9, 130.9, 130.7, 130.7, 130.5, 130.4, 129.9, 129.8, 128.7, 113.7, 55.5, 54.6, 54.4, 45.9, 45.6, 45.5, 45.2, 41.8, 41.7, 41.6, 35.4, 35.3, 33.2, 33.2, 31.9, 29.7, 27.2, 27.1, 22.7, 14.4, 14.1, 13.1, 11.8.
HRMS (ESI) *m/z* calcd for $[C_{34}H_{35}ClN_6O_4S + H]^+$ = 659.2129, found 659.2207.

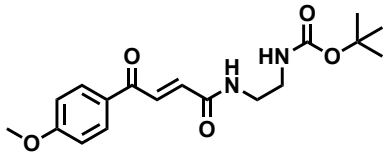

JP-2-216

General Procedure A was followed with *trans*-3-(4-methoxybenzoyl)acrylic acid (54.2 mg, 0.26 mmol), HATU (124.1 mg, 0.33 mmol), DIPEA (0.13 mL, 0.79 mmol), and *N*-boc-ethylenediamine (0.1 mL, 0.62 mmol). The crude residue was purified by silica gel chromatography (0-5% MeOH in DCM followed by 0-100% EtOAc in Hexanes) to afford 38.0 mg (42%) of the title compound as a brown residue, and 101.8 mg of a double addition byproduct. LRMS (ESI) of byproduct *m/z* calcd for $[C_{25}H_{40}N_4O_7 + H]^+$ = 509.3, found 509.3.

^{1}H NMR (500 MHz, $CDCl_3$) δ 8.1 – 8.0 (m, 2H), 7.9 (d, *J* = 14.96 Hz, 1H), 7.1 (s, 1H), 7.0 – 6.9 (m, 3H), 5.0 (d, *J* = 6.18 Hz, 1H), 3.9 (s, 3H), 3.5 (q, *J* = 5.48 Hz, 2H), 3.4 (q, *J* = 5.77 Hz, 2H), 1.4 (s, 9H).

^{13}C NMR (126 MHz, $CDCl_3$) δ 187.9, 164.9, 164.2, 157.1, 134.6, 133.2, 131.3, 130.0, 114.1, 80.0, 55.6, 41.4, 40.1, 28.4.

LRMS (ESI) *m/z* calcd for $[C_{18}H_{24}N_2O_5 + Na]^+$ = 371.2, found 371.1.

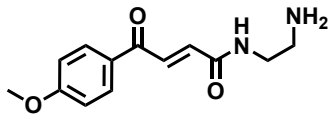

JP-2-218

General Procedure E was followed with **JP-2-216** (19.0 mg, 0.05 mmol), and TFA (0.13 mL, 1.8 mmol) for 40 minutes. The crude material was used without further purification.

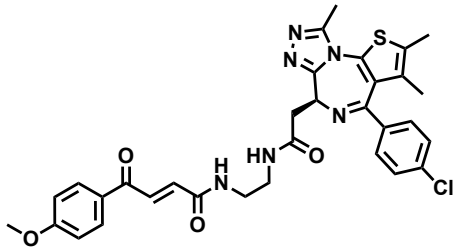

JP-2-219

General Procedure A was followed with (6S)-4-(4-chlorophenyl)-2,3,9-trimethyl-6H-thieno[3,2-f][1,2,4]triazolo[4,3-a][1,4]diazepine-6-acetic acid (JQ1-Acid) (24.6 mg, 0.06 mmol), HATU (27.0 mg, 0.07 mmol), DIPEA (0.04 mL, 0.23 mmol), and **JP-2-218** (13.5 mg, 0.05 mmol). The crude residue was purified by silica gel chromatography (0-6% MeOH in DCM) to afford 17.4 mg (51%, 2 steps - *E:Z* = 98:2) of the title compound as a yellow foam.

^{1}H NMR (600 MHz, $CDCl_3$) δ 8.02 – 7.98 (m, 2H), 7.95 (t, *J* = 5.6 Hz, 1H), 7.88 (s, 1H), 7.82 (q, *J* = 5.4 Hz, 1H), 7.39 – 7.36 (m, 2H), 7.29 (d, *J* = 7.4 Hz, 2H), 6.96 – 6.91 (m, 2H), 6.89 (d, *J* = 15.0 Hz, 1H), 4.71 (dd, *J* = 7.9, 6.2 Hz, 1H), 3.87 (s, 3H), 3.55 (qdt, *J* = 10.9, 6.8, 3.5 Hz, 5H), 3.46 (dd, *J* = 14.7, 6.2 Hz, 1H), 2.73 (s, 3H), 2.39 (s, 3H), 1.66 (s, 3H).

^{13}C NMR (151 MHz, $CDCl_3$) δ 188.0, 171.3, 164.8, 164.3, 164.0, 156.0, 150.4, 136.9, 136.4, 135.1, 132.6, 132.0, 131.2, 131.2, 131.0, 130.6, 130.2, 129.9, 128.7, 114.0, 55.5, 54.2, 40.3, 39.0, 38.9, 29.7, 14.4, 13.1, 11.8.

HRMS (ESI) *m/z* calcd for $[C_{32}H_{31}ClN_6O_4S + H]^+$ = 631.1816, found 631.1899.

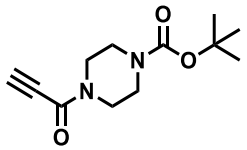

S1

To a solution of Boc-piperazine (7.2 g, 38.94 mmol) and DMAP (237 mg, 1.95 mmol) in DCM (45 mL) was added propiolic acid (3.0 g, 42.83 mmol) at ambient temperature. Next, DCC (5.6 g, 27.25 mmol) in DCM (5 mL) was added dropwise to the mixture at 0 °C, the mixture was stirred and warmed to ambient temperature over 1 hour. Once LCMS monitoring showed complete consumption of starting material, the reaction mixture was quenched with saturated $NaHCO_3$ aq. (20 mL) and extracted with EtOAc (20 mL x 3). The combined organic layers were washed by brine (50 mL), dried over Na_2SO_4, filtered and concentrated *in vacuo*. The crude residue was purified by silica gel chromatography (0-100% EtOAC in Petroleum Ether) to afford 7.2 g (78%) of the title compound as a yellow solid.

^{1}H NMR (400 MHz, $CDCl_3$) δ 3.75 (dd, *J* = 4.3, 6.2 Hz, 2H), 3.65 - 3.59 (m, 2H), 3.49 (dd, *J* = 4.3, 6.1 Hz, 2H), 3.45 - 3.40 (m, 2H), 3.16 (s, 1H), 1.48 (s, 9H).

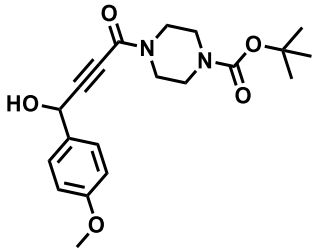

S2

To a solution of **S1** (2.0 g, 8.40 mmol) in THF (30 mL) was added dropwise n-BuLi (4.0 mL, 10.08 mmol) at -70 °C. The reaction was stirred at -70 °C for 30 mins. Then 4-methoxybenzaldehyde (914 mg, 6.72 mmol) and TMSCl (1.8 g, 16.80 mmol) was added dropwise to the mixture at -70 °C, the mixture was stirred and warmed to ambient temperature over 3 hours. The reaction mixture was quenched with ice water (200 mL), and extracted with EtOAc (200 mL x 2). The combined organic extracts were washed with brine (300 mL), dried over Na_2SO_4, filtered and concentrated *in vacuo*. The crude residue was purified by silica gel chromatography (0-100% EtOAc in Petroleum ether) to afford 1.3 g (41%) of the title compound as a white solid.

LCMS Rt = 0.454 min, M+23 (397.0), 71.7%.

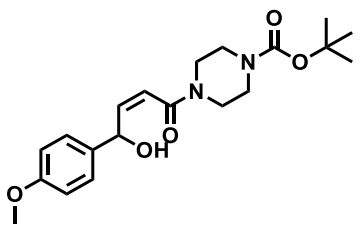

S3

A mixture of **S2** (300 mg, 0.80 mmol) and Lindlar's catalyst (30 mg) in THF (10 mL) was stirred at ambient temperature under a H_2 atmosphere (10 psi) for 2 hours. The reaction mixture was filtered and concentrated under reduced pressure to afford 300 mg of the title compound as a yellow solid, which was used without further purification.

^{1}H NMR (400 MHz, $CDCl_3$) δ 7.37 (d, J = 8.6 Hz, 2H), 6.90 - 6.86 (m, 2H), 6.28 (dd, J = 6.6, 11.9 Hz, 1H), 6.18 - 6.11 (m, 1H), 5.55 (br d, J = 5.1 Hz, 1H), 4.42 (br s, 1H), 3.81 - 3.79 (m, 3H), 3.68 - 3.61 (m, 2H), 3.49 - 3.41 (m, 6H), 1.48 (s, 9H).

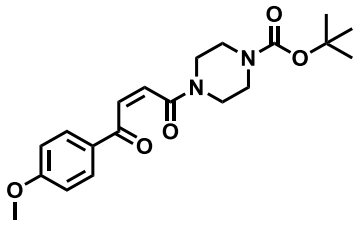

LE-21-PX17

To a mixture of **S3** (150 mg, 0.40 mmol) in DCM (5 mL) was added DMP (186 mg, 0.44 mmol) at 0 °C. The mixture was stirred and warmed to ambient temperature over 2 hours. The reaction mixture was filtered and concentrated *in vacuo* The crude residue was purified by silica gel chromatography (0-100% EtOAc in Petroleum Ether) to afford 53 mg (35%- *E:Z* = >99:<1) of the title compound as a white solid.

^{1}H NMR (400 MHz,$CDCl_3$) δ 7.98 - 7.93 (m, 2H), 7.03 (d, J = 11.9 Hz, 1H), 6.98 - 6.92 (m, 2H), 6.56 (d, J = 12.0 Hz, 1H), 3.89 (s, 3H), 3.65 (br s, 2H), 3.52 - 3.44 (m, 6H), 1.49 - 1.47 (m, 9H).

^{13}C NMR (126 MHz, $CDCl_3$) δ 188.6, 166.7, 164.0, 154.5, 134.4, 131.1, 129.7, 128.7, 114.0, 80.2, 55.5, 46.1, 41.1, 28.4.

HRMS (ESI) *m/z* calcd for $[C_{20}H_{26}N_2O_5 + Na]^+$ = 379.1820, found 379.1735.

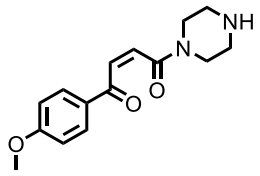

S4

General Procedure E was followed with **LE-21-PX17** (100.0 mg, 0.26 mmol), and TFA (0.4 mL) for 1 hour. The crude material was used without further purification.

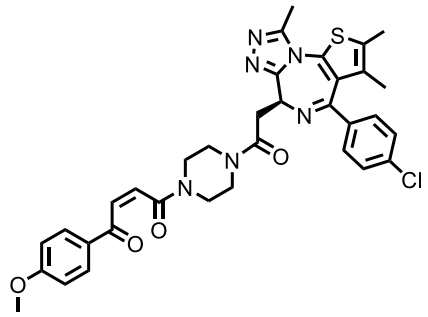

FB-84-GG64

General Procedure A was followed with (6S)-4-(4-chlorophenyl)-2,3,9-trimethyl-6H-thieno[3,2-f][1,2,4]triazolo[4,3-a][1,4]diazepine-6-acetic acid (JQ1-Acid) (144.0 mg, 0.36 mmol), HATU (152.1 mg, 0.40 mmol), DIPEA (0.16 mL, 0.94 mmol), and **S4** (100.0 mg, 0.36 mmol). The crude residue was purified by Prep-HPLC (NH_4HCO_3) to afford 31.2 mg (13%, 2 steps - *E:Z* = >99:<1) of the title compound as a white solid.

^{1}H NMR (500 MHz, $CDCl_3$) δ 7.89 (d, *J* = 8.5 Hz, 2H), 7.36 – 7.30 (m, 2H), 7.28 (d, *J* = 8.2 Hz, 2H), 6.99 (s, 1H), 6.93 – 6.85 (m, 2H), 6.52 (d, *J* = 11.8 Hz, 1H), 4.76 – 4.70 (m, 1H), 3.81 (s, 5H), 3.73 (s, 2H), 3.65 – 3.39 (m, 6H), 2.60 (s, 3H), 2.35 – 2.31 (m, 3H), 1.61 (d, *J* = 0.9 Hz, 3H).

^{13}C NMR (126 MHz, $CDCl_3$) δ 188.6, 169.3, 166.8, 164.0, 155.8, 149.9, 136.8, 136.7, 134.6, 134.5, 132.2, 131.1, 130.9, 130.7, 130.5, 129.8, 129.7, 128.7, 114.1, 55.6, 54.6, 54.4, 46.4, 45.9, 45.3, 41.7, 41.4, 41.2, 35.3, 14.4, 13.1, 11.9.

HRMS (ESI) *m/z* calcd for $[C_{34}H_{33}ClN_6O_4S + Na]^+$ = 679.2020, found 679.1867.

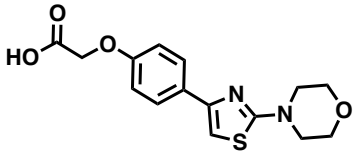

JP-2-215

A solution of *tert*-butyl 2-(4-(2-morpholinothiazol-4-yl)phenoxy)acetate (40.0 mg, 0.11 mmol) in 4 M hydrochloric acid in dioxane (0.7 mL) was stirred at ambient temperature overnight. The reaction mixture was diluted with toluene and the volatiles were removed *in vacuo* to yield a yellow-white solid which was used without further purification.

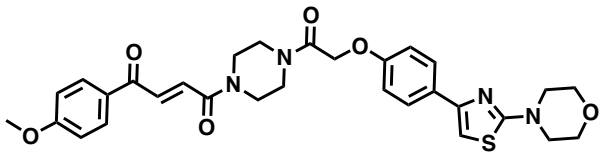

JP-2-217

General Procedure A was followed with 2-(4-(2-morpholinothiazol-4-yl)phenoxy)acetic acid (35.00 mg, 0.11 mmol), HATU (49.9 mg, 0.13 mmol), DIPEA (0.06 mL, 0.33 mmol), and **JP-2-196** (36.9 mg, 0.13 mmol). The crude residue was purified by silica gel chromatography (0-5% MeOH in DCM) to afford 34.6 mg (55%, 2 steps - *E:Z* = 93:7) of the title compound as a beige powder.

^{1}H NMR (700 MHz, $CDCl_3$) δ 8.03 (d, *J* = 8.6 Hz, 2H), 7.96 (dd, *J* = 14.9, 4.6 Hz, 1H), 7.79 – 7.76 (m, 2H), 7.43 (d, *J* = 14.7 Hz, 1H), 6.99 – 6.94 (m, 4H), 6.68 (s, 1H), 4.76 (d, *J* = 3.3 Hz, 2H), 3.89 (s, 3H), 3.85 – 3.82 (m, 4H), 3.73 (q, *J* = 6.3 Hz, 1H), 3.68 (p, *J* = 5.5 Hz, 5H), 3.64 – 3.59 (m, 2H), 3.54 – 3.50 (m, 4H).
^{13}C NMR (151 MHz, $CDCl_3$) δ 187.5, 171.2, 166.9, 164.4, 164.3, 157.1, 151.2, 135.1, 131.3, 130.8, 129.9, 129.3, 127.6, 114.5, 114.1, 100.5, 68.2, 68.0, 66.2, 55.6, 48.6, 46.1, 45.7, 45.2, 42.4, 42.0.
HRMS (ESI) *m/z* calcd for $[C_{30}H_{32}N_4O_6S + H]^+$ = 577.2043, found 577.2122.

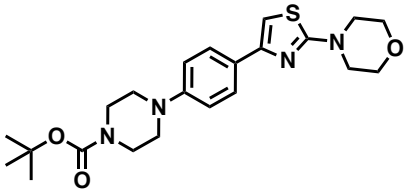

JP-2-221

A mixture of 4-(4-bromo-2-thiazolyl)morpholine (120.0 mg, 0.51 mmol), 4-(4-*tert*-butoxycarbonylpiperazinyl)phenylboronic acid pinacol ester (210.6, 0.54 mmol), cesium carbonate (485.9 mg, 1.5 mmol), and tetrakis(triphenylphosphine)palladium(0) (66.4 mg, 0.05 mmol) was suspended in DMF (12 mL) and stirred at 100 °C overnight. The reaction was quenched with 5% $LiCl_{(aq)}$ (60 mL) and extracted 3 times with DCM. The organic extracts were washed again with 5% $LiCl_{(aq)}$ and the organic extract was dried over Na_2SO_4, vacuum filtered, and the volatiles were removed *in vacuo*. The crude residue was purified by silica gel chromatography (0-50% EtOAc in Hexanes) to afford 28.8 mg (32%, BRSM) of the title compound as a white solid.
^{1}H NMR (700 MHz, $CDCl_3$) δ 7.75 – 7.72 (m, 2H), 6.93 – 6.90 (m, 2H), 6.65 (s, 1H), 3.85 – 3.81 (m, 4H), 3.58 (t, *J* = 5.2 Hz, 4H), 3.52 (dd, *J* = 5.9, 3.9 Hz, 4H), 3.16 (t, *J* = 5.1 Hz, 4H), 1.49 (s, 9H).
^{13}C NMR (126 MHz, $CDCl_3$) δ 171.1, 151.8, 150.7, 127.3, 127.2, 127.0, 116.8, 116.3, 99.7, 79.9, 66.3, 49.2, 48.6, 28.5.
LRMS (ESI) *m/z* calcd for $[C_{22}H_{30}N_4O_3S + H]^+$ = 431.6, found 431.2.

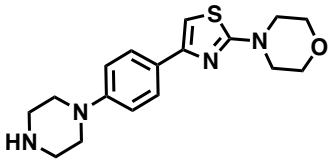

JP-2-223

General Procedure E was followed with **JP-2-221** (33.6 mg, 0.07 mmol), and TFA (0.18 mL, 2.4 mmol) for 30 minutes. The crude material was used without further purification.

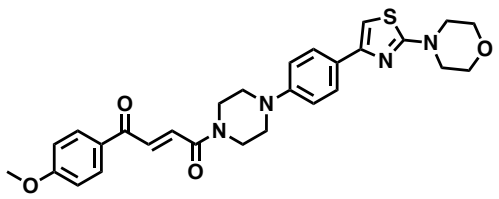

JP-2-224

General Procedure A was followed with *trans*-3-(4-methoxybenzoyl)acrylic acid (19.3 mg, 0.09 mmol), HATU (43.8 mg, 0.10 mmol), DIPEA (0.04 mL, 0.23 mmol), and **JP-2-223** (23.0 mg, 0.07 mmol). The crude residue was purified by silica gel chromatography (0-100% EtOAc in Hexanes) to afford 18.6 mg (51%, 2 steps - *E:Z* = 47:53) of the title compound as a light orange foam.

^{1}H NMR (700 MHz, $CDCl_3$) δ 8.07 – 8.03 (m, 2H), 7.99 (d, *J* = 14.8 Hz, 1H), 7.77 – 7.73 (m, 2H), 7.54 – 7.50 (m, 1H), 7.00 – 6.96 (m, 2H), 6.95 – 6.91 (m, 2H), 6.66 (s, 1H), 3.91 (t, *J* = 5.2 Hz, 2H), 3.89 (s, 3H), 3.83 (t, *J* = 4.9 Hz, 4H), 3.81 (d, *J* = 5.1 Hz, 2H), 3.52 (t, *J* = 4.9 Hz, 4H), 3.26 (q, *J* = 4.9 Hz, 4H).

^{13}C NMR (126 MHz, $CDCl_3$) δ 187.7, 171.2, 164.2, 164.1, 151.6, 150.1, 134.6, 131.3, 130.0, 127.7, 127.1, 116.4, 114.1, 99.9, 66.3, 55.6, 49.7, 49.1, 48.6, 45.9, 42.1.

HRMS (ESI) *m/z* calcd for $[C_{28}H_{30}N_4O_4S + H]^+$ = 519.1988, found 519.2067.

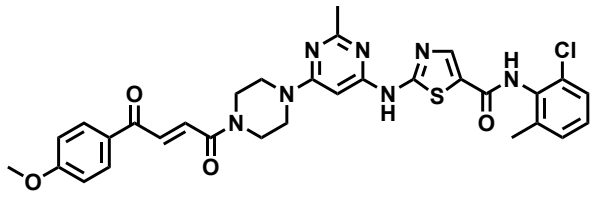

JP-2-227

General Procedure A was followed with *trans*-3-(4-methoxybenzoyl)acrylic acid (7.0 mg, 0.03 mmol), HATU (12.8 mg, 0.03 mmol), DIPEA (0.02 mL, 0.13 mmol), and *N*-deshydroxyethyl dasatinib (10.0 mg, 0.02 mmol). The crude residue was purified by silica gel chromatography (0-6% MeOH in DCM) to afford 12.8 mg (90% - *E:Z* = 93:7) of the title compound as a yellow solid.

^{1}H NMR (700 MHz, $CDCl_3$) δ 8.00 – 7.95 (m, 3H), 7.92 (d, *J* = 14.9 Hz, 1H), 7.42 (d, *J* = 14.9 Hz, 1H), 7.24 (d, *J* = 7.7 Hz, 1H), 7.15 – 7.07 (m, 2H), 6.95 – 6.91 (m, 2H), 5.87 (s, 1H), 3.83 (s, 3H), 3.77 (t, *J* = 5.3 Hz, 2H), 3.70 (p, *J* = 5.2 Hz, 4H), 3.62 (d, *J* = 5.5 Hz, 2H), 2.45 (s, 3H), 2.26 (s, 3H).

^{13}C NMR (126 MHz, $CDCl_3$) δ 188.0, 166.5, 164.6, 164.4, 162.8, 156.9, 140.4, 138.6, 135.0, 132.4, 131.4, 131.0, 129.7, 129.1, 128.1, 127.1, 125.6, 114.2, 83.1, 55.5, 45.5, 43.9, 43.6, 41.8, 29.6, 25.4, 18.7.

HRMS (ESI) *m/z* calcd for $[C_{31}H_{30}ClN_7O_4S + H]^+$ = 632.1769, found 632.1848.

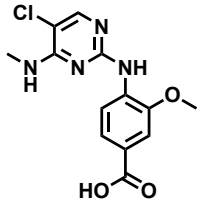

JP-2-241

A mixture of 2,5-dichloro-N-methyl pyrimidin-4-amine (106.2 mg, 0.60 mmol) and 4-amino-3-methoxybenzoic acid (111.8 mg, 0.67 mmol) was dissolved in a 1:1 mixture of Dioxane:H_2O (4 mL). A solution of 4 M HCl in dioxane (0.15 mL) was added and the reaction mixture was stirred at 100 °C overnight. A white precipitate formed upon

cooling which was filtered and washed with H_2O to afford 78.7 mg (43%) of the title compound as a white powder which product was used without further purification.
^{1}H NMR (500 MHz, DMSO) δ 9.17 (s, 1H), 8.55 (d, *J* = 5.8 Hz, 1H), 8.29 (d, *J* = 8.5 Hz, 1H), 8.18 (s, 1H), 7.63 (d, *J* = 8.5 Hz, 1H), 7.55 (s, 1H), 3.93 (s, 3H), 2.98 (d, *J* = 4.6 Hz, 3H).

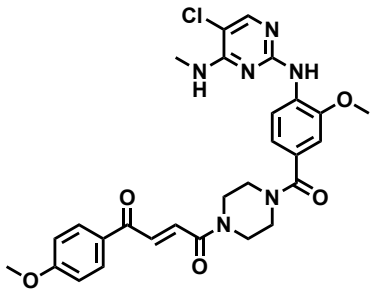

JP-2-244

General Procedure A was followed with **JP-2-241** (21.3 mg, 0.07 mmol), HATU (34.2 mg, 0.07 mmol), DIPEA (0.05 mL, 0.3 mmol), and **JP-2-196** (20.8 mg, 0.07 mmol). The crude residue was purified by silica gel chromatography (0-8% MeOH in DCM) to afford 23.3 mg (60%, 2 steps - *E:Z* = 91:9) of the title compound as a yellow film.
^{1}H NMR (700 MHz, $CDCl_3$) δ 8.58 (d, *J* = 8.2 Hz, 1H), 8.06 – 8.02 (m, 2H), 7.99 (d, *J* = 14.9 Hz, 1H), 7.93 (s, 1H), 7.67 (s, 1H), 7.47 (d, *J* = 14.9 Hz, 1H), 7.04 (d, *J* = 1.8 Hz, 1H), 7.02 (dd, *J* = 8.3, 1.8 Hz, 1H), 7.00 – 6.96 (m, 2H), 5.34 (q, *J* = 4.9 Hz, 1H), 3.93 (s, 3H), 3.89 (s, 3H), 3.81 – 3.59 (m, 8H), 3.11 (d, *J* = 4.9 Hz, 3H).
^{13}C NMR (126 MHz, $CDCl_3$) δ 187.5, 170.9, 164.3, 164.3, 158.6, 147.6, 135.1, 131.7, 131.4, 130.9, 129.9, 120.3, 116.9, 114.2, 109.7, 105.7, 56.0, 55.6, 46.1, 42.5, 28.2.
HRMS (ESI) *m/z* calcd for $[C_{28}H_{29}ClN_6O_5 + H]^+$ = 565.1888, found 565.1968.

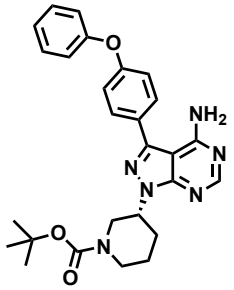

JP-2-242

A mixture of (4-phenoxyphenyl)boronic acid (60.6 mg, 0.28 mmol), *tert*-butyl (*R*)-3-(4-amino-3-iodo-1*H*-pyrazolo[3,4-*d*]pyrimidin-1-yl)piperidine-1-carboxylate (117.1 mg, 0.26 mmol), tetrakis(triphenylphosphine)palladium (28.4 mg, 0.03 mmol), and potassium carbonate (105.0 mg, 0.79 mmol) was suspended in a 1:1 mixture of Dioxane:H_2O (4 mL) and the reaction mixture was stirred at 90 °C for 5 hours. The solvent was removed *in vacuo*, and the crude residue was purified by silica gel chromatography (0-70% EtOAc in Hexanes) to afford 127.1 mg (99%) of the title compound as a yellow foam.
^{1}H NMR (500 MHz, $CDCl_3$) δ 8.37 (s, 1H), 7.65 (dd, *J* = 8.1, 6.1 Hz, 2H), 7.41 – 7.36 (m, 2H), 7.15 (dd, *J* = 8.4, 6.4 Hz, 3H), 7.08 (d, *J* = 7.9 Hz, 2H), 5.64 (s, 2H), 4.84 (tt, *J* =

10.9, 4.4 Hz, 1H), 4.47 – 4.03 (m, 2H), 2.85 (td, *J* = 13.0, 3.0 Hz, 1H), 2.32 – 2.14 (m, 2H), 1.88 (d, *J* = 7.9 Hz, 1H), 1.75 – 1.63 (m, 1H), 1.44 (s, 9H).

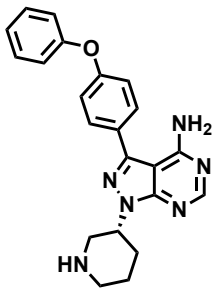

JP-2-246

General Procedure E was followed with **JP-2-242** (37.2 mg, 0.08 mmol), and TFA (0.19 mL, 2.5 mmol) for 30 minutes. The crude material was used without further purification.

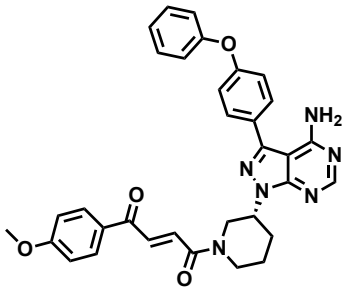

JP-2-247

General Procedure A was followed with *trans*-3-(4-methoxybenzoyl)acrylic acid (24.5 mg, 0.09 mmol), HATU (40.7 mg, 0.11 mmol), DIPEA (0.05 mL, 0.29 mmol), and **JP-2-246** (27.8 mg, 0.07 mmol). The crude residue was purified by silica gel chromatography (0-5% MeOH in DCM) and then by reverse phase silica gel chromatography (5-95% MeCN in H_2O) to afford 16.9 mg (41%, 2 steps - *E:Z* = 85:15) of the title compound as a white solid.

^{1}H NMR (700 MHz, $CDCl_3$) δ 8.38 – 8.31 (m, 1H), 8.07 – 8.03 (m, 1H), 8.00 – 7.97 (m, 1H), 7.97 – 7.85 (m, 1H), 7.67 – 7.62 (m, 2H), 7.55 – 7.41 (m, 1H), 7.40 – 7.36 (m, 2H), 7.17 (t, *J* = 7.3 Hz, 1H), 7.16 – 7.13 (m, 2H), 7.08 (d, *J* = 8.0 Hz, 2H), 7.00 – 6.96 (m, 1H), 6.96 – 6.92 (m, 1H), 5.64 (s, 2H), 4.96 – 4.87 (m, 2H), 4.55 – 4.49 (m, 1H), 4.22 (dd, *J* = 13.6, 4.1 Hz, 1H), 4.11 (d, *J* = 13.8 Hz, 1H), 3.92 (dd, *J* = 13.4, 9.9 Hz, 1H), 3.88 (d, *J* = 13.3 Hz, 3H), 3.48 (dd, *J* = 12.6, 10.6 Hz, 1H), 3.28 (td, *J* = 13.2, 2.9 Hz, 1H), 3.08 (ddd, *J* = 13.7, 11.1, 3.2 Hz, 1H), 2.45 – 2.33 (m, 1H), 2.28 (dd, *J* = 13.7, 4.1 Hz, 1H), 2.05 (ddt, *J* = 12.1, 7.5, 3.7 Hz, 1H), 1.81 – 1.71 (m, 1H).

^{13}C NMR (151 MHz, $CDCl_3$) δ 187.7, 187.6, 164.7, 164.4, 164.2, 164.1, 158.6, 158.6, 157.8, 156.4, 156.3, 155.8, 155.7, 154.3, 154.3, 144.1, 144.0, 134.4, 134.1, 132.0, 131.9, 131.3, 131.3, 130.0, 127.8, 127.6, 124.1, 119.6, 119.1, 114.1, 114.0, 98.6, 98.6, 55.6, 55.6, 53.4, 52.4, 50.1, 46.3, 46.2, 42.5, 30.3, 30.0, 25.3, 23.7.

HRMS (ESI) *m/z* calcd for $[C_{33}H_{30}N_6O_4 + H]^+$ = 575.2329, found 575.2406.

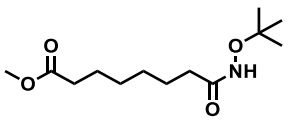

DD-1-42-P1

General Procedure D was followed with suberic acid monomethyl ester (500 mg, 2.66 mmol), T3P (1.66 mL, 2.79 mmol), DIPEA (1.38 mL, 7.98 mmol), and O-*tert*-Butylhydroxylamine hydrochloride (400 mg, 3.19 mmol). The reaction was quenched with 5% LiCl (aq) (60 mL) and extracted 3 times with EtOAc. The organic extracts were washed again with 5% LiCl (aq) and the organic extract was dried over Na_2SO_4, vacuum filtered, and the volatiles were removed *in vacuo*. The crude residue was purified by silica gel chromatography (0-100% EtOAc in Hexanes) to afford 573 mg (83%) of the title compound as a slightly yellow, thick oil.

^{1}H NMR (500 MHz, $CDCl_3$) δ 3.65 (s, 3H), 2.29 (t, J = 7.5 Hz, 2H), 2.14 – 2.01 (m, 1H), 1.62 (qd, J = 12.9, 8.0 Hz, 4H), 1.33 (p, J = 3.7 Hz, 4H), 1.25 (s, 9H).

^{13}C NMR (151 MHz, $CDCl_3$) δ 174.4, 172.2, 81.9, 51.6, 34.1, 33.4, 28.9, 26.4, 25.4, 24.8, 14.3.

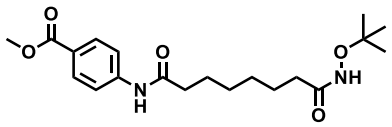

DD-1-47-P1

Methyl ester **DD-1-42-P1** (100 mg, 0.39 mmol) was dissolved in MeOH (2.0 mL) and 2M LiOH (aq, 0.77 mL) was added dropwise. The reaction mixture was stirred at ambient temperature overnight, and upon completion was quenched with 1M HCl (10 mL) and extracted 3 times with DCM. The organic extracts were washed again with brine and the organic extract was dried over Na_2SO_4, vacuum filtered, and the volatiles were removed *in vacuo*. The crude material was used without further purification.

A modified **General Procedure A** was followed with crude residue, HATU (147 mg, 0.39 mmol), DIPEA (0.2 mL, 1.16 mmol), and methyl 4-aminobenzoate (64 mg, 0.42 mmol). The reaction mixture was stirred at 100 °C for two days. The reaction was quenched with 5% LiCl (aq) (20 mL) and extracted 3 times with EtOAc. The organic extracts were washed again with 5% LiCl (aq) and the organic extract was dried over Na_2SO_4, vacuum filtered, and the volatiles were removed *in vacuo*. The crude residue was purified by silica gel chromatography (0-100% EtOAc in Hexanes) to afford 55 mg (38%) of the title compound as a beige solid.

^{1}H NMR (500 MHz, DMSO) δ 10.20 (s, 2H), 7.89 (d, J = 3.0 Hz, 2H), 7.72 (d, J = 3.0 Hz, 2H), 3.81 (s, 3H), 2.34 (t, J = 8.3 Hz, 2H), 1.99 (t, J = 7.9 Hz, 2H), 1.30 – 1.24 (m, 5H), 1.13 (s, 9H).

^{13}C NMR (126 MHz, DMSO) δ 171.9, 170.4, 165.8, 143.7, 130.2, 123.6, 118.3, 80.1, 51.8, 36.4, 32.3, 28.3, 26.4, 25.0, 24.9, 20.6.

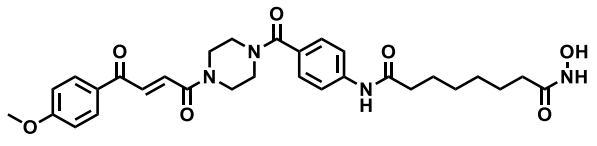

DD-1-073-P1

Methyl ester **DD-1-47-P1** (55 mg, 0.15 mmol) was dissolved in MeOH (6.0 mL) and 2M LiOH (aq, 0.90 mL) was added dropwise. The reaction mixture was stirred at ambient temperature for 7 days. The volatiles were removed *in vacuo*, and the off-white residue was dissolved in water and acidified with 1M HCl until a beige precipitate was formed that was vacuum filtered and dried under vacuum (40 mg) and the resultant material was used without further purification.

A modified **General Procedure A** was followed with crude residue, HATU (42 mg, 0.11 mmol), DIPEA (0.08 mL, 1.16 mmol), and **JP-2-196** (33 mg, 0.12 mmol) and stirred overnight. The reaction was quenched with 5% LiCl (aq) (20 mL) and extracted 3 times with EtOAc. The organic extracts were washed again with 5% LiCl (aq) and the organic extract was dried over Na_2SO_4, vacuum filtered, and the volatiles were removed *in vacuo*. The crude residue was purified by silica gel chromatography (0-10% MeOH in DCM) to afford 62 mg (66%) of the *tert*-butyl protected hydroxamic acid, which was dissolved in TFA (5.0 mL) and stirred at 35 °C overnight. The volatiles were removed *in vacuo* and the brown residue was dissolved in DCM, adsorbed onto silica gel and was purified by silica gel chromatography (0-10% MeOH in DCM, 0.1% AcOH) to afford 27mg (49%, 2 steps - *E:Z* = 97:7) of the title compound as a beige film.

^{1}H NMR (500 MHz, MeOD) δ 8.07 (dd, J = 8.9, 3.0 Hz, 2H), 7.92 (d, J = 15.1 Hz, 1H), 7.71 (d, J = 8.1 Hz, 2H), 7.52 (d, J = 15.2 Hz, 1H), 7.45 (d, J = 8.1 Hz, 2H), 7.11 – 7.06 (m, 2H), 3.91 (s, 3H), 3.85 – 3.45 (m, 8H), 2.41 (t, J = 7.4 Hz, 2H), 2.11 (t, J = 7.4 Hz, 2H), 1.69 (dp, J = 36.6, 7.0 Hz, 4H), 1.48 – 1.35 (m, 4H).

^{13}C NMR (126 MHz, MeOD) δ 189.4, 174.8, 172.6, 166.7, 166.0, 142.1, 135.9, 132.9, 132.4, 132.3, 131.3, 131.0, 129.3, 120.7, 115.3, 56.2, 47.1, 43.2, 37.9, 33.7, 29.9, 29.8, 26.6, 26.6.

HRMS (ESI) *m/z* calcd for $[C_{30}H_{36}N_4O_7 + Na]^+$ = 587.2476, found 587.2482.

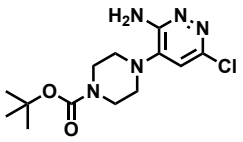

JP-2-238

A mixture of 3-amino-4-bromo-6-chloropyridazine (108.5 mg, 0.52 mmol) and 1-boc-piperazine (461.9 mg, 2.5 mmol) was dissolved in a THF (1 mL) and the reaction mixture was stirred at 80 °C for overnight. The solvent was removed *in vacuo*, and the crude residue was purified by silica gel chromatography (0-100% EtOAc in Hexanes) to afford 147.4 mg (90%) of the title compound as a yellow foam.

^{1}H NMR (500 MHz, $CDCl_3$) δ 6.73 (s, 1H), 5.12 (s, 2H), 3.60 – 3.55 (m, 4H), 3.00 (t, *J* = 5.0 Hz, 4H), 1.48 (s, 9H).

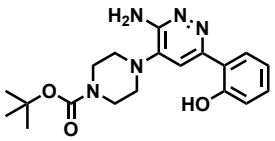

JP-2-243

A mixture of **JP-2-238** (122.3 mg, 0.39 mmol), 2-hydroxyphenyl boronic acid (138.4 mg, 1.00 mmol), [1,1′-Bis(diphenylphosphino)ferrocene]dichloropalladium(II) (34.5 mg, 0.05 mmol), and potassium carbonate (186.1 mg, 1.35 mmol) was suspended in a 1:1 mixture of MeCN:H_2O (2.5 mL) in a sealed tube, and the reaction mixture was stirred at 120 °C for 45 minutes. The solvent was removed *in vacuo*, and the crude residue was purified by silica gel chromatography (0-100% EtOAc in Hexanes) to afford 21.2 mg (15%) of the title compound as a white-yellow powder.

^{1}H NMR (500 MHz, $CDCl_3$) δ 7.57 (dd, *J* = 8.0, 1.6 Hz, 1H), 7.29 (ddd, *J* = 8.5, 7.2, 1.6 Hz, 1H), 7.05 (dd, *J* = 8.2, 1.2 Hz, 1H), 6.91 (td, *J* = 7.6, 1.3 Hz, 1H), 4.88 (s, 2H), 3.65 (t, *J* = 5.0 Hz, 4H), 3.10 (t, *J* = 5.0 Hz, 4H), 1.50 (s, 9H).

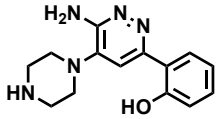

JP-2-248

General Procedure E was followed with **JP-2-243** (11.2 mg, 0.03 mmol), and TFA (0.09 mL, 0.96 mmol) for 1 hour. The solvent was removed *in vacuo*, and the crude residue was purified by silica gel chromatography (0-20% MeOH in DCM with 0.1% Et_3N) to afford 6.2 mg (76%) of the title compound as a yellow oil.

^{1}H NMR (600 MHz, DMSO) δ 7.92 (dd, *J* = 8.3, 1.6 Hz, 1H), 7.48 (s, 1H), 7.24 (ddd, *J* = 8.4, 7.3, 1.6 Hz, 1H), 6.89 (dtd, *J* = 8.2, 3.6, 1.2 Hz, 2H), 6.23 (d, *J* = 6.0 Hz, 1H), 4.01 (s, 1H), 3.04 (t, *J* = 5.0 Hz, 4H), 2.98 – 2.91 (m, 4H).

LRMS (ESI) *m/z* calcd for $[C_{14}H_{17}N_5O + H]^+$ = 272.3, found 272.1.

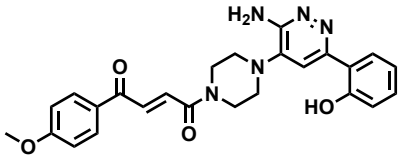

JP-2-249

General Procedure A was followed with *trans*-3-(4-methoxybenzoyl)acrylic acid (12.5 mg, 0.06 mmol), HATU (27.7 mg, 0.07 mmol), DIPEA (0.05 mL, 0.29 mmol), and **JP-2-248** (16.4 mg, 0.06 mmol). The crude residue was purified by silica gel chromatography (0-10% MeOH in DCM) to afford 25.5 mg (92%, 2 steps - *E:Z* = 92:8) of the title compound as a white-yellow powder.

^{1}H NMR (700 MHz, $CDCl_3$) δ 8.02 (d, *J* = 8.5 Hz, 2H), 7.97 (d, *J* = 14.9 Hz, 1H), 7.54 (d, *J* = 8.0 Hz, 1H), 7.48 (d, *J* = 14.9 Hz, 1H), 7.30 (s, 1H), 7.26 (t, *J* = 1.7 Hz, 1H), 7.00 (d, *J* = 8.1 Hz, 1H), 6.96 (d, *J* = 8.6 Hz, 2H), 6.89 (t, *J* = 7.5 Hz, 1H), 3.92 (t, *J* = 5.0 Hz, 2H), 3.87 (s, 3H), 3.86 – 3.83 (m, 2H), 3.16 (t, *J* = 5.2 Hz, 4H), 2.47 (br s, 2H).

^{13}C NMR (151 MHz, $CDCl_3$) δ 187.8, 164.6, 164.5, 158.7, 155.0, 154.1, 140.6, 135.3, 131.5, 131.1, 130.9, 129.8, 125.3, 119.1, 118.4, 117.5, 114.3, 111.6, 55.7, 49.6, 49.1, 49.1, 45.9, 42.1.

HRMS (ESI) *m/z* calcd for $[C_{25}H_{25}N_5O_4 + H]^+$ = 460.1979, found 460.1983.

Supporting References for Methods

1. Xu, T.; et al. ProLuCID: An improved SEQUEST-like algorithm with enhanced sensitivity and specificity. J. Proteomics 2015, 129, 16-24.
2. Schanda, P.; et al. SOFAST-HMQC experiments for recording two-dimensional heteronuclear correlation spectra of proteins within a few seconds. J. Biomol. NMR 2005, 33, 199-211.
3. Krysztofinska, E. M.; et al. Structural and functional insights into the E3 ligase, RNF126. Sci. Rep. 2016, 6, 26433.
4. King, E. A.; et al. Chemoproteomics-Enabled Discovery of a Covalent Molecular Glue Degrader Targeting NF-κB. Cell Chem. Biol. 2023, 30 (4), 394-402.